University Mohamed Khider of Biskra
Exact sciences and sciences of natural and life
Material sciences

MASTER MEMORY

Matter
Sciences
Physics

Material physics

Energetic physics

Réf. :

Prsented by:
Loucif Narimane
Mameri Foulla

Le : 27/6/2022

Study of perovskite based tandem solar cells

Jury:

Dr	Tibermacine Toufik	Professor	Med Khider University-Biskra	President
Dr	Mancer Mansoura	MCB	Med Khider University-Biskra	Examiner
Dr	Abdeslam N.Amele	MCB	Med Khider University-Biskra	Supervisor

Academic Year: **2021-2022**


بسم الله الرحمن الرحيم

اهداء

بعد بسم الله الرحمان الرحيم والصلاة والسلام على أشرف المرسلين سيدنا وحبيبنا محمد وعلى أله وصحبه الميامين ومن تبعهم بإحسان الى يوم الدين.

اهدي ثمرة جهدي المتواضع الى من لم تدخر نفسا في تربيتي.... **امي الحنونة**

الى من تشققت يداه في سبيل رعايتي .... **ابي الغالي**

الى **اخوتي** و**اخواتي** و**زوجة اخي** و**زوج اختي** الكرام حفضهم الله الى كافة **أصدقائي** و**رفاق الدراسة** وفقكم الله

الى كل من نصحني ووجهني وكل من ساهم في إتمام هذا البحث. **خوتي** و**اخواتي** و**زوجة اخي** و**زوج اختي** الكرام حفضهم الله الى كافة **أصدقائي** و**رفاق الدراسة** وفقكم الله

الى كل من نصحني ووجهني وكل من ساهم في إتمام هذا البحث.

جزاكم الله عني ألف خير

لوصيف نريمان

اهداء

الى من بلغ الرسالة وأدى الأمانة ونصح الامة. الى نبي الرحمة ونور العالمين سيدنا محمد صلى الله عليه السلام

الى اعز الناس وأقربهم الى قلبي الى ***والدتي العزيزة: بقة مباركة*** ووالدي **العزيز: عبد العزيز** الذي كانا بدعائهما المبارك أعظم الأثر في تسيير البحث حتى ترسو هذه الصورة

الى من ساندني وخطا معي خطواتي ***زوجي العزيز: عمارة لحسن*** الذي تحمل الكثير. ووقوفي في هذا المكان ما كان ليحدث لولا تشجيعه المستمر لي.

اميرتي وفلذتي كبدي، ابنتي ***اميرة*** التي حرمت مني طيلة هذه الفترة التي قضيتها في اعداد هذا البحث.

الى امي الثانية سعيدة التي كانت دائما تساندني بدعائها، الى من حبهم يجري في عروقي اخواتي عمار وزهراء وعبد الحق وكاميليا، الى احبتي حفيظة وأخي نذير، الى حبيبة قلبي ابنة اختي رحيل.

واهداء خاص الى الدكتور جبنون رشيد الذي لولاه لما وصلتو لهذه المرحلة.

اهدي لكم هذا العمل المتواضع راجية من المولى عز وجلى ان يجد القبول والنجاح.

معمرى فلة

Acknowledgments

Thank first and foremost to Allah, the Most Gracious, the Most Merciful without his grace this thesis would never have been finished on time

Then we should mention everyone who contributed to complete this work.

Foremost my utmost gratitude goes to my supervisor, ***Dr.Abdeslam Noura Amele*** *to whom I would express my sincere thanks .I am very grateful for her support, her patience and her valuable advice for completing this study*

I addition to our consultant, we would like to thank the thesis jury members Professor ***Tibermacine Toufik*** *as president assuring the defence of our master degree,*

And the Dr ***Mancer Mansoura*** *for her examination.*

Narimane and foulla

Abstract

Photovoltaic research communities have seen a remarkable increase in the efficiency of perovskite solar cells, and their tandem configurations. Especially those based on organo-lead-halide showing great promise for overcoming the S-Q limit as well as their stability and environmental friendliness. At the first, free lead perovskite solar cell was performed under the Atlas–Silvaco simulator and the compared results were obtained with sufficient agreement for J-V characteristics. Solar cells used perovskite ($CH_3NH_3GeI_3$) and ($CH_3NH_3PbI_3$) are employed separately to build top solar cells. $SrSnO_3$ and TiO_2 have been involved as electron transport materials while Cu_2O has been included as a whole transport material. The effect on light is explored through the shape variation of conduction band energy. The influence of $SrSnO_3$ and TiO_2 is also studied when using the $MAPbI_3$ perovskite solar cell. The two-junction tandem device was chosen to operate under planar and spectral light available in the Silvaco package library (solar example 03). The tunnel layer used consists of (P^+ and N^+)-silicon. The organic-inorganic mechanically stacked tandem is constructed by using the lead-free absorber ($MAGeI_3$) as top cell connected to the bottom inorganic solar cell. The inorganic solar cell is made of CdS (n-type, Nd=1e18 cm^{-3})-CIGS (p-type, Na=2e16 cm^{-3})-Silicon (substrate).

Key words: Solar cell, Perovskite, Tandem, Organic-inorganic Material

Résumé

Les communautés de recherche photovoltaïque ont témoigné une augmentation remarquable de l'efficacité des cellules solaires à pérovskite ainsi leurs configurations en tandem. En particulier ceux à base d'organo-halogénure de plomb très prometteurs pour surmonter la limite S-Q ainsi que leur stabilité et leur respect de l'environnement. Au début, la cellule solaire à pérovskite sans plomb a été réalisée sous le simulateur Atlas – Silvaco et les résultats comparés ont été obtenus avec un accord suffisant pour les caractéristiques J-V. Les cellules solaires utilisant le pérovskite ($CH_3NH_3PbI_3$) et ($CH_3NH_3GeI_3$) sont employées séparément pour construire les top cellules solaires. $SrSnO_3$ et TiO_2 ont été impliqués en tant que matériaux de transport d'électrons tandis que Cu_2O a été inclus en tant que matériau de transport de trous. L'effet sur la lumière est exploré à travers la variation de forme de l'énergie de la bande de conduction. L'influence de $SrSnO_3$ et TiO_2 est également étudiée lors de l'utilisation de la cellule solaire pérovskite $MAPbI_3$. Le dispositif tandem à deux jonctions a été choisi pour fonctionner sous une lumière planaire et spectrale disponible dans la bibliothèque de packages Silvaco (exemple solaire 03). La couche tunnel utilisée est constituée de (P^+ et N^+) silicium. Le tandem organique-inorganique empilé mécaniquement est construit en utilisant l'absorbeur sans plomb ($MAGeI_3$) comme cellule top connectée à la cellule solaire inorganique du bas. La cellule solaire inorganique est constituée de CdS (type n, Nd=1e18 cm^{-3}) -CIGS (type p, Na=2e16 cm^{-3}) -silicium (substrat).

Mots clés : Perovskite, cellule solaire, Tandem, Organique-inorganique Matériaux

Table Of Contents

General Introduction

Improving the performance of the photovoltaic (PV) device is critical in order to strengthen its competitiveness with a conventional electricity source. Crystalline silicon solar cells have controlled the PV market for years, with current market share of 90%. Where only a slight improvement of their efficiency has been reached over the past 15 years, in which the wafer size efficiency as high as 25.6% has been reported, that is close to the maximum efficiency theoretical 29.4% [Loper et al, 2014; Richter et al, 2013]. Consequently, to overcome Shockley–Queisser (SQ) single junction limit, tandem solar cells have attracted a potential interest for efficiencies beyond which has driven researchers to develop thin-film tandem solutions for high-performance solar cells and to low cost. Perovskite solar cells have recently appeared as a promising candidate for photovoltaics building the third-generation concept. In addition to good efficiencies and ease of fabrication, a mainly great feature is their tunable band gap range (1.48 and 2.3 eV) which makes association with other solar cells in tandem device structuration possible.

Also, since the perovskites processing conditions as importantly the low temperature are achieved, this allow them to be integrated monolithically as the top component of tandem structures without harmful the bottom cell. Nowadays, the experimental results and modeling indicate that efficiencies above 25% are already reached [Todorov et al, 2016]. Consequently, the perovskite optimization and solving its stability limitations could lead to a commercially practical technology.

In this concept and for the purpose to investigate the perovskite materials and solar cells based, then to be able to build the tandem solar cell, this work aims to cover the major characteristics of solar cell devices, perovskite physical properties and modeling the tandem configuration. Thus, one can find in this manuscript three chapters.

The first chapter contains an introduction to the solar cell where the motivation behind the appealing interest to solar cell and proper energy. An overview of light properties, photovoltaic principle and solar cells characterization are followed. Then, recombination and quantum efficiency solar cell are treated in this chapter.

The second chapter deal with the tandem configurations. It studies the top electrodes (TMO, ITO, IZO and Ag-Nanowires), and their constituent metal. The absorber Material (Perovskite) is reviewed through the band tuning and its site substitutions. As well, the recombination layer

has been studied. Then, the electron and hole transport layers and the charge carriers transport modeling are given at the end of this part.

The third chapter holds some simulation attempts of perovskite solar cell and tandem devices. The solar cells used perovskite lead free ($CH_3NH_3GeI_3$) and with lead (Pb) such as ($CH_3NH_3PbI_3$) in construction with $SrSnO_3$ and TiO_2 as electronic transport materials and Cu_2O as hole transport material.

References of General Introduction

[Loper et al, 2014] P. Loper, B. Niesen, S.J. Moon, S. Martin De Nicolas, J. Holovsky, Z. Remes, M. Ledinsky, F.J. Haug, J.H. Yum, S. De Wolf, C. Ballif, Organic-inorganic halide perovskites: Perspectives for silicon-based tandem solar cells, IEEE Journal of Photovoltaics 4 1545-1551, 2014.

[Richter et al, 2013] A. Richter, M. Hermle, S.W. Glunz, Reassessment of the Limiting Efficiency for Crystalline Silicon Solar Cells, IEEE Journal of Photovoltaics 3 1184-1191, 2013

[Todorov et al, 2016] T. Todorov, O. Gunawana and S. Guhab, 'A road towards 25% efficiency and beyond: perovskite tandem solar cells', The Royal Society of Chemistry, Mol. Syst. Des. Eng., 1, 370–376, DOI: 10.1039/c6me00041j, 2016,

CHAPTER I

SOLER CELL BACKGROUND

Problematic and Motivation

Photovoltaic means energy and as it is evident, the energy is connected to climate change which stands as an enormous problem and a real threat seriously reckon after the cold war This fact of global warming can't be refuted especially because of the new catastrophic nature phenomena. During the last decade and particularly the last summer (2021), wildfires have practically incinerated many countries, as well as Austria, Canada, Greece, Turkey, Palestine and Algeria too where the temperatures soar above 45 degrees Celsius.

The scientific consensus concerning this prolonged extreme weather, newly, happening worldwide, is due to climate change, continuously exacerbating by human interference [Stocker et al, 2013; Cook et al, 2016].

Despite the Fossil fuels (gas) still provide 80 % of global energy consumption, including 65 % supply of global electricity generation, [KWES, 2016] have long been regarded as the main offender behind this environmental crisis. whereas, the sun can wreak havoc on a greenhouse earth with a polluted atmosphere, it is also considered as a solution for breaking free from the reliance on fossil fuel.

Estimated to be 23,000 terawatts a year [R. and M. Perez, 2010], the total potential solar energy available on earth is a reservoir of solar energy, which eclipses all other finite and renewable resources.

Indeed, solar power suffer of limitation as any other energy source; knowing that solar irradiance is not mostly uniform all the time since it is dependent on seasonal variations, shading from local weather, and on time of day. Nevertheless, in combination with other renewables, new advances in energy storage, and a restructuring of national power grids to more localized systems, solar modules easily have the capability to provide the twenty terawatts' years annual global energy consumption [R. and M. Perez, 2010] in this time, a hug shift societal and political has already made headway away from fossil fuel energy sources towards carbon neutral energy generation. But it does not serve that much since the turn of the millennia, the large majority of the two billion dollars spent on climate change related lobbying of the U.S Congress was from fossil fuel and transportation corporations, and their associated trade affiliations.[Brulle ,2018] In spite of the efforts made to encourage investment in solar modules as the feed-in tariffs which have been

established in many countries, it is still unlucky an balanced economic requirement that most feed-in tariff policies constantly are reduced to keep the energy market competitive and fair.[Karneyeva and Wüstenhagen, 2017]

As the progressiveness of carbon capture technology, it is a costly mitigator of climate change. Carbon capture does not treat the reality that fossil fuels are a shrinking continuously, limited source of energy. Nevertheless, in counteracting the effects of climate change, the carbon capture will still be indispensable up until the consumption of fossil fuels is significantly reduced [Zweibel, 2010]

It is not sur whether the evolution of substituted energy sources will involve nuclear power, which is full of drawback due to negative cultural views of course, termination costs and waste management, and is not renewable energy. since, renewables, by definition, are the only available long-term energy source. With the race for clean energy to meet the goals of the Paris Agreement, there has been an increase in the widespread deployment of photovoltaics on rooftops and solar farms in the past 10 years.

The overall installed PV capacity worldwide exceeded 100 gigawatts (gigawatt peak), at the end of 2012. [Hodes,2013] and about one-third of all newly installed electricity generation is anticipated to come from photovoltaics by 2030. [Hodes,2013] Then, 72% of all investment in new generation capacity is expected to be reliable on renewable energy by 2040. Even if the investment in solar energy is second only to wind energy but it increases rapidly. [Michael and Chairman, 2017]

Government tariffs across Europe have stimulated growth and investment in solar energy, despite the budget cuts, and the more importantly, the tipping point for PV return-on investment which carries solar energy up to grid cost-equality with other energy sources as a result to the continuing decline in the prices of crystalline silicon (c-Si) [Docampo et al,2013].

Significantly, over the past 40 years, the average price of 1 watt (power) of silicon PV has decreased from $100 to about $0.5, and it is expected to drop to less than $0.2 for sunny areas; Renewable energy supply auctions have shown solar energy prices dropping from $250/MWh in 2010 to less than $50/MWh by 2016 [IRENA, 2016]

Thin-film photovoltaic light absorbing semiconductors are the principal angle of a large established scientific community, with the goal of providing a semiconducting material to compete with well-known crystal-based (c-Si) and amorphous silicon (a-Si) solar module materials. Inorganic replacements include cadmium telluride (CdTe), copper indium gallium selenide (CIGS) and copper-zinc-tin sulfide (CZTS).

Typically, the thin-film active materials have lower efficiency, and depend on utilizing cheaper processing techniques and less bulk material in order to produce a cost-competitive device. As example, CdTe solar cells managed to occupy a small part of the PV market (1.8 GWp in 2012). But since, Cadmium is known as a toxic substance and Tellurium as rare-earth element. Both are factors that can hinder wider spread of CdTe uses. As much as CdTe, CIGS PV has comparable issues, containing two rare-earth elements: Indium and Gallium and the only possible promising emergent inorganic photovoltaic technology is CZTS, because it uses elements abundantly available in the earth. However, world-class CZTS solar cells have a power conversion efficiency (PCE) of 10%approximately, remarkably weaker than any silicon-based PV. However, there is other alternative thin-film PV technology like Organic carbon-based PVs (OPVs), which is a concurrent to the inorganic photovoltaic cells that use mixed semiconductors polymers and fullerenes or small molecule acceptors, as well as Dye sensitivity Solar cells (DSSC)

Indeed, in 2006 a remarkable progress in PV domain emerged with the perovskite sensitized solar cells (PSSC) fabrication of. The solar cell based on a metal-organic hybrid semiconductor in a nano-porous titanium dioxide (TiO2) layer, realized a 2.2 %.PCE of [Green et al,2014; Kojima et al,2009] $CH_3NH_3PbBr_3$ was used as a metalorganic. The last decade has seen intensive research on perovskite based photovoltaic. Since that date, a speed advancement has been recorded in PCE and the world-record perovskite solar cell reached 23.3 % PCE [NREL, 2018]. Evidently, up today, perovskites are the fastest-growing solar technology in comparison to the single junction organic cells which surpassed 14% recently despite the intense research for twice as long

I-1 Introduction

In this chapter, the solar cell is introduced in first, then a quick view of light, the major source of photoenergy is given followed the photogenerated electron transport via the band structure for inorganic material. The absorbed solar irradiation and Shockley-Quiesser limit tracked by the characterization of solar cell and finally the recombination and quantum efficiency in solar cell is explored.

I.2 Solar cells Introduction

Throughout the last decades, ascending CO_2 emissions and energy shortage triggered grave environmental and political problems. This is because of the deficiency of coal, oil and gas and essentially the increased energy consumption, which become a significant issue to develop a green approach qualified to outface human beings' energy demand. To date, many energy sources such as solar energy, wind energy, nuclear energy have been remarkably progressed over the last years [Armaroli et al,2007]. Solar energy owns non-exhausting obvious advantages, including low environmental impact and low cost plus unlimited high energy of electromagnetic radiation ($12e10^5$TW/hour) to our Earth. Furthermore, it uses solar cells providing more efficient, harmless and cleaner means compared with other techniques. Also, a more efficient energy transportation and storage step is achieved by the immediate conversion of solar energy into electricity. So briefly, how to capture solar energy in maximum cost-efficient balance way is the typical aim of this technology. And yet, this technology started to arouse extensive and global attentions since 1954 when the first modern p-n solar cell in Bell Laboratories using silicon with a delivered efficacy of 6%. After that, Si based solar cell technology dominates the current PV market by achieving a high efficiency (above 26 % versus a "modest" fabrication costs) due to the effective advancement in both essential physical understanding and device engineering of this technology.

In counterpart, considerable other thin film technologies (ex: GIGS, CdTe, and GaAs...ect) exhibited promising efficiencies too and GaAs single-junction solar cell under one-sun illumination reaches an efficiency of 28.8% as shown in Figure I.1 [Yihou, 2017]

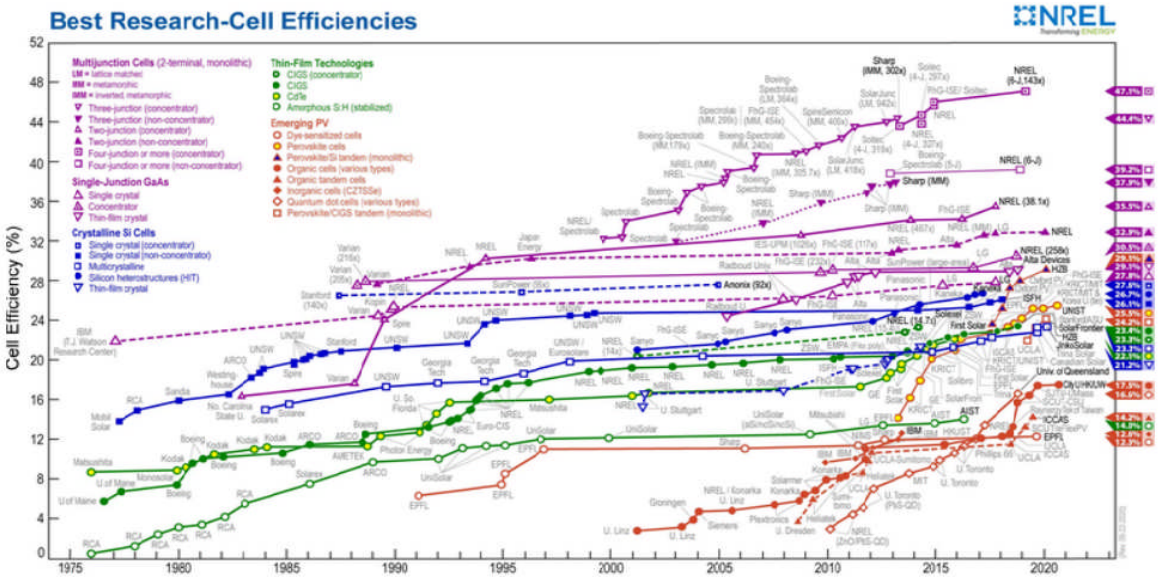

Figure 1.1 State-of- art PVs technology, reproduced from [NREL,2016]

Despite, the bill of modules for the precedent technologies is remarkably rises when the high-temperature or vacuum processing conditions are involved. During the past years, countless next-generation solar technologies were rapidly and unprecedentedly emerged among them, dye-sensitized solar cells (DSCs) [Docampo et al, 2014] and quantum-dot solar cells (QDSCs) [Yuan et al, 2016] organic photovoltaics (OPVs) [Pivrikas et al, 2007], considering a low-temperature solution processing by roll-to-roll printing and coating to reduce effectively the material and fabrication cost. Indeed, nowadays, perovskites have drawn incredible research interest because they proved an increased power conversion efficiency above 22%, which is progressing toward other thin film and Si technologies Figure I-2. Taking into account their short development period compared to inorganic based photovoltaic technologies, the results of organic solar cell are continually impressive [Green et al, 2014].

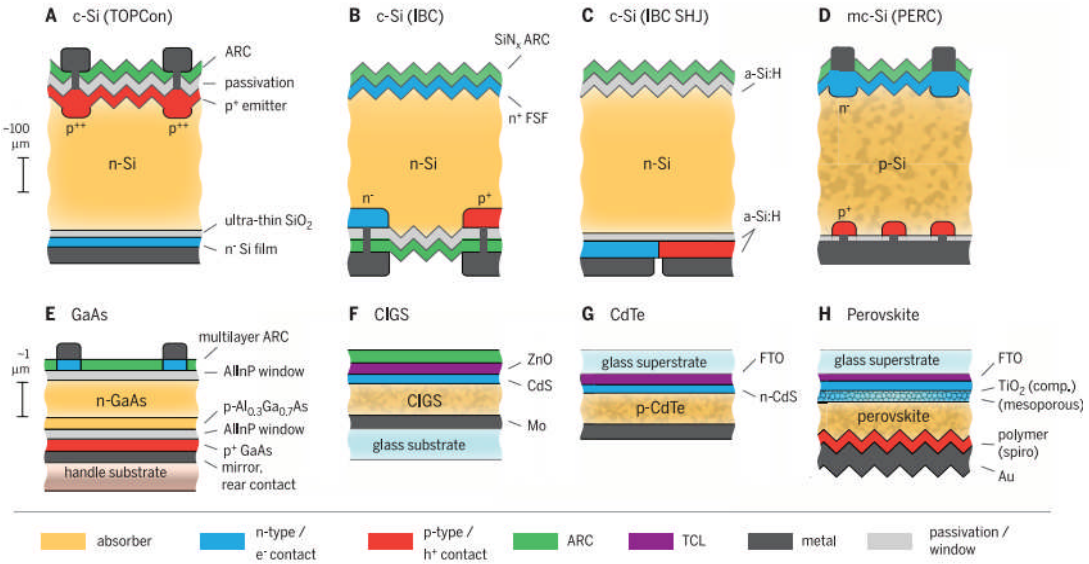

Figure I-2: Layer and contact geometry for solar cells with record efficiencies above 20%:(A) TOPCon crystalline Si (Fraunhofer). (B) IBC crystalline Si (SunPower). (C) Heterojunction IBC crystalline Si (Panasonic). (D) Multicrystalline Si (Trina Solar). (E) GaAs thin film (Alta Devices). (F) CIGS thin film (ZSW Stuttgart). (G) CdTe thin film (First Solar). (H) Perovskite thin film (KRICT) [Polman et al, 2016].

I-3 A quick overview of light properties

Only a portion of global energy emitted by the sun and incident on the earth is the visible light and forms a small subset of electromagnetic spectrum as the sunlight is considerate as a form of electromagnetic radiation as shown in figure I-3(a). The electromagnetic spectrum describes light as a wave with a specific wavelength. But, during experiments measuring the spectrum of wavelengths from heated objects in the late 1800's, a clear divergence of the wave-based view of light could not be explained using the wave-based equations of light. This discrepancy was resolved in the early 1900's by Planck [Yihou, 2017] when he proposed that the total energy of light is composed of almost identical energy elements, or a quanta-of-energy and followed by Einstein, where he correctly distinguished the values of these quantum energy elements while considering the photoelectric effect consisting on the release of electrons from certain metals and semiconductors when struck by light.

Quantum mechanics today describes both the observations of the wave nature and the particle nature of light. The photon, as well as all other quantum mechanical particles (electrons, protons, etc.), is described as a wave packet. A wave packet is defined as a set of waves which can interact

in certain way and it can appear either spatially localized (similar to a square wave resulting from accumulation of an infinite number of sine waves) and behaves like a particle, or can just alternatively appear as a wave. Consequently, the concept of wave-particle duality emerges depending on the situation, a photon appears as either a wave or a particle. Figure I-3 (b) shows the diagram where the relative wavelengths of blue, red and black light waves are represented. A sight of this waves illustrates that the blue light has the shorter wavelength compared to red (long wavelength.) and black and this means that it carries more energy (highest frequency). Figure I-3 (c) show the spectrum of only the visible light.

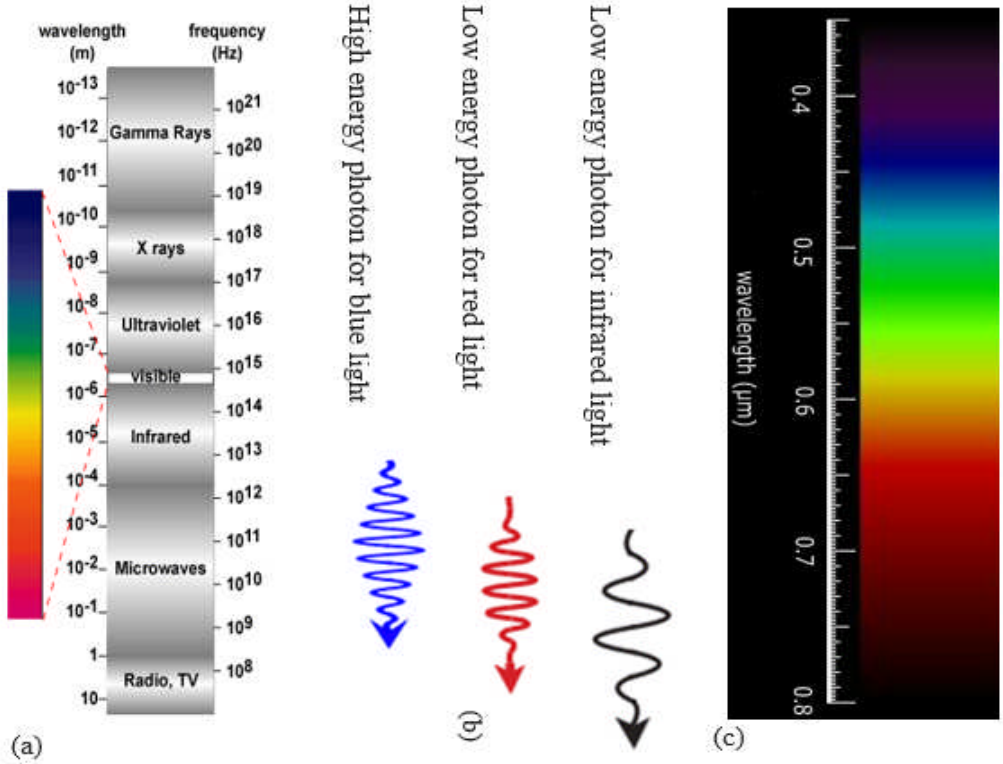

Figure I-3: (a)Sunlight electromagnetic spectrum (b)The relative wavelengths of blue, red and black light. (c) the visible light spectrum.

It is conventional to characterize a photon, one can use either a wavelength (λ) or equivalently its energy (*E*). These two physical quantities are inversely related by the equation given as:

$$E = h.c/\lambda \qquad \text{I-1}$$

Where h is Planck's constant (h= 6.626 × 10^{-34}joule·s), $c$is the speed of light (c= 2.998 × 10^{8} m/s) and $h.c$= 1.99×10^{-25}joules-m.

Often the unit of energy used is the electron volt (eV) rather than the joule (J) when dealing with particles such as photons or electrons. The electron volt is the energy required to raise an electron by 1 eV, and thus a photon with an energy of 1 eV = 1.602 x 10-19 J. Accordingly to that, the hc constant in the equation I-1, can be changed in terms of eV, h = (1.99×10^{-25}joules-m) × (1ev/1.602 ×10^{-19}joules) = 1.24×10^{-6}eV-m. And in addition to that the units for λ will be in µm which gives hc= (1.24×10^{-6}eV-m) ×(10^{6}µm/m). By expressing the new transformed I-1 equation which relates the energy and wavelength of a photon, as shown in the following equation:

$$E(eV) = 1.24/\lambda \qquad \text{I-2}$$

Many key properties of incident solar energy are important to determine how incident sunlight interacts with a photovoltaic converter or other object. The major characteristics of incident solar energy are: -spectral content of the incident light, the intensity of radiant energy and the strike angle of the solar radiation falling on the photovoltaic material; plus, the energy radiated from the sun all over the year or day for a specific surface.

known as photovoltaics (often abbreviated as PV), the solar cell convert light into electricity. in 1839, the photovoltaic effect was observed by Edmond Becquerel for the first time [Yi Hou,2017] and described as a process where semiconducting materials under illumination can produce directly photocurrent and photovoltage.

I-4 Photovoltaic principal

photoelectric and photovoltaic effects are similar phenomenon, whereby light induces a release of charge carriers from a material and are emitted only when the energy of the incoming light exceeds a material dependent value, known as the material's work function ($\varphi < hc/\lambda$). The photoelectric effect is experimental evidence for the particle like (part of the wave-particle duality) nature of light, but it causes only ejection of free charges and without using the photon to generate functional current [Cook et al, 2016].

Different from, conductors containing free charges completely non-localized or insulators where the free charges are hardly removed, semiconductors in between, have a hefty amount of delocalized free charges and electronic properties amid those of the conductor and insulator.
Solid-state physics, elucidates these properties through the electronic band structure of quantum mechanical, giving energetic positions description that electrons can take within a solid. Whereas, the intrinsic semiconductors, at room temperature, have bands that are statistically possible to be partially filled with electrons at any time. The band of the highest occupied electron energy levels known as the valence band is established by the outer shell valence electrons of the material.

VB separates from a lower empty energy band, known as the conduction band, by a band gap E_g depleted of electron energies. The incident photons need to have energies equal to or greater than $E_g$to excite electrons in or above the CB. The exited electrons possess excess heat energy so by means of heat treatment they can relax near the edge of the conduction band. [KWES, 2016, R. and M. Perez, 2015].
Generally, conductance and valence bands are the terms used to represent the electronic band structure of inorganic semiconductors formed by the crystal structure of the material from the overlapping electronic structure of the atoms of its constituents [KWES, 2016, R. and M. Perez, 2015]. But photovoltaics also contains the use of organic semiconductors where they instead have a band-like structure determined by the molecular orbital bonding of its constituents' organic atoms. The highest occupied molecular orbital is known by HOMO and the lowest unoccupied molecular orbit is LUMO and they are equivalent to the valence and conduction bands. [Brulle, 2018; Karneyeva and Wüstenhagen, 2017]
Overall, the process of photoexcitation is described as photoexcited electron through the forbidden band leaving behind a quasiparticle known as a hole. If this pair (electron-hole) stay bound, its known as an exciton or rapidly disassociate, emerging a free electron and hole [Zweibel, 2010; Hodes,2013].

Thus, in order to accomplish the photovoltaic process and using photovoltaic electromotive force to generate a photocurrent, the electron and the hole have to be selectively dissociated and separated, exiting the photoactive semiconductor. These free charges are involved into two different processes [Green et al,2014] as follow:

- Charge diffusion driven by charge concentration (charge immigration to lower concentration region),
- Drift of charges produced due to an in-built or external electric field.

  An in-built electric (embedded)field is engendered when a p-type semiconductor with electronic band structure favorable accepting electrons is brought into contact with an n-type semiconductor that favorably donates electrons.

  The resulting p-n junction attains an energetic balance through a region called the space charge region (SCR) or depletion region and characterized by an electric field continually growing until that region is totally depleted from intrinsic charge carriers [Green et al,2014] the extraction of the selective charge without obstruction requires also interfaces with semiconductors having a band structure that produces a well aligned affinity(ex: hole)for one charge and unaligned affinity for the other charge (ex: electron) [Docampo et al, 2013].In case where the photogenerated charges persist as a tightly bound exciton, it will diffuse until it either recombines or meets an interface with a material that has a band structure making it energetically favorable to dissociate across the interface, rather than remaining as a bound state.

I-5 Transport of a photogenerated electron through the band structure of inorganic material

the following equation (Equation I-3) describes the resulting transported electron and hole currents

$$\begin{cases} J_n = q.n.\mu_n E + qD_n \frac{dn}{dx} \\ J_p = q.p.\mu_p E - qD_p \frac{dp}{dx} \end{cases} \quad \text{with } D_{n,p} =.\mu_{n,p}\,.\frac{K_B.T}{q} \qquad \text{I-3}$$

Where n and p, $.\mu_{n,p}$ and $D_{n,p}$are the electron and hole density, mobility and diffusivity respectively, q is the electron charge, and E is the electric field.

The term $q(n/p)\mu_{n,p}E$describes the drift process while the term $qD_{n,p}\frac{dn/p}{dx}$ describes the diffusion.

I-5-1 Absorbing Solar Irradiation

The earth is irradiated by an extra-terrestrial spectral irradiance called AM0 (AM: Air Mass) coming from the sun. AM0 spectrum is appropriate for evaluating the solar cells performance used in space. When this solar irradiance passes through the atmosphere and received at the Earth's surface is called AM1.5, it is not uniform, but a normalized spectral irradiance

characterizes the amount of available sunlight at all wavelengths, which attain the Earth's surface at mid-latitudes. Then, when some light is attenuates and absorbed by 1.5 thickness of atmosphere caused by the incident angle of sunlight, which is 48.2° at mid-latitudes. These standardized spectral irradiances are presented on Figure I-4-a, depending on wavelength λ or photon energy E_λ and includes the circumsolar AM1.5 Global and AM1.5 Direct, where AM1.5 Direct is valuable for concentrator solar cells that use light scattered around the Sun from a solid angle (2.5 half angle).

As shown in Figure I.4-b, the Air Mass is the path length which light goes through the atmosphere normalized to the shortest path length when sun is at zenith angle. The Air Mass quantifies the reduction of power loss of light caused by air and dust as it passes through the atmosphere. The Air Mass is defined by equation I-4 as:

$$AM = 1/\cos\,\theta \qquad \text{I-4}$$

The excellent choice of the light spectra when using flat solar cells is the AM1.5 G (G stands for global). The sunlight intensity is normalized and measured in suns, with 1 sun equivalent to 1000 W/m^2 of AM1.5 illumination [Pickard, 2017]. Also, to describe the quality of a solar cell the power conversion efficiency (PCE) is used. It is the ratio of the power generated by the solar cell to the power of the illumination incident on the cell solar, and it is given in percentage. Figure I.4 -c shows, AM1.5 solar spectrum with distinct dips due to molecular absorption in Earth's atmosphere. As already said before**, p**hotons with energies smaller than E_g are not absorbed, while photons with energies larger than E_g are not fully converted to electrical energy because of thermalization of charge carriers. The maximum power generated by the cell is limited by voltage loss relative to the band gap voltage. Inset electronic band structure with the separation of the quasi-Fermi levels determining the open-circuit voltage V_{oc} [Polman, 2016]

I-6 The Shockley–Queisser Limit

A direct band gap availability in semiconductors is essential for the absorption of light for PV applications. A small band gap semiconductor with $E_\gamma \geq E_g$ for a hefty amount of the AM1.5 spectrum will therefore absorb almost all the arriving photon. While, a PV large band gap semiconductor will result in only a fraction of the short wavelength where high-energy sunlight is able to excite charges from the VB. Nevertheless, this does not mean that PV should rely only on small bandgap semiconductors because photons beyond the bandgap energy ($E\gamma > EG$) do not transmit this energy directly into more free charges, but actually they transfer increased

kinetic energy on same number of charges. Although the charge excitation happens, the excess energy is unexploited and transformed as thermal energy where the excited electrons thermalized back down to the edge of the CB as shown in figure I-4-d.

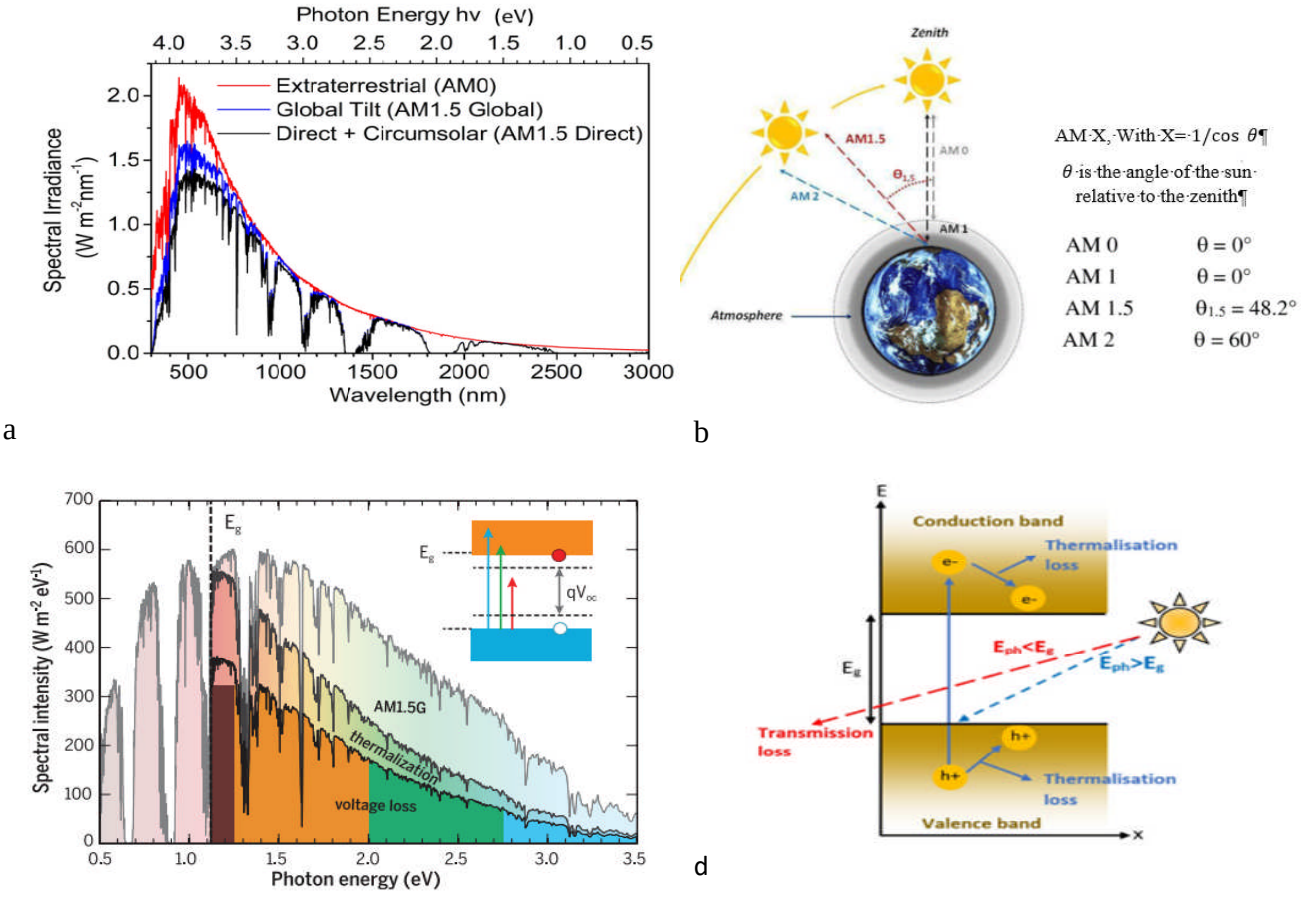

Figure I-4: a/ Normalized spectral irradiance AM0 and AM1.5. The AM1.5 spectrum is considered by two ways: AM1.5Gand considers both direct and diffuse radiation, used for maximum flat solar cells and considers the Earth as a plane with a horizontally tilted steradian field of view, AM1.5 Direct is commonly used for concentrators and considers direct sunlight incident on a plane normal to the Sun [Hossain, et al,2021]- b/ Air mass calculation- c/ AM1.5 solar spectrum with distinct dips due to molecular absorption in Earth's atmosphere[Polman, 2016] -d/ Schematic representation of power losses in single-junction solar cells viz. thermalization and transmission loss [Jaya et al,2021].

Eventually, and despite the existing of some ways to collect the resulting heat, the PCE of a solar cell relies on the balance between failed out the energy of photon as heat versus absorbing thoroughly and intensively the spectral radiation as possible. Regardless the band gap, the solar

cell under illumination will always seek for the balance with its environment by radiating the heat.

Actually, it is possible to combine this comprehension of the detailed balance and accounting the possible lost recombination of photogenerated charge, in order to calculate the maximum theoretical efficiency PCE of solar cells depending on band gap, called by many names such as the radiative efficiency limit, the detailed balance limit, Shockley–Queisser limit, Shockley Queisser Efficiency Limit or also known as SQ Limit. Note that SQ Limit use a single p-n junction to collect power from the cell where the only loss mechanism is radiative recombination in the solar cell.

Figure I-5shows the Shockley Queisser Efficiency limit solar cell as function of band gap. As it can be depicted from the figure that the maximum efficiency 33.7% occurs for semiconductor having a band gap of 1.34 eV.

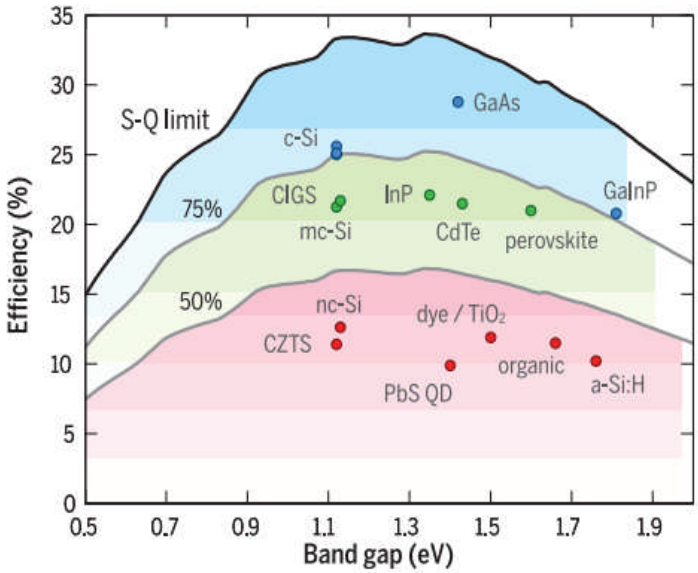

Figure I-5: Theoretical Shockley-Queisser detailed-balance efficiency limit as a function of band gap (black line) and 75% and 50% of the limit (gray lines). Rerecord efficiencies for different materials are plotted for the corresponding band gaps [Polman2016].

As it is distinguishable from the last figure, there are three classes of PV materials: (1st) ultrahigh-efficiency mono crystalline materials with efficiencies higher than 75% of the S-Q limit for the corresponding band gap: homojunction and heterojunction Silicon (Si), gallium arsenide (GaAs) and gallium indium phosphide (GaInP); (2nd) high-efficiency multi- and polycrystalline materials (50 to 75% of the S-Q limit) : Si, $Cu(In,Ga)(Se,S)_2$:(CIGS), CdTe, methyl ammonium lead halide perovskite [$CH_3NH_3Pd(I,Cl,Br)_3$], and InP; and (3rd) low

efficiency materials (<50% of the S-Q limit): micro or nanocrystalline and amorphous Si, organic and polymer materials and quantum dot materials.

Indeed, to overcome the S-Q limit and reaching higher PCE levels some approaches and materials are involved. For example, perovskite materials and/or tandem large band gap perovskite/ perovskite (or silicon) structures [Sista et al, 2009; Uzu et al, 2015].

Currently there are no ubiquitous perovskite materials around the ideal 1.34 eV band gap, but perovskites have tunable bandgap crystal structures that are further elucidated later in the next chapter [Tai et al, 2011; Wang, et al,2014]. Solar cells can also be stacked on top of each other building tandem and intended to accumulate photons of different energies by having different bandgap semiconductors with.

Because of their important property of having a continuously tunable bandgap, which allows the PV based perovskite materials to considerably collect photons with wavelengths of light and unlike solar cells-based c-Si or CIGS, solar cells perovskite do not need extra phonon to liberate the electrons which means that they can be manufactured as very thin films using a technique knowing as solutions processing. Perovskite structures are also much more tolerant to defects than silicon and that eliminates the need of high cost and high energy machinery that silicon production requires. Yet, the tandem perovskite/ Si can reduce its parasitic losses and achieve a PCE of 29.6 % [Sista et al, 2009]. And other studies for a perovskite/CIGS tandem cell using an oscillator model involving the n-k optical data calculated similar PCE (29%) [De Vos, 1980; Rau and Werner, 2004]

Different types of tandem devices would emerge only by counting the terminal electrodes as Figure I-6 shows, tandem cell usually referred as monolithic 2-terminal devices with only 2 metal electrodes and all layers touching and alternative tandem concepts using stacked sub-cells with three- or four-terminal connections have been presented in literature [Shrotriya et al, 2006b; Hadipour et al., 2007; Tvingstedt et al., 2007].

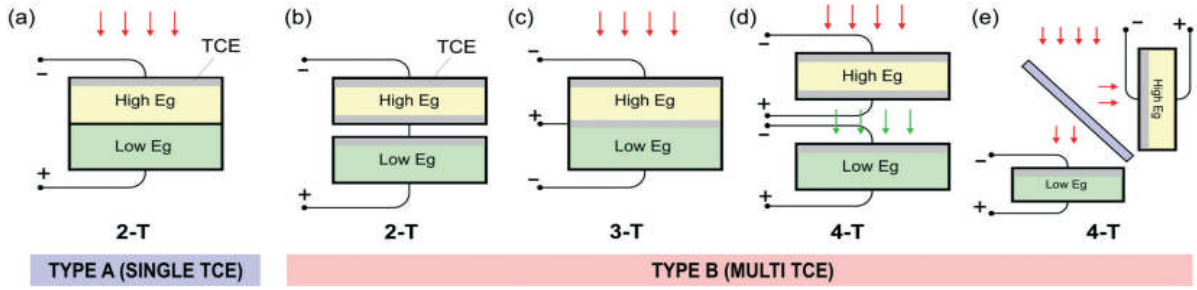

Figure I-6 Types of tandem solar cell device based on the number of transparent conductive electrodes (TCEs) and terminal connections: (a) type A: single TCE, two-terminal monolithic; and type B with multiple TCEs: (b) two-terminal mechanically stacked, (d) 4-terminal mechanically stacked, (c) 3-terminal monolithic stack and (e) 4-terminal spectrum-split [Todorov, 2016].

I-7 Solar Cells Characterization

I-7-1 Current-voltage characteristics

A simple PV solar cell device exhibits diode behavior and it is best modelled by Shockley ideal photodiode equation I-5. The current density-voltage (J-V) characteristics of a perovskite solar cells can be described by an equivalent electric circuit showed in Figure I.7 a

$$J(V) = J_{ph} - J_D = J_{ph} - J_0\left(e^{\frac{eV}{K_B.T}} - 1\right) \qquad \text{I-5}$$

J_{ph} is the photocurrent provided by the photoactive absorbing layer, the J_D diode current (also known as dark diode current) and J_0 the diode reverse saturation current. As the applied voltage (V) increases, the diode current faces the photocurrent, rises exponentially [Green et al,2014]. by considering the parasitic losses and a non-ideal diode, the equation I-5 turns into Equation I-6.

$$J(V) = J_{ph} - J_0\left(e^{\frac{e(V+JR_S)}{nK_B.T}} - 1\right) - \frac{V+JR_S}{R_{Sh}} \qquad \text{I-6}$$

Where R_S is the series resistance that takes into account all the processes opposing the generation and extraction of photocurrent and R_{sh} the shunt resistance is against all parallel circuit paths that avoid or select one or more of charge-generating layers. It is due mainly to the fabrication defects and can lower the open circuit voltage. K_B is the Boltzmann constant, and T(kelvin) is the

temperature and *n* is the diode ideality factor which is a measure of the type recombination occurring in solar cell. When *n*=1 (ideal diode) then all recombination happen outside the depletion region of the photoactive absorbing layer.

However, this circuit model (Figure I-7-a) does not entirely describe a perovskite solar cell because of the ion migration and charge transport modulations at charge extraction interfaces. – developed in chapter II and III-. Even though the accurate model is yet under discussion and intensive debate, it is of interest to mention it in this work and it rely on circuit modeling and the functionality of perovskite PV devices shown in figure I-7-f) [Moia et al, 2016].

Several important solar cell parameters can be extracted from the J-V curves, including short-circuit current density J_{SC}, open-circuit voltage V_{OC}, and fill factor FF.

Obviously, the solar cell does not generate any power at either-short circuit or open-circuit condition. The point where the solar cell generates the maximum power is defined as maximum power point (MPP), and the corresponding current density and voltage are J_{MPP} and V_{MPP}.

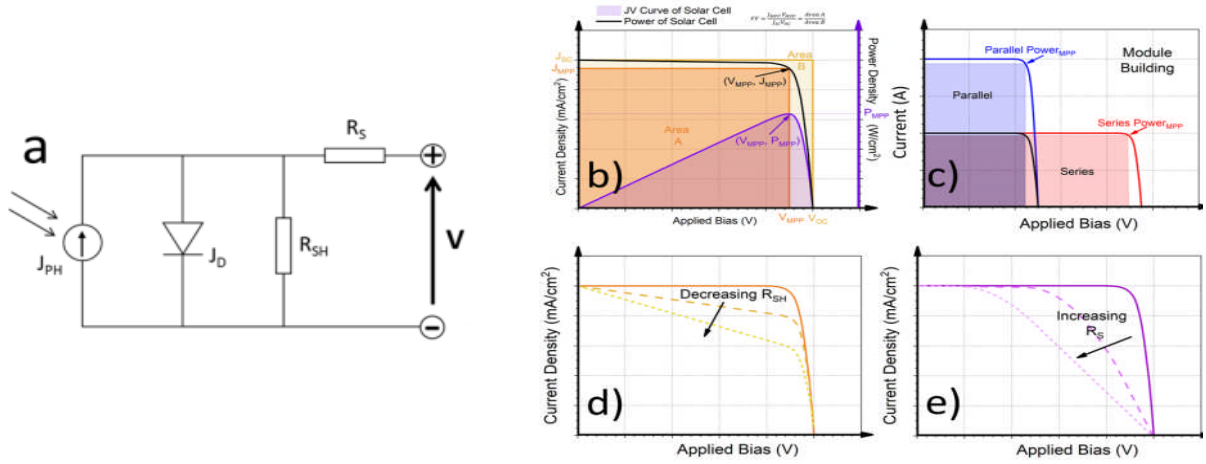

f)

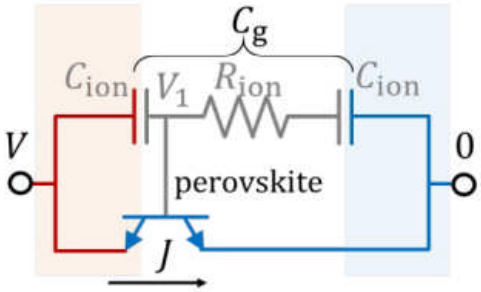

$$J = J_{s1}\left[e^{\frac{qV_1}{k_BT}} - e^{\frac{q(V_1-V)}{k_BT}}\right]$$

V_1: voltage on the base of the transistor element in the circuit model,

J_{s1}: the saturation current density of interface at dark equilibrium

- hole conduction dominant
- electron conduction dominant
- ionic conduction
- p − type material
- n − type material

Figure I-7: Solar cell operation and response. a) solar cell diode circuit generating photovoltage V with J_{PH} photocurrent density. b) JV curve and power density output of a solar cell at applied bias V. c) Current-voltage curves of modules made of equivalent solar cells connected in either series or parallel and their associated maximum power points. d) JV curves indicated with dotted curves demonstrate decreasing R_{SH}. e) JV curves indicated with dotted curves demonstrate increasing R_S[Michael,2018]. f) A perovskite solar cell forming a mixed ionic-electronic conducting diode where changes from the dark equilibrium distribution of mobile ionic charge that occurs with time constant $\left(\frac{R_{ion}C_{ion}}{2}\right)$ result in a change in electrostatic potential V_1, relative to dark equilibrium. This gates electronic charge transfer across the perovskite HTM interface in a manner analogous to the base of a bipolar transistor [Moia et al,2019].

I-7-2 J_{SC} -Short Circuit Current

When there is no applied voltage, the solar cell photocurrent density is J_{SC}. Obviously, the photocurrent is proportional to received photons, since it is often higher for absorbing layers having a narrow band gap which absorb broader range of energies photons. This photocurrent

can be affected in various ways, it can be reduced by undesirable charge recombination during charge generation, excitons diffusion when charges are bound and or free charge transport inside the active material, charge transfer and extraction between all layer charge interfaces and metal contacts. Consequently, increasing the amount of light collected by the photoactive layer results in an increase in photocurrent which leads to expand sufficiently the thickness of the absorbing layer in order to absorb a large number of photons, without losing too many photogenerated charges by recombination over the process of exciton diffusion or free charge transport. So, perovskites with its notable charge mobilities, allows perovskite active layers extracting charge across micron thick films. Furthermore, another reason to enlarge the perovskite thickness is the fact of photon recycling. Itis a process that increases the obtained J_{SC} without being affected necessarily by recombination [Pazos et al, 2016] because the long-lived free charges can recombine with other free charges and generate a photon which next re-excites the perovskite.

I-7-3 V_{OC}-Open Circuit Voltage

The produced voltage by the solar cell when no current flows is V_{OC}. This occurs when the electric field due to the applied voltage cancels the built-in potential of the device. if an electric field is necessaire to carry the current out of the photoactive layer, then this point of cancellation leads to photogenerated charges not drawn from the device. In the background of PSCs, there is delicate controversy about the required conditions to extract charges out of perovskite active layer. V_{OC} can be influenced by many factors as instance if the bandgap of the photoactive layer decreases, it decreases too. But the band structure of perovskite is not the only influencer, the band structure and work functions of the used charge-selective semiconductors and metal electrodes also effect the V_{OC}. In general, the layers must have charge affinity well-aligned with the active layer without an excess of energy that impedes the charge exit from the active layer and their thickness must balance between being thick enough to form a full layer to efficiently select charges, and not so thick as to motivate loss of charge extraction. Theoretically, perovskite solar cells have shown unusual responses for charge-selective layers with non-ideal alignment and revealed also to maintain high V_{OC} even in their absence [Ravishankar et al, 2018].

I-7-4 FF-The Fill Factor

The ratio of area A to area B is the fill factor given in percentage. As shown in figure I-7-b, the area B corresponds to a product of the J_{SC} and V_{OC}, and area A corresponds to the maximum power point (P_{MPP}) at the product of maximized voltage and current. Using the notation of the maximum power point voltage (V_{MPP}) and current (J_{MPP}), FF is defined by equation I-7.

$$FF = \frac{J_{MPP}V_{MPP}}{J_{SC}V_{OC}} = \frac{Area\ A}{Area\ B} \qquad \text{I-7}$$

The fill factor is usually below 1 and as high is its value as good the solar cell is. Good fill factors are typically approaching 80 %, these high values are completely dependent on high shunt resistance and low series resistance [Nelson, 2003; Stolterfoht et al,2017].

I-7-5 PCE Power Conversion Efficiency

The power conversion efficiency is the most important parameter of a solar cell, determined by the ratio of maximum extracted power relative to the incident power onto the solar cell. PCE is given by equation I-8 [Nelson, 2003]

$$PCE = \begin{cases} \frac{P_{out}}{P_{in}} = \frac{P_{MPP}}{P_{in}} \\ \frac{P_{MPP}}{P_{in}} = \frac{J_{MPP}V_{MPP}}{P_{in}} = \frac{J_{SC}V_{OC}\,FF}{P_{in}} \end{cases} \qquad \text{I-8}$$

As the equation I-8 shows,$J_{SC}, V_{OC}\ and\ FF$are amid other parameters that can affect the PCE.

J-V characteristics is usually enough to define the PCE of solar cells, as for the case of Si, GaAs, CIGS, CdTe devices. But this is not the situation for the perovskites, since a discrepancy is often observed between J-V sweep forward (short-circuit to open-circuit) and J-V sweep backward (open-circuit to short-circuit), known as J-V hysteresis [Becquerel, 1839]. As it is shown in Figure I-8, even if the backward sweep often gives better photovoltaic metrics compared to those measured from the forward sweep, still delivers well performance than the backward (inverted hysteresis)

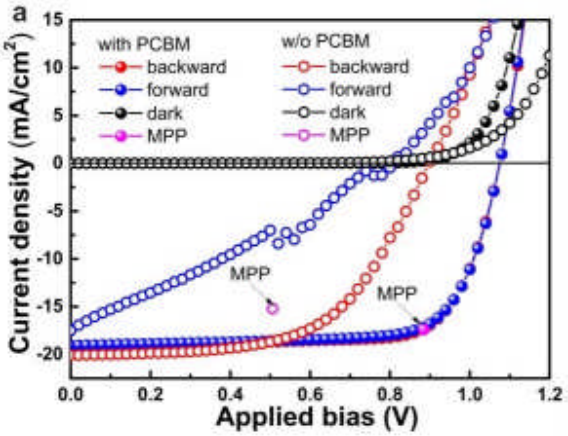

Figure I.8: J-V hysteresis and MPP measurements of perovskite solar cells. a, The J-V behavior of perovskite solar cells with and without hysteresis (the structure is glass/FTO/TiO2/with or without PCBM/Spiro-OMeTAD/Au) [2phdthese].

I-7-6 R_{SH} -Shunt Resistance

As already mentioned, the shunt resistance of solar cell is resistance opposite to current avoiding the photoactive absorbing layer or any charge transport layers involved which means he higher is its value the less leakage currents are. In thin-film solar cells field, this is obvious due to the uniformity of all layers caused during film fabrication opening pathways to currents, resulting in a loss in R_{SH}. In these cases, these layers do not complete charge transport leading to generate a maximum V_{OC}.

The shunt resistance is defined as the inverse of slope of a current-voltage sweep from the current axis, at short circuit condition (V=0). Figure I-7-d demonstrates the effect of a reduction in shunt resistance on J-V solar cell's characteristics.

I-7-7 R_S- Series Resistance

The series resistance includes all the processes against the extraction of the charge from the solar cell. This is caused by several factors that are closely related. Series resistance can be high if the charge carrier mobilities of constituent layers are low, or their thickness is considerable thick even for charges which diffuse and may be trapped and/or recombined. A high density of defects in any layers or interfaces would increase the probability of recombination too which decrease the

mobility of the photogenerated carriers. Also, if there is any energy barrier, this can cause non ideal charge affinity alignment which hold the photogenerated charges to go out the solar cell. Rs can be calculated as the slope of a current-voltage characteristic from the voltage axis, and can be approximated by taking the inverse of the slope at the open circuit voltage V_{OC} [Denhoff and Drolet, 2009]. FigureI-7-e demonstrates the effect of increased series resistance on JV solar cell's characteristics.

I-8 Recombination and Quantum Efficiency in solar cell

I-8-1 Recombination of charge carriers

Although perovskite solar cells have been shown to have a significant low rate of trap-assisted recombination [Shi et al, 2015; Sum et al, 2014] compared to inorganic solar cells, it is still important to mention charge recombination's forms involved in reducing device performances [Zhao et al, 2015]. Shockley Reed Hall (SRH) recombination is a type of recombination due to the band gap traps and it is non-radiative given the Shockley–Read–Hall equation [Selberherr, 1984]

$$R_{SRH} = \frac{C_n C_p \Sigma_T}{C_n(n+n_1)+C_p(p+p_1)}(np - n_i^2) \qquad \text{I-9}$$

With $C_n, C_p$are the capture coefficients for electrons and holes, respectively. C_n represents the probability of conduction band electron captured per unit time when the trap (band gap) is filled by a hole and able to capture the electron. In the same way, C_p is the probability for the valence band hole captured by the filled trap with electron and able to capture the hole per unit time. And the constants $n_1 = n(f_{T,n}^{-1} - 1)$ and$p_1 = p(f_{T,p}^{-1} - 1)^{-1}$.The interface traps $\Sigma_{T,p}$

For perovskite absorber layer, typically the intra band gap traps are due to iodine (I) species because of their low activation energy. Positive iodine vacancies, negative iodine interstitial ionic species and crystal lattice lead (Pb) vacancies in perovskite have been also accounting as trap sites [Shi et al, 2015; Sherkar et al,2017] nevertheless, an interesting advantage is identified for metal-halide perovskites where the accumulated negative iodide vacancies at crystal grain boundaries and interfaces are neutral when filled with photogenerated charges. Which means that the filled traps interfere with highly mobile holes. And since perovskite grain boundaries are rich sites with defect densities, they act as charge trap regions so it is possible to mainly reduce the influence of traps if

compact perovskites with large crystal grains and a low density of grain boundaries can be fabricated.

Among the needed properties of perovskites, the most one is its ultra-long carrier diffusion length 'more than 1 µm in thin films and more than 175 µm in single crystals' [Dong et al,2015]
These values are quite longer than the absorption depth, thereby guarantee an efficient carrier collection as mentioned before. Charge carriers transport in perovskites is strongly depend on electron and hole effective masses where the low electron mass of 0.2 m_e of perovskite is very close to those for semiconductor GaAs, which benefits principally from the strong spin-orbit coupling effect in the electronic band structure because of the presence of heavy Pb atoms [Brenner et al,2016]. But, even in polycrystalline thin film perovskite, the free electrons and holes have a modest mobility in the range of 10-30 cm^2/V s.As a result, even that the modest mobility of perovskites cannot compete that of GaAs, its long carrier lifetimes (100 ns to >1 µs) leading to long diffusion lengths, which guarantees efficient collection. carriers for layers of µm-thickness.

Thus, the lifetime of charge carrier is as important as the diffusion length. It determines the time window, able to extract charges to contacts before they recombine represented by the schematic diagram on Figure I-9.

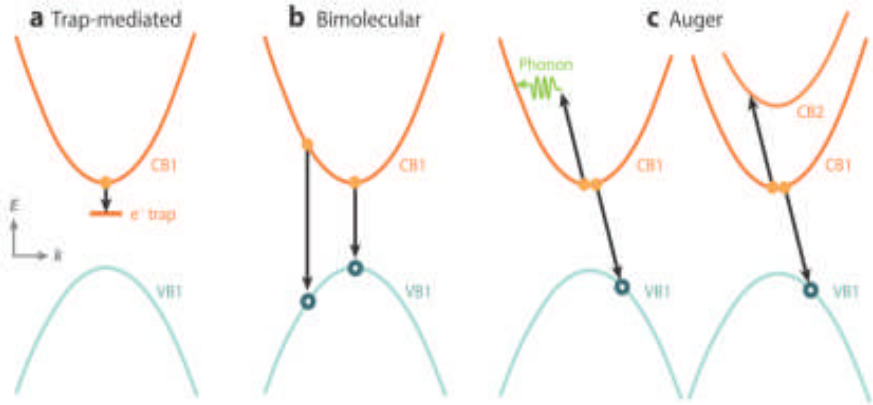

Figure I-9: The three different recombination mechanisms in perovskite [Herz,2016].

$n(t)$ is the decay of a free-charge-carrier density and is expressed by the rate equation I- 10

$$\frac{dn}{dt} = -k_3 n^3 - k_2 n^2 - k_1^{total} n \qquad \text{I-10}$$

n is the photogenerated carrier density and t is time. The three terms were ascribed to three charge carrier annihilation processes: (1) first-order trap-assisted recombination; (2) second-order radiative band-to-band recombination; and (3) third-order Auger recombination. These three different recombination mechanisms contribute to the effective total recombination rate R (n, t). For the trap-related recombination, and are in about $(10s\ to\ 100s) \times 10^{-9}$

Herek_2 is rate of bimolecular recombination (band-to-band recombination), k_3 is Auger recombination rate which is strongly dependent on the charge-carrier density, k_1 is the rate constant associated with monomolecular recombination (trap-related recombination) and as it is reasonably assumed that the density of photogenerated electrons and holes (n=p) are equal then the monomolecular recombination rate (k_1^{total}=k_2p_0+k_1^{nr}). Consequently, it comprises two contributions: the first term (k_1^{r}=k_2p_0) is known by the recombination of photogenerated electrons (n) with a constant dopant hole density (p_0) which should be radiative as it is fundamentally the same mechanism as the bimolecular recombination of photogenerated electrons (n) with photogenerated holes (p=n). The presence of doping hence introduces a radiative "pseudo-monomolecular" decay component at low charge-carrier densities. The second term (k_1^{nr}) is due to SRH recombination [Harrison, 1989] that may act as recombination centers if both types of carriers are trapped. In this case, charge-recombination tends to be nonradiative. Shockley–Read–Hall recombination is dominant process at low charge density for halide perovskites with lead that exhibit nonradiative monomolecular rates [Eisberg and Resnick, 1974; Blakemore, 2008; Wang et al,2014]. In contrast, radiative monomolecular decay channels is potentially the dominant type recombination in tin (Sn) based perovskites because of their unintentionally high levels of p-doping [Milot, 2016].

As practical example, and since lead and tin-based perovskites are mainly direct band gap semiconductors, while, the bimolecular (band-to-band) recombination between electrons and holes should be radiative. the Auger recombination, strongly depends on electronic band structure involving electron–hole recombination through energy transfer to a third charge-carrier, it is

nonradiative mechanism where the spin-orbit coupling induces additional bands, the resulted high Auger recombination rate constant of (0.2-1.6) $\times 10^{-28}$is significantly large making it of important concern for laser as it competes with bimolecular recombination at the high charge-carrier densities required for lasing. But it could not hinder the applications of perovskite in photovoltaics [Michael and Herz, 2016].

I-8-2 Quantum Efficiencies

I-8-2-1 ERE-External radiative efficiency

the percentage of total recombination that results in the emission of light is known as external radiative efficiency (ERE) it has been identified as an efficient indicator of solar cell. The trap-assisted nonradiative recombination pathways must be minimized while radiative recombination can lead to photon recycling. So, accordingly, to that, it appears counterintuitive, a bright luminescing solar cell is always a good device. a typically Perovskites EREs is up to 4%, exceeding common EREs of c-Si solar cells [Snaith, 2018].

I-8-2-2 IQE-Internal quantum efficiency

while the more traditional indicator of solar cells performance is the internal quantum efficiency (IQE). Which is the percentage of the number of photons absorbed relative to the number of photogenerated charges extracted. It depicts all of the processes that suppress generation, transport and transfer of charge from the photoactive absorbent layer.

I-8-2-3 EQE-External quantum efficiency

However, the relevant performance metric to compare solar cells is the external quantum efficiency (EQE). It is the number of collected charges by the electrodes relative to the number of incident photons at every specific wavelength. It is given by equation I-11 as follows [Nelson, 2003]

$$EQE(\lambda) = \frac{Jhc}{p(\lambda)\lambda.q} \qquad \text{I-11}$$

where $P(\lambda)$ is the incident power of photons as a function of wavelength λ, $\frac{hc}{\lambda.}$is the energy of one photon, J is the photocurrent and q the electronic charge.

This parameter also considers the photons that do not attain the active layer or are not absorbed. Such loss of incident photons is typically due to parasitic absorption and reflection taking place at the front facing encapsulation surface and electrodes. Most thin-film photovoltaic devices use transparent conductive oxides which have a photon transmission less 90 %. Other back-contact solar cell architectures decrease this loss by putting all charge-selective electrodes at the back of the solar cell at the rear of the photoactive absorbing layer [Jumabekov et al, 2016].

References of chapter I

[Stocker et al, 2013] T. F. Stocker, Q. Dahe, G.-K. Plattner, L. V. Alexander, S. K. Allen, N. L. Bindoff, F.-M. Bréon, J. A. Church, U. Cubash, S. Emori, P. Forster, P. Friedlingstein, L. D. Talley, D. G. Vaughan, S.-P. Xie, 'Climate Change 2013- the Physical science Basis', part of the working group I contribution to the fifth assessment report of the intergovernmental panel on climate change, 2013

[Cook et al, 2016] J. Cook, N. Oreskes, P. T. Doran, W. R. L. Anderegg, B. Verheggen, E. W. Maibach, J. S. Carlton, S. Lewandowsky, A. G. Skuce, S. A. Green, D. Nuccitelli, P. Jacobs, M. Richardson, B. Winkler, R. Painting, K. Rice, 'Consensus on consensus: a synthesis of consensus estimates on human-caused global warming', Environ. Res. Lett.,11, 2016

[KWES, 2016] Key World Energy Statistics Agency for Natural Resources and Energy, IEA Int. Energy Agency, 2016

[R. and M. Perez, 2015] R. Perez, M. Perez, 'update 2015- A fundamental look at supply side energy reserves for the planet', Int. Energy Agency SHC Program. Sol. Updat62, 4. 2015

[Brulle, 2018] R. J. Brulle,' the climate lobby: a sectoral analysis of lobbying spending on climate change in the USA', 2000 to 2016, Clim. Change, 149, 289, DOI 10.1007/s10584-018-2241-z, 2018.

[Karneyeva and Wüstenhagen, 2017] Y. Karneyeva, R. Wüstenhagen, Energy Policy, vol. 106, issue C, pages 445-456, 2017

[Zweibel, 2010] K. Zweibel, Should solar photovoltaics be deployed sooner because of long operating life at low, predictable cost? Energy Policy, vol 38, issue 11, Pages 7519-7530, 2010

[Hodes, 2013] G. Hodes, Science, Applied physics. Perovskite-based solar cells, 342, 317, 2013

[Green et al, 2014] M. A. Green, A. Ho-Baillie, H. J. Snaith, The emergence of perovskite solar cells,Nat. Photonics, 8, 506, 2014.

[Michael and Chairman, 2017] Michael Liebreich, Chairman of the Advisory Board Bloomberg New Energy Finance, 6, 2017

[Docampo et al, 2013] P. Docampo, J. M. Ball, M. Darwich, G. E. Eperon, H. J. Snaith, Efficient organometal trihalide perovskite planar-heterojunction solar cells on flexible polymer substrates, Nat. Commun 4, pages 2761, 2013

[Pickard, 2017] W. F. Pickard, A simple lower bound on the EROI of photovoltaic electricity generation, Energy Policy,vol 107, pages 488, 2017

[IRENA, 2018] Renewable Energy Auctions, International Renewable Energy Association 2018.

[Rao et al, 2016] S. Rao, A. Morankar, H. Verma, P. Goswami, J. Appl, 'emerging photovoltaics: organic, copper zinc-tin-sulphide, and perovkite-baased solar cells', Chem.,1, 2016

[Kojima et al, 2009] A. Kojima, K. Teshima, Y. Shirai, T. Miyasaka, Organometal Halide Perovskites as Visible-Light Sensitizers for Photovoltaic Cells, J. AM. CHEM. SOC., 131, 6050–6051, 2009

[Armaroli et al, 2007] N. Armaroli, V. Balzani, Angew, The future of energy supply: Challenges and opportunities, Chem. Int. Ed., 46, 52, 2007.

[R. F. Service, 2005] R. F. Service, Science (Washington, D. C.), 309, 548, 2005.

[Polman et al, 2016] A. Polman, M. Knight, E. C. Garnett, B. Ehrler, W. C. Sinke, Photovoltaic materials: Present efficiencies and future challenges, 352, aad4424, Science 2016.

[Pivrikas et al, 2007] A. Pivrikas, N. Sariciftci, G. Juška, R. Österbacka, Progress in Photovoltaics: Research and Applications, 15, 677, 2007

[Docampo et al, 2014] P. Docampo, S. Guldin, T. Leijtens, N. K. Noel, U. Steiner, H. J. Snaith, Lessons Learned: From Dye-Sensitized Solar Cells to All-Solid-State Hybrid Devices Adv. Mater. 2014.

[Yuan et al, 2016] M. Yuan, M. Liu, E. H. Sargent, Detecting trap states in planar PbS colloidal quantum dot solar cells, *1*, 16016, *Nature Energy* 2016.

[Tai et al, 2011] C.-H. Tai, C.-H. Lin, C.-M. Wang and C.-C. Lin, Int. J.Photoenergy, Three-Terminal Amorphous Silicon Solar Cells, 813093, 2011.

[Wang, et al, 2014] L. Wang, et al., Proceedings of the 29th EUPVSEC, pp.2043–2045, 2014.

[Sista et al, 2009] S. Sista, Z. Hong, M. H. Park, Z. Xu and Y. Yang, Intermediate Layers in Tandem Organic Solar Cells, Adv. Mater.,22, E77–E80,2009.

[McMeekin et al, 2016] D. P. McMeekin, et al., Amixed -cation leadmixed-halide perovskite absorber for tandem solar cells, Science, 351, 151–155,2016.

[Uzu et al, 2015] H. Uzu, M. Ichikawa, M. Hino, K. Nakano, T. Meguro, J. L.Hernandez, H.-S.Kim,N.-G. Park and K. Yamamoto, High efficiency solar cells combining aperovskite and a silicon heterojunction solar cells via an optical splitting system, Appl.Phys.Lett, , 106, 013506,2015.

[A. De Vos and J. Phys, 1980] A. De Vos, J. Phys. D: Appl. Phys,Detailed balance limit of the efficiency of tandem solar cells, 13, 839,1980.

[U. Rau and J. H. Werner,2004] U. Rau and J. H. Werner, Appl. Phys. Lett, Radiative efficiency limits of solar cells with lateral band-gop fluctuations, 84, 3735,2004.

[A. E. Becquerel,1839] A. E. Becquerel,Acarban-metal junction prepared by cvd technique as x-ray photo voltaic cell ,*Comptes Rendus L'Academie Des Sci*, *9*, 145,1839.
[A. Einstein,1905] A. Einstein, *Ann. Phys*,Über einen die Erzeugung und Verwandlung des Lichtes betreffenden heuristischen Gesichtspunkt, , *17*, 132,1905.
[Charles Kittel,2004] Charles Kittel, *Introduction to Solid State Physics, 8th Edition*, Wiley, 2004.

[R. M. Eisberg and R. Resnick,1974] R. M. Eisberg and R. Resnick, *Quantum Physics of Atoms, Molecules, Solids, Nuclei, and Particles*,New York: Wiley, 1974.

[J. Nelson,2003] J. Nelson, *The Physics of Solar Cells*, Imperial College Press, 2003.

[Pazos et al,2016] L. M. Pazos-Outón, M. Szumilo, R. Lamboll, J. M. Richter, M. Crespo-Quesada, M. Abdi-Jalebi, H.J. Beeson, M. Vrućinić, M. Alsari, H. J. Snaith, B. Ehrler, R. H. Friend, F. Deschler, Photon recycling in lead iodide perovskite solar cells,*Science,351, 6280,* 1430-1433,2016.
[Ravishankar et al,2018] S. Ravishankar, S. Gharibzadeh, C. Roldán-Carmona, G. Grancini, Y. Lee, M. Ralaiarisoa, A. M.Asiri, N. Koch, J. Bisquert, M. K. Nazeeruddin, Influence of Charge

Transport Layers on Open-Circuit Voltage and Hysteresis in Perovskite Solar Cells, , *2*, 788, *Joule* 2018.

[H. J. Snaith, Present,2018] H. J. Snaith,Present status and future prospects of perovskite photovoltaics, *Nat. Mate, 17,* 372,2018.

[M. W. Denhoff, and Drolet,2009] M. W. Denhoff, N. Drolet, *Sol. Energy Mater. Sol. Cells*, *93*, 1499, 2009.

[Shi et al,2015] D. Shi, V. Adinolfi, R. Comin, M. Yuan, E. Alarousu, A. Buin, Y. Chen, S. Hoogland, A. Rothenberger, K. Katsiev, Y. Losovyj, X. Zhang, P. A. Dowben, O. F. Mohammed, E. H. Sargent, O. M. Bakr, Solar cells. Low trap-state density and long carrier diffusion in organolead trihalide perovskite single crystals, *347, 6221*, 519-522, *Science* 2015.

[Sherkar et al,2017] T. S. Sherkar, C. Momblona, L. Gil-Escrig, J. Ávila, M. Sessolo, H. J. Bolink, L. J. A. Koster, Recombination in Perovskite Solar Cells: Significance of Grain Boundaries, Interface Traps, and Defect Ions, *ACS Energy Lett.*, *2*, 1214,2017.

[Sum et al,2014] T. C. Sum, N. Mathews, *Energy Environ. Sci.* 2518,2014.

[Zhao et al,2015] D. Zhao, M. Sexton, H. Y. Park, G. Baure, J. C. Nino, F. So, *Adv. Energy Mater*, *5*, 6, 1401855,2015

[W. A. Harrison,1989] W. A. Harrison, *Electronic Structure and the Properties of Solids: The Physics of the ChemicalBond*, Dover Publications, 1989.

[J. S. Blakemore,2008] J. S. Blakemore, *Solid State Physics, 2nd Edition*, Cambridge University Press, 2008.

[Wang et al,2014] B. Wang, X. Xiao, T. Chen, Perovskite photovoltaics: a high-efficiency newcomer to the solar cell family,*6*, 12287-12297 *Nanoscale* 2014.

[Stolterfoht et al,2017] M. Stolterfoht, C. M. Wolff, Y. Amir, A. Paulke, L. Perdigón-Toro, P. Caprioglio, D. Neher, *Energy Environ. Sci.*, *10*, 1530,2017.

[Denhoff and Drolet,2009] M. W. Denhoff, N. Drolet, *Sol. Energy Mater. Sol, 93,* 1499, *Cells* 2009.

[Jumabekov et al,2016] A. Jumabekov, E. Della Gaspera, Z. Xu, A. Chesman, J. van Embden, S. Bonke, Q. Bao, D. Vak, U.Bach, *J. Mater* Back-contacted hybrid organic–inorganic perovskite solar cells,. *Chem*, *4* 3125, *C* 2016.

[ASTM, 2012] "ASTM Standard G173-03- Standard Tables for Reference Solar Spectral Irradiances: Direct Normal and Hemispherical on 37: httpsttps://compass. astm.org/EDIT/html_ annot.cgi? G173+03, 2012

[Selberherr, 1984] Selberherr, S,'Analysis and Simulation of Semiconductor Devices; Springer-Verlag: Vienna, 1984

[Michael and Herz, 2016] Michael B. Johnston and Laura M. Herz','Hybrid Perovskites for Photovoltaics: Charge-Carrier Recombination, Diffusion, and Radiative Efficiencies', ACC Chem. Res 49, 1, 146–154, 2016

[Yi Hou,2017] Yi Hou, Rational Interfaces Design of Efficient Organic–inorganic Hybrid Perovskite Solar Cells, der Friedrich-Alexander-Universität Erlangen-Nürnberg,2017

[Green et al,2014] M. A. Green, A. Ho-Baillie, H. J. Snaith, *Nat. Photonics*, *8*, 506, 2014

[Kojima et al,2009] A. Kojima, K. Teshima, Y. Shirai, T. Miyasaka, *J. AM. CHEM. SOC*., *131*, 6050–6051,2009

[Jaya et al,2021] Jaya Madan, Karanveer Singh, & Rahul Pandey, Comprehensive device simulation of23.36%efficient two-terminal perovskite-PbS CQD tandem solar cell for low-cost applications,2021

[Hossain, et al,2021] Hossain, M. I. *et al*. Perovskite/perovskite planar tandem solar cells: A comprehensive guideline for reaching energy conversion efficiency beyond 30%. *Nano Energy* 79, 105400. https://doi.org/10.1016/j.nanoen.2020.105400 (2021).

[Michael,2018] Michael Wong-Stringer, Optimisation of Fabrication Processes for Stable and Scalable Perovskite Solar Cells,2018

[Brenner et al,2016] T. M. Brenner, D. A. Egger, L. Kronik, G. Hodes, D. Cahen, *Nature Reviews Materials*, *1*, 15007, 2016

[Dong et al,2015] Q. Dong, Y. Fang, Y. Shao, P. Mulligan, J. Qiu, L. Cao, J. Huang, *Science*, aaa5760,2015

[Herz,2016] L. M. Herz, *Annu. Rev. Phys. Chem.*, *67*, 65,2016

CHAPTER II

Tendam Perovskite soler cells

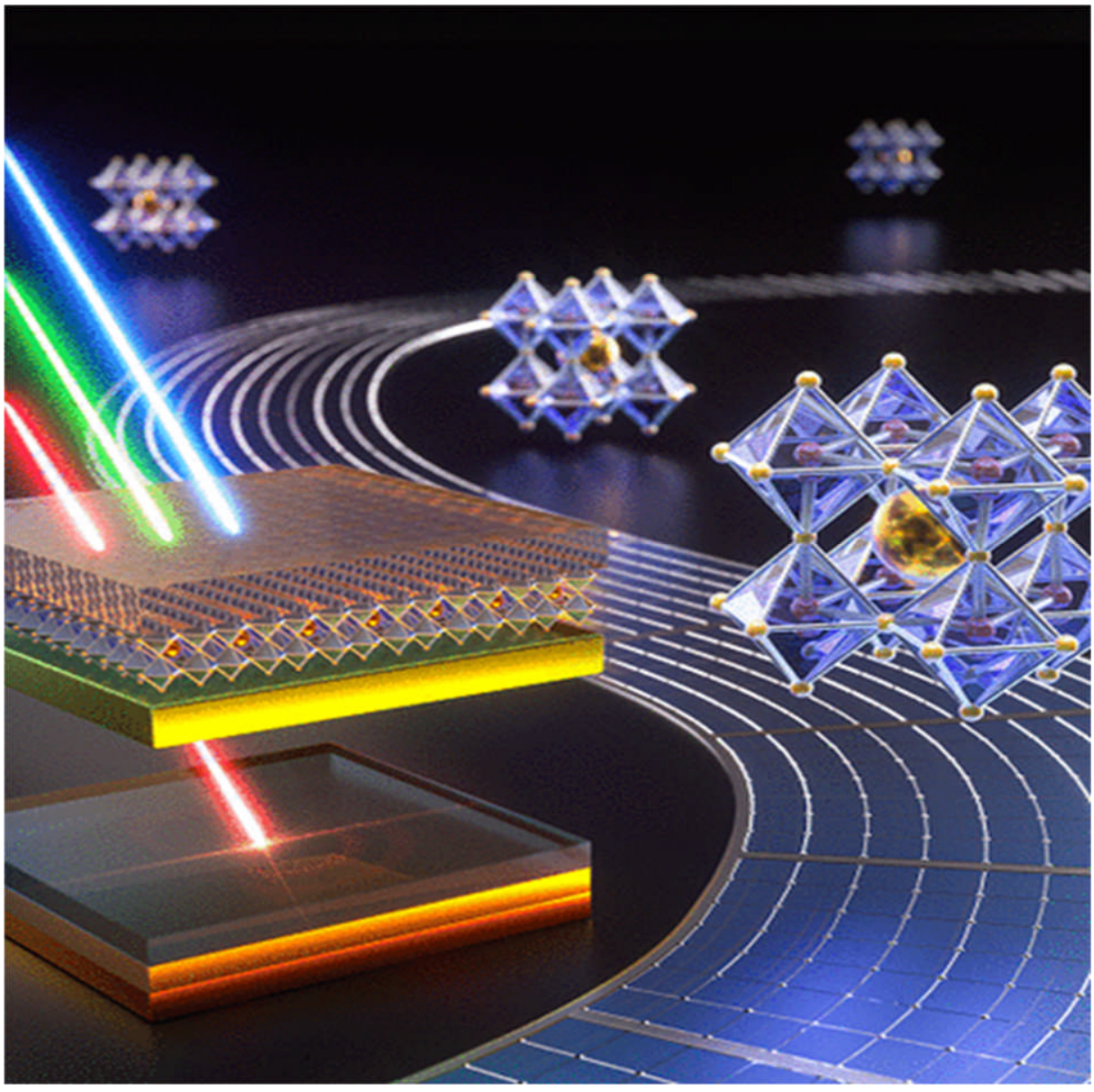

Chapter II- Tandem Perovskite-Solar Cells

II-1 Introduction

the conventional technology of solar cells was based on crystalline silicon occupying almost 90% of the photovoltaic (PV) market, and their production costs have reduced dramatically in the past decade. Si based solar cells have achieved an average panel power conversion efficiency [PCE] of around 20% for modules in mass production. And a record cell efficiency of 26.7% has been achieved, which is very close to the S-Q limit of single-junction solar cells [Lee et al., 2012; Zhou et al., 2014; Dong et al., 2015]. In fact, to obtain higher efficiency, an alternative material is thus needed which also offers PV market diversity.

Recently, perovskite solar cells (PSCs) with low production expenses gain a significant interest technologically [Green et al., 2014]. The PSCs PCE has progressed from the initial 3.8% to a now certified 25.5%, within ten years only [Laboratory, 2019].

Since the solar irradiation spectrum has a wide energy distribution, while the semiconductor material can only absorb a part of the photons with energy above the bandgap, so, in the case of a single junction, the PCE cannot surpass the S-Q limit because of the loss of energy absorption below the bandgap and hot charge carriers loss by thermal relaxation [Malinkiewicz et al., 2013]. Afterwards, forming tandem solar cells (TSC) by integrating high-efficiency wide-bandgap (top cell) with low-bandgap (bottom cell) has been considered as a good plan to enhance their PCE beyond the S-Q limit [Rong et al., 2018].

At this stage, various researchers were investigating on perovskite solar cells and its tandem configurations with plenty of various approaches in order to reach higher performances.

The concentrated exploration of thin-film solar cells aimed for modeling thickness and material type layered structures and to study the consequence of device design and materials parameters on their photovoltaic performance.

The function of preferred hole transport material (HTM) on the solar cells results with copper conductors (CuI) and thiophene polymer (PTAA) group touched a relatively higher PCE due to their wide bandgap, high conductivity, and superior chemical interaction with the perovskite absorber layer was reported for PSCs [Kai Tan et al., 2016]. After, a structured PSC without HTM realized above than 15% PCE [Lin et al., 2014], then, electrically organic solar cells (OSCs) had been simulated at different charge carrier mobilities where they realized maximum OSC's

efficiency at maximum short-circuit current at electron and hole mobility of $0.5^{10} \times 10^{-6}$ m^2/v s [Narender et al. 15].The organic-inorganic PSC was designed and considered the effect of both active layer thickness and defect density, on the solar cell production where it was obtained 31.77 % PCE and Jsc of ~ 25.6 mA /cm^2 [Ucha et al., 16]. Afterwards, lead-based organic-inorganic PSC was studied with the CuI HTM where it was analyzed that CuI HTM can be used with $CH_3NH_3PbI_3$ and can replace spiro-MeOTAD, which is an expensive HTM for lead-based organic-inorganic PSCs [Zulqarnain Haider et al., 2018]. Lead-based PSCs were also studied and performance optimized by varying the active material thickness and its doping levels where the achieved energy conversion was up to 30.15 % [Abdel Hadi et al. 18]. Also, the effect of annealing nanostructured CuO/TiO_2 heterojunction SCs shown that with an annealed sample in the range of 300 K to 423.15 K, the modification in solar cell efficiency is important [Enebe et al., 2019].

The instability of PSCs is mainly related to ecological effects. However, PSCs are still far from industrial uses as a clean and renewable source of energy due to their main reliability on lead material to absorb sunlight, as it is a detrimental material for the environment. Lead pollution can cause long-term ecological damage due to high degradation time and high toxicity.

In this part of study, the perovskite material will be first studied, then the tandem configurations. Then the layers constituting the TSCs will discuss in term of materials and their properties with the focus on the top-cell development to improve their performance. Firstly, an introduction of different types of transparent electrodes with high transmittance and low sheet-resistance used in tandem solar cells. Then a discussion of the wide-bandgap perovskite absorber for top-cells development is followed, especially the approaches to gain perovskite layers with convenient efficiency and stability. In addition, as a special functional layer in tandem solar cells, the recombination layers play an important role in device performance, wherein different configurations are summarized. The transport equations adopting drift diffusion model are also discussed briefly as well as recombination processes

II-2 Perovskite

First reported by Weber the metal-halide perovskites have formula structure of ABX_3 as shown in Figure II-1. The A^+ is monovalent cation typically: methylammonium (MA^+: CH3NH3+), formamidinium (FA^+: $HC(NH2)_2^+$), Cs^+, Rubidium (Rb^+), or their mixtures; B^{2+} is a divalent cation generally bivalent metal such as Pb^{2+}, Sn^{2+}, Ge^{2+}, or their mixtures too while $X^-$is monovalent anion such as halide like I^-, Br^-, Cl^-, or their combinations [eijtens et al,2018; Green et al,2014; Stoumpos et al,2015]Where the cations A fill the 12-fold coordinated holes within the cavity and the metallic cations B and the anions X built BX_6^{4-} octahedra [Hui Li and Wei Zhang,2020]. The structure thermodynamically stable for different perovskites relays on their composition. As example the $MAPbI_3$ is stabilized under tetragonal structure while the tri-cation perovskite FA/MA/Cs is habitually stabilized under cubic structure at ambient temperature [Jena et al,2019].. As light absorbers metal halide perovskites are good for both top and bottom cells in TSCs due to their tunable band gaps from 1.17eV to 3.10 eV by compositional engineering as illustrated in Figure II-2 [Noh et al,2013; Luo et al,2020].. In TSCs, when considering the long-term energy yields to have highly efficient PSCs, the PSCs are used as upper cells since their band gaps (1.60 eV) is close to the ideal band gap regions (1.67 eV−1.75 eV for top cells) [Shen et al,2020; Anaya et al,2017 ; Kojima et al,2009]. Lately, it is also possible to employ low band gap PSCs as bottom cells in all perovskite TSCs (all PTSCs) due to the improvement of stability and PCE of low band gap perovskites [Kulbak et al,2015, Park,2015].

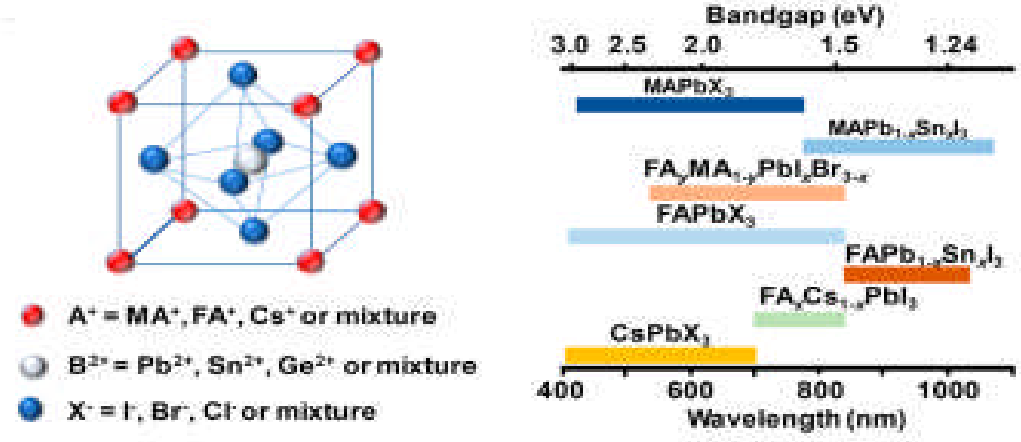

Figure II-1: left- Crystal structure of perovskite materials. right- Band gap values for perovskite materials [Anaya et al, 2017].

Due to their optimal band gaps, Si with band gap of 1.12 eV [Liang et al,2019] and CIGS (in highly efficient CIGS solar cells) with 1.08 eV to 1.15 eV [Ramanujam and Singh,2017; Chantana et al,2020] represent the advantageous absorber materials for bottom cells [Eperon et al,2017]. Also, the combination of PSCs with the third generation PVs (dye-sensitized solar cells (DSSCs), organic PVs (OPVs), quantum dot solar cells (QDSCs)) draws some attention owing to their enhancement in PCEs, processing compatibility with PSCs, and low-cost. Besides to the tunable band gaps, the high structure tolerance is a major additional advantage of perovskites for TSCs where it can reduce the firm requirement of lattice match between sub-cells. The tolerance t is defined by Goldschmidt factor [Travis et al,2016] which is a function of the radius of the constituent atoms r_A, r_B and r_X and given as follows:

$$t = \frac{r_A + r_B}{\sqrt{2}(r_A + r_X)} \qquad \text{II-1}$$

The value of Goldschmidt factor (t) must be in the range of 0.81− 1.0 in order to maintain a three-dimensional metal halide perovskite structure, while fort higher than 1.00, the formed structures are hexagonal. And for t less than 0.81, the formed structures are non-perovskite [Manser et al,2016]. The ratio of the distance A−X to the distance B−X in an idealized solid sphere model is 0.81−1.11. The octahedral factor μ (the ratio r_B/r_X) is 0.44−0.90 [Green et al,2014].

The lattice parameters of perovskites are tuned easily in a wide region only via halide substitution (as instance: the lattice constants for $MAPbI_3$ is 6.39 Å, $MAPbCl_3$ is 5.78 Å and $MAPbBr_3$ is 6.04 Å) [Yin et al, 2015].

Moreover, the electrical tolerance also makes PSCs suitable candidates in TSCs that can effectively diminish the deep defect centers (the non-radiative Shockley−Read−Hall) originating from defects of surface and bulk induced by the lattice mismatch between sub-cells [Hui Li and Wei Zhang,2020].

Perovskites exhibit good defect tolerance principally since dominant intrinsic defects create shallow levels in the valence band (VB) or conduction band (CB). This is partly the reason for the high carrier mobility of 1.60−1.70 cm^2/ Vs, which is higher than 1 µm electron-hole diffusion lengths, and higher than 1 µs minority carrier lifetime [Tong, et al ,2019] that are especially 2T TSCs important parameters due to the increase in film thickness. The VB or CB defect states are due to the high formation energy of deep levels which in their turn are caused by the strong Pb

lone-pair s orbital and I p orbital antibonding coupling and the high $MAPbI_3$ ionicity as illustrated on Figure II-2 [Park,2015; Yin et al ,2014; Snaith ,2013]

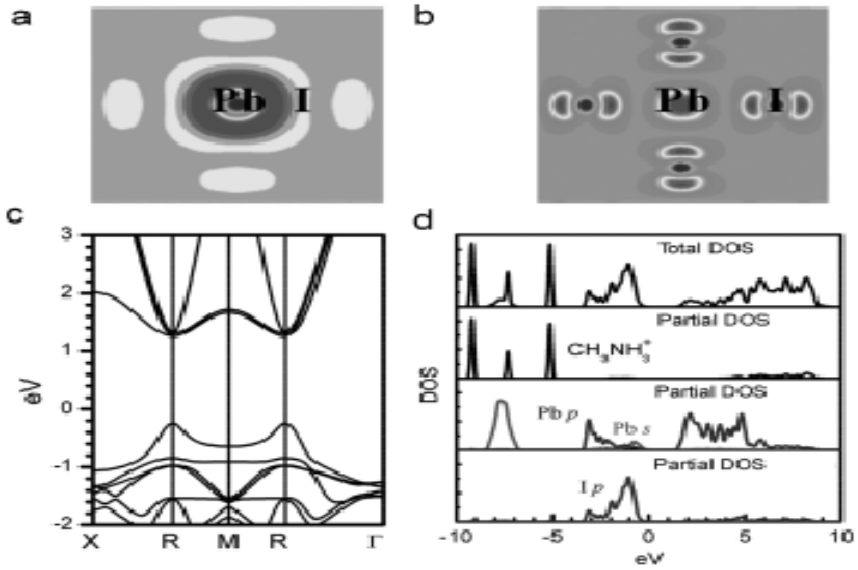

Figure II-2: (a, b) CB minimum and VB maximum partial charge density of $MAPbI_3$, respectively. (c) Band structure of $MAPbI_3$. (d) Total density of states (DOS) and MA^+, Pb, I partial DOS. The zero in DOS is referred to VBM. The Pb partial DOS enlarged by five times for clear indication of s orbital contribution [Yin et al ,2014].

Furthermore, because of the high absorption coefficient which is about 1.5×10^4 cm−1 at 550 nm of perovskites, the perovskites thickness is only around to∼500 nm. This caused a great reduce to the material cost [Park,2015; Green et al ,2014]. As additional advantage of PSCs for TSCs, their compatibility with solution and vacuum fabrication methods where the PSCs with high PCEs are easily fabricated via low temperature solution technics instead of needing high temperature leading to other layers' stability as shown in Figure II-3. This is a key issue to obtain high PCEs especially in 2T TSCs. High PCEs of PSCs with different device structures make it feasible to obtain TSCs by combining with other types of solar cells having different device structures.

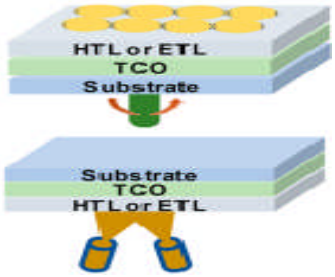

Figure II-3: a spin-coating solution method (top) and a vacuum thermal evaporation method (bottom) for perovskite films. Schematic representation of PSCs structures [Hui Li and Wei Zhang,2020]

II-3 The tandem configurations

The tandem arrangements permit the absorption of high-energy photons in the top-cell, that makes high voltage to decrease the thermalization loss, and also allows the lower-cell to absorb transmitted low energy photons, leading to a wider harvest of the solar spectrum. It has been reported that theoretical maximum efficiency of Si based tandem cells could be increased from 29 to 42.5% [Bremner et al., 2008].

As already mentioned, the halide perovskite and Si have different bandgaps, and the bandgap of perovskite materials could achieve a bigger bandgap over composition engineering [Jesper Jacobsson et al., 2016]. Therefore, the PSCs can be used as top cells and the Si cells as bottom cells, that are added to tandem perovskite/Silicon solar cells. First established 2T monolithic perovskite/Si SCs of 1 cm cube, achieved a 1.65 V of V_{OC} and 13.7 % PCE [Mailoa et al.2015].

II-3.1 Top electrodes

Just one front transparent electrode is necessary in a 2T perovskite/Si TSCs, according to the requirements given as follows:

1st, the materials deposition process has negligible damage to the subcells. No reaction with the underlayer is allowed as long as the energetic atom is producing during deposition. Otherwise, an additional electrode buffer layer is needed to protect the carrier transport layer despite the fact that it can produce current loss.

2nd, in order to produce photocurrent more effectively by the bottom cells, the electrodes must have high-transmittance in the infrared and visible spectrum region. Plus, the parasitic absorption and reflection loss in this contact layer need to be taken into account to rise the photocurrent. More importantly, besides optical transmittance and electron collection, other parameters such as band-gap alignment, scale-production and costs also need to be considered. Based on these requirements, the materials under choice are divided into five categories.

Considering the low sheet resistance, the high transmittance in the near infrared and visible spectrum region, transparent metal oxides (TMOs) are promising electrode materials which could be deposited by sputtering and to overcome the damage during the deposition process MoO_x buffer layer is inducing. Precious metals such as Ag and Au are opaque and thick so they are not a

qualified because they prevent the sunlight to penetrate and induce the production of the photocurrent. As a result, ultrathin metal electrode with a thickness less than 10 nm manufactured by evaporated and employed as the top electrode. Silver nanowires, also are taken as electrodes with TMOs or transport layer to improve charge carrier collection ability.

Graphene with excellent physical (carrier mobility equal to15.000 $cm^2V^{-1}s^{-1}$of) and mechanical properties is a good material for electrodes, especially for fabrication of flexible devices grown by chemical vapor deposition.

II-3.1-1 TMOs

TMOs are materials used for top electrodes due to their small sheet resistance, high conductivity, high transmittance in near infrared and visible spectrum region. In addition, TMOs including indium tin oxide (ITO), indium zinc oxide (IZO) and doping with transition metals could upgrade the top electrodes properties.

II-3.1-2 ITO

ITO is one of the TMOs widely explored materials for top electrodes. In 2017, a 150 nm ITO was taken as front contact to minimize the parasitic absorption [Bush et al., 2017] as illustrated in Figure II-4. And by implementing antireflection coating MgF_2 on the top in order to reduce the reflection loss the top electrodes of ITO, producing was revealed to produce an efficiency of 15.7% in single junction cell with a record near infrared transmittance of about 92% so the efficiency of 25.7% in the a 4-Terminal tandem cells [Zhang et al., 2018].

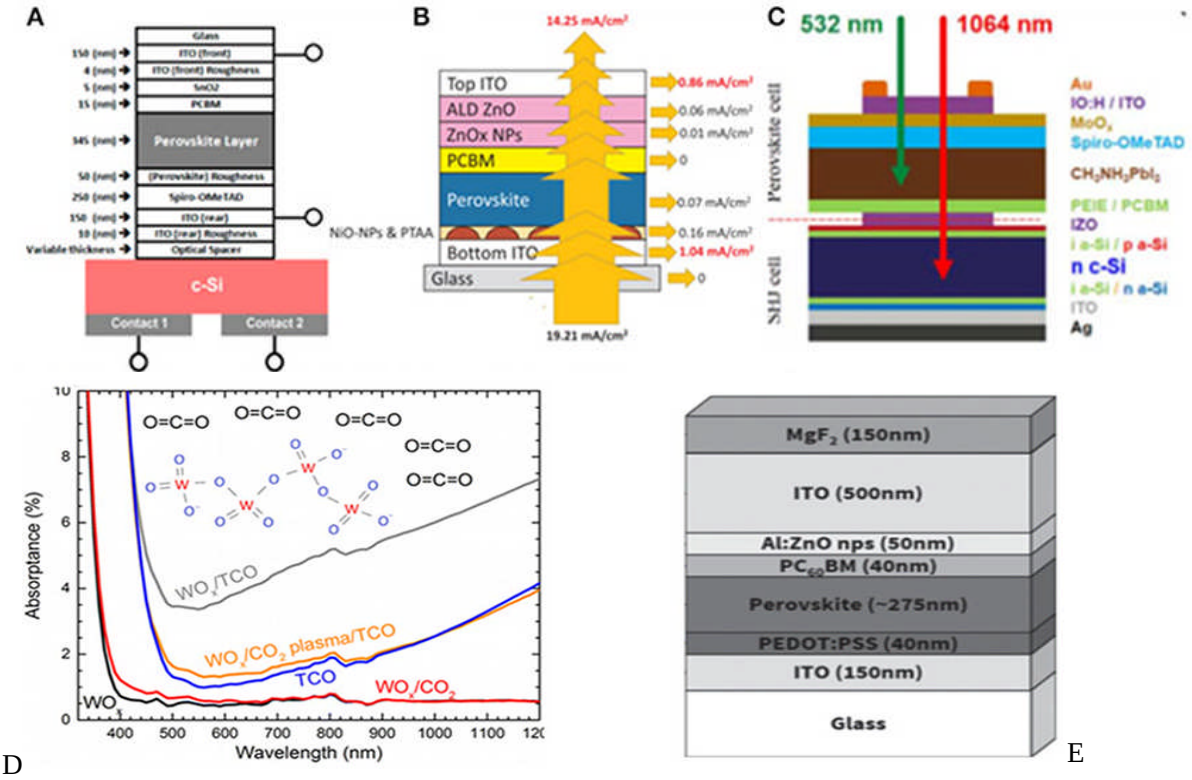

Figure II-4 : A- Device structures of 2T perovskite/Si TSC. B- Detailed analysis of the optical loss of ST-PSCs in the NIR (800–1,200 nm). The thickness of the ITO layer is fixed at 140 nm. C- Schematic of perovskite/Si monolithic TSCs. D- Absorption spectra and tauc plots of MoO_x, WO_x and V_2O_x layers evaporated about 10 nm thick on glass. E- Illustrative schematic of the device architecture showing the ITO electrode encapsulation layer [Liu et al, 2020]

However, additional efficiency optimization is limited by the deposition process which damages the subsequent transport layer where a MoO_x buffer layer strategy was proposed to solve this problem [Song et al., 2016]. MoO_x buffer layer had a bilayer front electrode of hydrogenated indium oxide (IO:H) and ITO. Finally, an optimized efficient tandem device is attained due to the reduction of carrier recombination.

The instability problem is one of some disadvantages for MoO_x buffer layer still persist which was mostly induced by the chemical reaction of MoO_x with the iodide in the perovskite. Overall, MoO_x served usually as a buffer layer for the n-i-p structure. Whereas, for the p-i-n structure, ZnO and SnO_2were employed as buffer layer.

A perspective was proved while using solution-treated ZnO nanoparticles as a hole-blocking layer and sputtering buffer layer to replace MoO_x in inverted PSCs with ITO sputtered at 500 nm directly

on the ZnO nanoparticles, achieving small sheet resistance of ≈9.9 Ω/ sq after 100°C annealing [Bush et al., 2016]. But there was a large interfacial barrier standing between the ZnO and ITO layers hindering carrier extraction which could be eliminated by using the zinc oxide nanoparticles doped with aluminum (2% in mole) (AZO) buffer layer in TSCs. Consequently, improvements were reached on the efficiency to 18.0%, and a J_{SC} of 13.3 mA/ cm^2.

Plus ZnO, the SnO_2buffer layer was introduced for the p-i-n structure where a 20 nm SnO_2 was made by atomic layer deposition this deposition technic is a powerful-in order to grow dense, conformal, and pinhole-free layer, thus prevent damage caused during the sputtering of the electrode. SnO_2buffer layer added by this technic yielded to an efficiency of 26.0% as well as the J_{SC} of 19.5 mA/ cm^2.

II- 3-1-3 IZO

IZO seems to be suitable for transparent conductive electrodes compared to ITO owing to its high carrier mobility and low carrier concentration. In addition, using ITO as the transparent electrode has some disadvantages such as a strong parasitic absorption in a thicker ITO layer or high sheet resistance in a thinner ITO layer.

By using the rear electrode of sputtered IZO with a sheet resistance of 35Ω/sq, an efficiency of 9% was obtained in the semitransparent PSCs without a buffer layer as shown in Figure II-5 [Werner et al., 2015], and the efficiency rises to 10.3% while adding MoO_x buffer layer. Then in 2018 a detailed guidelines for achieving a high-efficiency tandem devices was presented using a light trapping strategy [Jošt et al., 2018]. A textured light management foils on top of the IZO transparent contact was added to reduce the reflection in dual-textured perovskite/Si TSCs.

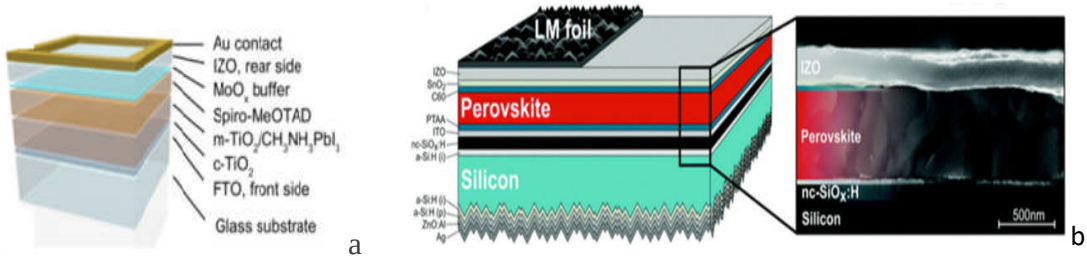

FIGURE II-5: a- Illustration of PSC schematic with a transparent rear electrode and Au contact. b- TSC device schematics of the experimentally realized architecture and SEM cross section image of the top cell [Liu et al, 2020].

Also, to diminish the barrier extraction of carrier at the IZO interface, a configuration was established of a sputtered ZnO:Al TMOs (IZO doped with Aluminum) layer and a metallic grid on

above the MoO_x buffer layer with an average transmission of 71% for photons in the wavelength of 800–1,000 nm as shown in Figure II-6 [Kranz et al. [2015]. By this method, it was possible to engineer near-infrared-transparent PSCs with a PCE of up to 12.1%, in addition to polycrystalline thin film tandem device with an efficiency of 19.5% combined with CIGS. Despite these results which show that AZO can be considered as a good electrode, AZO-embedded devices present high resistance and low fill factor, which is not ideal, and could be improved by multilayer electrodes adding a metal grid under the AZO layer [Roldán-Carmona et al, 2014] where a three-layer structure of AZO, silver and AZO as an electrode on a PET substrate in flexible thin-film solar cells was fabricated and attained a 7% of efficiency.

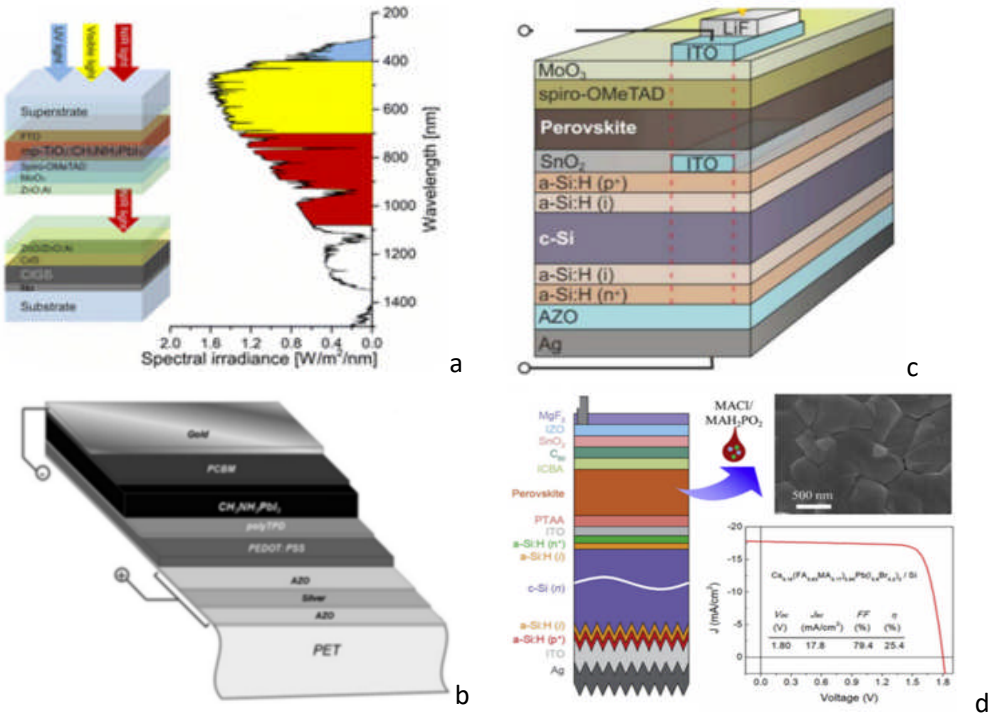

Figure II-6: a- Characterization of NIR-transparent Perovskite cell, b Schematic device design of the Si heterojunction/perovskite tandem solar cell .c- Schematic layout of the flexible PSC and chemical structure of the materials used as the electron and hole blocking layer. d- Schematic structure, J-V curves of $Cs0.15(FA_{0.83}MA_{0.17})_{0.85}Pb(I_{0.7}Br_{0.3})_3$/Si tandem device under forward and reverse scans with an inset photograph of the tandem device [Liu et al, 2020]

After that, the back contact of monolithic perovskite/Si tandem cells was fabricated by sputtering 70 nm AZO and 200 nm silver, yielding a stabilized output power of 18% and an open circuit voltage Voc of 1.78 V [Albrecht et al; 2016]. An optical optimization strategy of Si cells was

presented aiming to achieve a 25% high-efficiency device by changing ITO with c-Si:H as the *recombination layer*. Computationally, a proposed approach was established for trapping light in electrodes which used a textured foil on top of the Si cell substrate to reduce reflection, especially in the long-wavelength regime, which might improve the photocurrent.

Based on the multilayer stacking electrodes strategy and through the introduction of two types of additives (MACl and MAH_2PO) the grain engineering was verified to improve the grain morphology and extend the perovskite bandgap with the Cu grid electrode underneath IZO which can also reduce the electrodes sheet resistance as well as improve the fill factor (fill factor of 79.4% in a high tandem V_{OC} (1.80 V) and PCE of 25.4%).

To summarize, the doping (with H, Zn, etc) has attained good PV properties. However, In_2O_3:H could be damaged by water vapor diffusion. IZO can encourage parasitic absorption due to its amorphous nature. Other transition metals such as Mo, Ce, Ti, W, etc., could also be dopants but they are not considered in tandem cells due to their high annealing temperature, which was not well-suited with the undercoating process. Sputtered zirconium oxide (ZrO_2) doped with indium oxide (IZRO) with 2wt% ZrO_2 as transparent electrode allowing high electron mobility of 77 cm^2/V s and low square resistance of 18 Ω/sq in 100 nm films [Aydin et al. 2019]. In addition, it was proposed that doping by Zr can improved crystallinity which results in high conductivity and better efficiency of 26.2%. Additionally, the film thickness and annealing process also effect the layer microstructure of and its carrier transport property [Rucavado et al.]. such as IZRO annealing in neutral N_2 or reducing atmosphere H_2, persisted mostly amorphous while air-annealing leads to polycrystalline films with an average grain size extending from 350 nm to 500 nm. Moreover, the IZRO sputtered with different thickness from 100 nm to 15 nm, reached electron mobility of 100 and 50 cm^2/Vs, respectively. On the other hand, films annealed in H_2 confirmed high carrier density but low carrier mobility. Thus, doping with H, Zn, Zr, translation metals (Mo, Ce, Ti, W)..etc, can enhance the mobility of carriers and the optical transparency, allowing a higher solar cell efficiency of the comparing with the pure ITO.

II-3-1-4 Ag Nanowires

For large-area and flexible photoelectric applications, TMOs are not appropriate because of their high resistance, low thick layer conductivity, as well as poor mechanical properties. So, to resolve this problem, networks Ag nanowires (Ag-nw) were used as top electrodes enabling transmission as high as 90% with sheet resistances below 13 Ω/sq [Beiley et al. 2013]. This is well below the

commercial ITO of 36 Ω/sq, represented in Figure II-7 [De et al, 2009]. Nevertheless, due to the corrosion of halogenated species of perovskite, Ag-nw based contact was not stable and their contact could not collect the charge carriers efficiently. Filling materials under Ag-nm was explored [Beiley et al.] and ZnO nanoparticles was proposed as filler materials for the Ag-nw mesh that lowered the sheet resistance (from 16 Ω/sq to 14 Ω/sq). Consequently, as top electrodes the Ag-nanowires were combined with ZnO nanoparticles, realizing 5%efficiency in single junction cells. Moreover, it was predicted that by this such approach, the efficiency of GIGS/PSCs could reach as high as 20.7%.

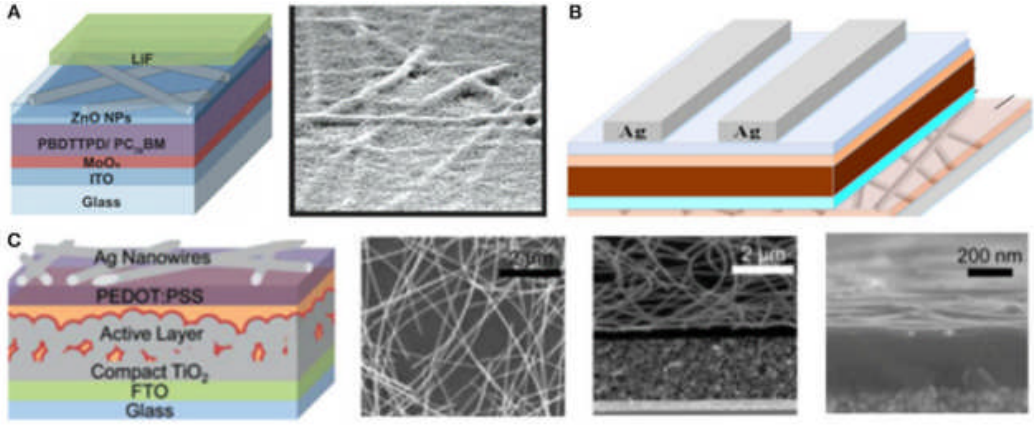

FIGURE II-7: A- The semi-transparent cell architecture schematic. B- Schematic diagram of semitransparent SSDSC device. C- Schematic illustration of the PVSK solar cell structure on an Ag-nw/LGO composite electrode [Liu et al, 2020]

Furthermore, an Ag-nw/PEDOT: PSS electrode was fabricated by spraying method, reaching more than 92% transmittance in solid-state dye-sensitized solar cells (SSDSCs) [Margulis et al., 2013]. The efficiency 3.6% of the cell was only 0.1% smaller than the standard (SSDSCs) where they were employing the evaporated silver electrode. Thus, via this approach, important insights are provided to realize high efficiency hybrid tandem PV (HTPV).

In 2019, a large size graphene oxide sheets with thickness of 60 µm was used in order to build a protective barrier to cover Ag-nw cracks [Chen et al, 2019]. And an average transmittance of 98.4 and 95.1 % was maintained by using the composite electrode of Ag-nw/Graphene Oxide maintained 98.4 and 95.1% average transmittance versus the original contact and gave a 9.62% power conversion efficiency. Overall, Ag-nw is a promising future electrode for flexible and large area PV devices.

II-3-1-5 Ultrathin Metal Electrode

In fact, the fabrication procedure of Ag-nw is complex, and variability in the applied force can cause short circuiting and incomplete electron transfer too, which results in a limited efficiency. Ultra-thin metal typically less than 10 nm thick, combining the advantages of high conductivity, good mechanical-flexibility and ease of fabrication without a pattern grid. In 2018, 2T tandem cells with 130 nm Ag electrodes were fabricated and reached an external quantum efficiencies with more than 80% in the near infrared region in Figure II-8 [Leijtens et al.2018b].

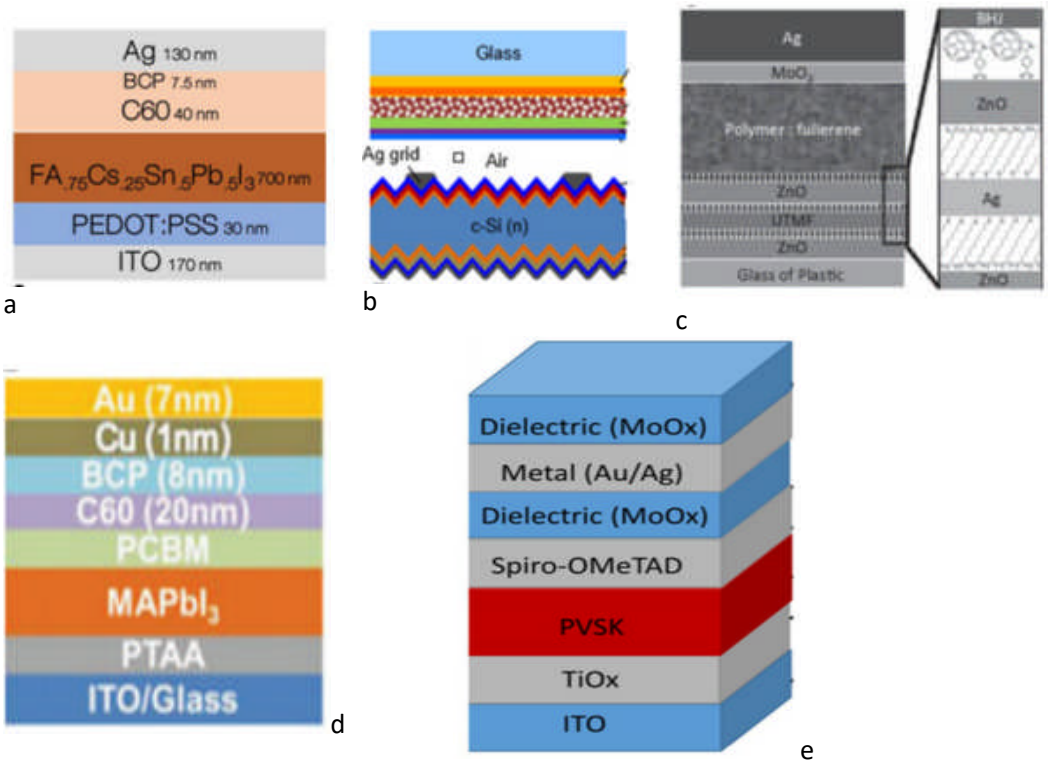

FIGURE II-8: a-Device schematic of the single junction solar cell. b-Schematic of the mechanically stacked 4T tandem. C- Schematic drawing of the PSC devices and the molecular structure of MUA and C60-SAM employed for interfacial modifications. d- Schematic drawing of tandem cells. e-Device structure of top illuminated perovskite solar cell [Liu et al, 2020]

But this efficiency was much lower than a single sub-cell, despite the high-efficiency sub-cells composition of TSC with record V_{OC} and FF values. This can be attributed to the high current losses due to reflection and parasitic absorption. In addition, precious metals such as Ag could not grow continually for its poor wettability, and this can be solved by via using TMOs as seed layer to grow metal oxide/thin metal/metal oxide tri-layer structure ‘MO/M/MO’.

A tri-layer structure in Ag films employing ZnO seed layer and a fullerene-based self-assembled monolayer was realized in order to achieve ohmic contact and enhance charge collection [Zou et al, 2014]. Thus, a low surface roughness, high transparency and low sheet resistance (8.61 Ω/sq) were achieved. Based on the model of dielectric/metal/dielectric (DMD) (MoO_x/Ag/MoO_x) a, an ultrathin gold seed under the silver layer as the front electrodes were fabricated with high conductivity and transparency [Yang et al, 2015] delivered 15.5% efficiency with neglected loss of V_{OC} and FF in 4T perovskite/CIGS tandem cells.

Also, by using an ultrathin 1nm of Cu on 7nm of Au metal electrode in semitransparent PSCs, the attained PCE was 16.5% [Chen et al, 2016] and when this cell is connected with Si the achieving efficiency rises to 23.0%. Furthermore, the tungsten trioxide (WO_3) was used in tri-layer structure WO_3/Ag/WO_3 as top electrode in planar devices [Loper et al, 2015] and aiming to tune the band gap mismatch between electrodes and perovskite, an additional layer WO_3/Ag/SnO_2 (WAS) was sputtered with aqueous soluble SnO_2 nanoparticles and achieved 14% efficiency [Liang et al, 2018]. Similarly, OMO top electrodes showed great potential in the PV-domain and might be explored further.

II-3-1-6 Graphene

Nowadays, the non-metal electrodes have attracted a special interest and have been developed, such as graphene which has high near-infrared transparency compared with the metal-based electrodes. Furthermore, the TSCs contact layer must possess high electrical conductivity and optimal transparency.

II-3-1-6 -a-Pristine Graphene

In 2013, graphene film were synthesized via CVD technique, resulting in 2,03 $cm^2V^{-1}s^{-1}$ charge-carrier mobilities (μ_p) with 3.61 cm^2 hole concentrations and transferred to Si-based devices, as presented in Figure II-9 [Gluba et al, 2013]. In addition, it was found that the charge-carrier mobilities and hole concentrations could be impacted by the deposition and subsequent crystallization of Si, as demonstrated by Raman backscattering spectroscopy and Hall-effect measurements. Shortly, the graphene layer was applied into TSCs where in 2015 and by using CVD a large-area single layer graphene was produced and transferred onto the PSCs achieving outstanding optical transmission (97.4%) [Lang et al, 2015]. They have attained a PCE of 13.2%

in 4T perovskite/Si TSCs, and notable open circuit voltages (~1V) in single cells, whose performance has already reached the Au electrodes standard.

In order to explore a manufacturing process more appropriate for industrialization, an advanced and economic technology was developed in 2019, presenting an approach of solution-processed graphene that could satisfy both conductivity and transmittance demand for electrodes using ethyl cellulose in the flexible PSCs resulting in a maximum efficiency of 15.71% [Yao et al, 2019].

CVD graphene was reported as transparent conductive electrode on a thin polyethylene naphthalate (PEN) rather than glass, and induced MoO_3as hole-doping to build flexible PSCs in 2016. As a result, PCE of 16.8% was achieved without hysteresis and superior bending stability [Yoon et al. 2017].

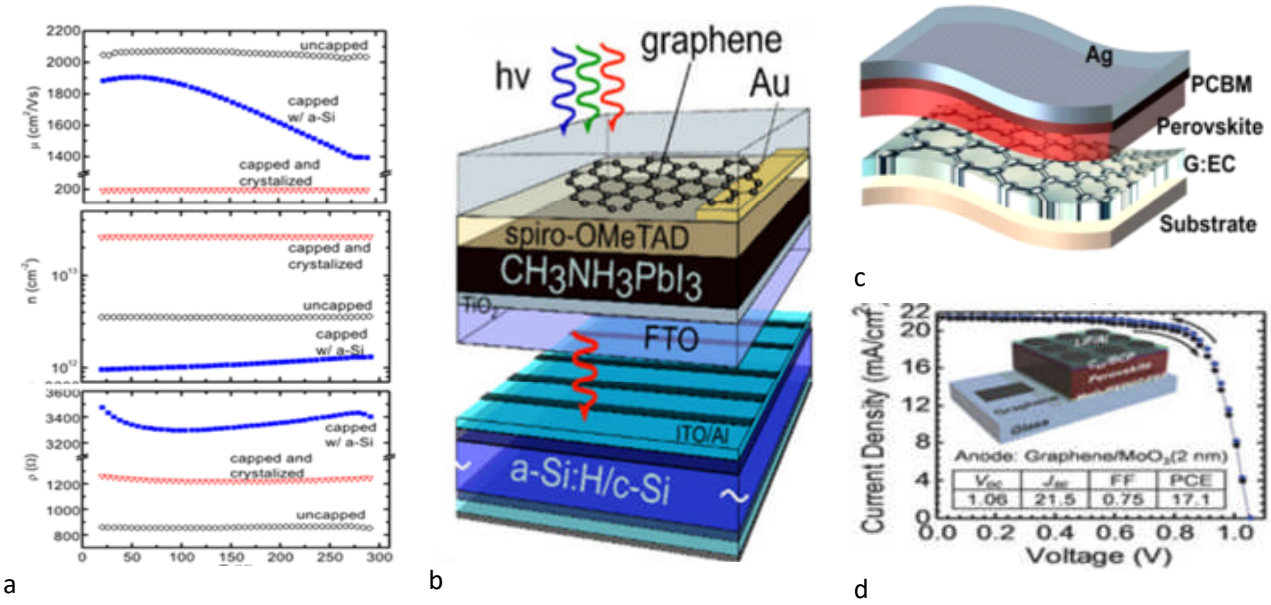

FIGURE II-9: a/ Temperature dependence of hall mobility, charge carrier density, and sheet resistance of bare graphene on a glass, capped with amorphous, and post-crystallized Si. b/Simplified sketch of a four terminal tandem solar cell consisting of graphene-based perovskite top solar cell and an amorphous c-Si bottom solar cell. c/The device structure of PSCs based on G:EC electrode. d/ Schematic structure of the inverted MAPbI3 PVSK solar cells utilizing graphene as a transparent anode [Liu et al, 2020]

Besides graphene, a proposed $CH_3NH_3PbI_3$/CNTs PSC with an energy-intensive vacuum process in direct derivation of the network of carbon nanotubes without hole transport layer as well as an Au electrode reaching 6.29% of efficiency [Li et al, 2014]. Spiro-OMeTAD as a hole transport layer was also incorporated which improved the efficiency up to 9.90%. It is convenient to note

that this property could be further improved by purification or chemical doping to increase the conductivity and work function.

II-3-1-6 -b-Doped Graphene

Aiming to improve conductivity and absorption including other photoelectric properties of electrodes, doping approach has been considered in carbon-based materials. Dopant graphene has a square resistance of 10 Ω/cm^2, while it is 377 Ω/cm^{2}for pure graphene [De and Coleman, 2010]. Habitually, the carbon nanotubes dispersion could be attained via both covalent or non-covalent modification and with a polymer. Single-walled carbon nanotubes embedded in a copper-phthalocyanine derivative (TSCuPc) were shown on a PET substrate as top electrodes in 2015 with an efficiency of 3.2% [Raissi et al, 2015]. Also, this layer can be used as an electron transport layer too, achieving an efficiency up to 7.4%.

In addition, incorporating graphene with ZnO nanocomposite in a-Si:H/lc-Si:H tandem cells allows better photon management. The J_{SC} increased by 41.8% by changing the thick of graphene/ZnO [Chawla et al, 2017]. Plus, high efficiency, the long-term stability also is with consideration for tandem cells achieved by doping the electrode. High stability in air was also realized and suggested by doping carbon electrodes with various concentrations of WO_3 nanoparticles [Bhandari et al, 2020]. Consequently, the graphene and its branching inset as top electrodes is beneficial for the industrialization of tandem cells as it also reduces manufacturing costs.

II-3-1-7 Conductors without precious metals

Recently, the transparent conductor without indium and precious metals was developed, due to the reaction of precious metals (such as silver, gold and indium) with any residual free halide of the perovskite where stabilized power conversion efficiencies of 7.6 ± 1.0%. was verified. a laminated top electrode has been proposed, consisting of a corrosion-resistant Ni mesh electrode embedded in a PET film with a silver-free transparent conductive adhesive (TCA), achieving an efficiency of 15.5% [Bryant et al, 2014]. Accordingly, the use of a precious metals free conductive polymer has revealed high potential in the realization of high efficiency cells.

II-3-2 Absorber Layers-Perovskite

As mentioned in section II- 2, due to their simple fabrication methods and superior electronic and optical properties perovskite materials have been used as absorbing layers in solar cells [Jiang et al., 2015]. One of the exceptional advantages of perovskites over other semiconductor materials is the possibility of tuning their absorption onset by ion replacement, resulting in tunable absorption edges in the wavelength range from 350 to 1,200 nm. For this reason, was considered an ideal candidate for TSCs. The perovskite wide-bandgap which was used in the top sub-cell can be obtained by introducing Br^-. But under light illumination, this can lead to segregation and phase separation in the high Br^-content perovskite active layer, which impairs PV performance and stands a challenge for the industrialization for high-efficiency of TSCs. Moreover, it is important and imperative to develop practical deposition methods to obtain conformal and high-quality perovskite films on textured Si.

II-3-2-1 Bandgap Tuning

The bandgap of perovskites can be adjusted by composition engineering [Jesper Jacobsson et al., 2016]. Generally, in the tandem configuration, the perovskite top-cell uses the short wavelengths of the solar spectrum also have been shown by simulations that a high-perovskites PCE top-cell with bandgap of ~1.70 eV to 1.85 eV can increase the PCE up to 30% [Lal et al., 2014; Yu et al., 2016]. Consequently, it is imperative to develop high-PCE PSCs with appropriate bandgap for tandem cell application. As well, it is also convenient point out that some perovskites with a relatively low bandgap of 1.55 eV also show exceptional PV performance for tandem devices.

II-3-2 -1-a- X Site Substitution-

Aiming to widen the perovskites bandgap, one of the usual approaches is to partially substitute $I^-$by Br^- to form mixed halide perovskites where, in 2013, the nature of excitons in MABr was discovered with a large bandgap, showing that the $MAPbX_3$ bandgap can be tuned through substitution $I^-$with Br^-[Tanaka et al., 2003]. In the same year, the bandgap of $MAPb(I_{1-x}Br_x)_3$ perovskites light absorbers was shown to increase with increasing Br^-fraction, leading to a tunable bandgap from 1.55 to 2.3 eV [Noh et al., 2013]. Subsequent studies have also been reported to adjust the bandgap and even the perovskites photoelectric properties via including Br^-, and this could come from MABr, FABr and $PbBr_2$ …etc [Jesper Jacobson et al., 2016].

Even if wide-bandgap of the perovskite can be obtained by the halide composition adjustment, segregation and phase separation were found in these mixed-halide wide-bandgap perovskite with high Br^-content under light illumination, which adversely affects PV performance. Light-induced halide segregation can conduct to the formation of I-rich domains and Br^--rich domains in the $MAPb(I_{1-x}Br_x)_3$thin films, leading to serious photo-instability issues in a wide range band gap at mixed-halide perovskite. Accordingly, there is an urgent demand to develop an easy way to stabilize wide-bandgap perovskite under illumination.

As a strategy, manufacturing larger grain size perovskite films to ameliorate their photo-stability. PTAA was first used to facilitate the growth of perovskite films with large grains [Bi et al., 2015] where via varying the grain size of the mixed-halide perovskite films, the $MAPb(I_{1-x}Br_x)_3$with a bandgaps (from 1.70 eV to 1.75 eV) were free degradation and stable under illumination continuous 1 sun for 30 min and the film of 1.70 eV bandgap exhibited an improved PCE (16.6%). In 2019, obtained perovskite films by adopting grain engineering, was found to possess large grain sizes (~1 μm) and a bandgap of 1.64 eV in top cell, realizing an efficient perovskite/Si tandem device of 25.4%. and they can preserve 91.5% of their initial PCE after constant illumination of simulated AM 1.5 G light for 250 h when encapsulated [Chen et al., 2019].

The improvement in photo-stability during this process is explained by the ion-migration suppression in a larger grain. It was also reported efficient wide bandgap perovskite top cells 1.67-eV employing triple-halide (chlorine, bromine, iodine) alloys to much the bandgap and stabilize the semiconductor under illumination. It deleted the phase segregation induced by light- in films even at 100-sun illumination intensity and less than 4% degradation in semitransparent top cells after 10,000 h of maximum power point operation at 60°C [Xu et al., 2020].

II-3-2 1-b- B Site Substitution

The B site in the perovskite structure can be occupied by cation (Pb^{2+} Cu^{2+}, Sn^{2+}, or Bi^{3+}) [Ju et al., 2017; Liu et al., 2017; Williams et al., 2017]. the Sn^{2+} based perovskite has been the most studied, but it absorbs in the near infrared region, and the bandgap can be decreased down to 1.17 eV. Knowing that the smaller bandgap Perovskites were usually applied in the bottom cell of perovskite/perovskite TSCs, B site substitution is not a good tactic for developing perovskite materials with large bandgap in the TPSCs top cell.

II-3-2 -1c- A Site Substitution

It is possible to replace the cation MA^+ by formamidinium $CH(NH2)_2^+$ abridged by FA^+ but its larger size can tilt the metal-halide octahedra, leading to decrease the bandgap of the perovskite, meaning that the bandgap of $MAPbI_3$ (1.6 eV) is larger than that of $FAPbI_3$ (1.45 eV) [Lee J. W. et al, 2015]. Also, the long-chain organic cations are regarded as interesting choice to substitute MA^+ cation. For example, Butamine $(CH_3(CH_2)_3(NH_3)^+$ abbreviated as BA^+ was a used cation to form two-dimensional (2D) perovskite with large bandgap [Smith et al, 2014]. The bandgap of 2D-perovskite $(CH_3(CH_2)_3)NH_3)_2(CH_3NH_3)_{n-1}Pb_nI_{3n+1})$ increases with the decreasing the value of *n*, from 1.53 eV of $CH_3NH_3PbI_3$ to 2.24 eV of $CH_3(CH_2)_3NH_3)_2PbI_4$ [Stoumpos et al, 2016]. $CH_3(CH_2)_3NH_3)_2(CH_3NH_3)_3Pb_4I_{13}$ is the frequently used 2D perovskite in PV application, which has a bandgap of 1.65 eV appropriate as top-cell of TSCs [Tsai et al., 2016; Liu et al., 2020a,b]. these 2D perovskite films also shows excellent moisture stability due to their long organic chains such as $CH_3(CH_2)_3NH_3)^+$.

In the past researches, the 2D PSCs exhibited poor PCEs of no more than 5% owing to its low carrier mobility and short diffusion length, caused by their large size spacers but by using pre-heated deposition to grow these films while the orientation of inorganic framework perpendicular to the substrates, consequently, this helped the charge transport, leading to an improvement of PCE of 12.5% without hysteresis. More than 60% of the efficiency was maintained under constant and standard (AM 1.5G) illumination after 2, 250 h by the unencapsulated 2D perovskite devices while it was remarkable for encapsulated devices, since they almost did not show any degradation under humidity or constant AM1.5G illumination [Tsai et al., 2016]. Yet, the PCE of two-dimensional perovskite devices still lagged behind their 3D counterparts.

Cs^+ cations have also been effectively used in perovskite where the bandgap of all inorganic perovskite $CsPbI_{1-x}Br_x$ increased by changing the halide from 1.73 eV for $CsPbI_3$ to 2.3 eV for $CsPbBr_3$. The rapid progress of inorganic perovskites-based solar cells has resulted in an inspiring PCE record from the initial 6.7% to nowadays 17.75% [Liang et al., 2016]. It was found that for increasing bandgap it is more ideal to use more Cs at A site rather than more Br at the X-site as it improves V_{OC} [McGehee's et al,2018]. The obtained perovskites bandgap of 1.68 and 1.75 eV and the high efficiencies of 17.4 and 16.3%, respectively [Bush et al., 2018]. But the inorganic

perovskite is unstable under ambient conditions, it rapidly degrade from the cubic black phase to the unwanted orthorhombic yellow phase, which damages the PV performance of cells.
To summarize, perovskite materials is an excellent choice for top sub-cell in TSCs, since it can fulfill the bandgap requirement through simple composition engineering, whereas in many other optoelectronic materials this is not offered.

II-3-3 Recombination Layers

The two sub-cells monolithic perovskite/Si tandem cells, are connected with a recombination layer or interconnecting layer that recombine entirely opposite electrons and holes from the electron transparent layer (ETL) and the hole transparent layer (HTL) of top and bottom sub-cells, respectively. A good interconnecting layer must realize a neglected voltage-loss and accordingly to this, the recombination layer has to submit some requirements:

- Its work function must efficiently gather electrons and holes form different transport layers, achieving minimal electrical losses.
- It can be manufactured at the low temperature without damaging the underneath layer.
- The transmittance should be high and do not influence the absorption of bottom cells to induce current-loss.

Considering these requirements, TMOs are excellent candidates, having the characteristics of high transmittance, high conductivity and low sheet resistance. Therefore, the ITO, IZO, and AZO are all common materials for recombination layers. But since the TMOs have a low shunt resistance, the voltage loss is induced. Accordingly, homogeneous Si materials are good candidates for the recombination layer plus the amorphous Si, p type Si, n type Si, hydrogenated microcrystalline Si (μc-Si:H) or doped-Si materials depositing by the low temperature plasma-enhanced CVD technique with higher shunt resistances [Liu et al, 2020]. Additionally, the doped organic molecular such as m-PEDOT:PSS/$PH_{1,000}$/ZnO and Spiro-OMeTAD/PEDOT:PSS/PEI/PCBM:PEI combined with bottom or to transparent layer can replace the Si materials at low temperature manufacturing process and then low costs. Nevertheless, the supplementary additional recombination layer would induce an unavoidable loss current. Thus, to solve this issue a so-called layerless recombination is proposed by combining ETL and HTL layer from different cells which could also simplify the manufacturing technology.

II-3-3-1 Si-based recombination layer

The low lateral conductivity of silicon-based materials can diminish V_{OC}-loss that can lead to high tandem cells efficiency. Monolithic tandem cells were first constructed in 2015 where the Si-based tunnel junction was deposited by plasma-enhanced-CVD (PECVD), which caused efficient recombination of the majority-carrier charges in tunnel junction, as presented on Figure II-10 and the ability for Si to work as recombination layer has been anticipated. The achieved V_{OC} and the efficiency were of 1.65 V and 13.7% respectively, while the device performance was limited by high-temperature-deposition mesoporous TiO_2 that must be removed. Moreover, the Silicon low lateral conductivity influenced extra efficiency improvement [Mailoa et al, 2015].

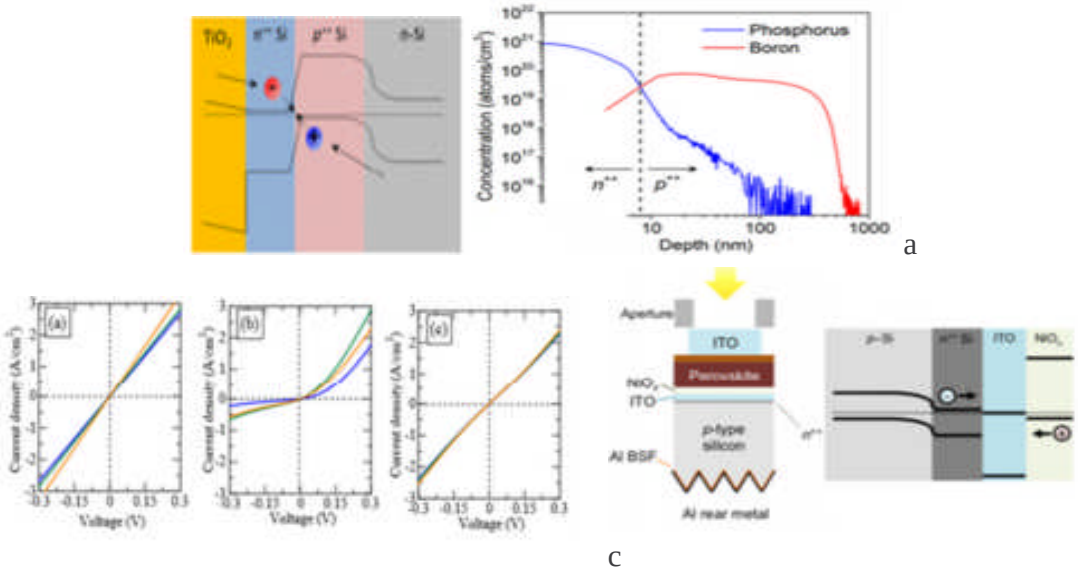

FIGURE II-10: a-Band diagram, and SIMS profile of the perovskite/Si cell tunnel junction interface. b- The characteristics of tunnel recombination junction structure using p-Cu_2O:N=n-a-Si:H, and Tunnel recombination junction structure using p-Cu_2O:N=n-µc-Si:H, C- Device structure of tandems with aluminum back surface filed (Al-BSF) p-type Si bottom cells and structure of the ITO/NiO_x recombination contact on a p-type Si cell [Liu et al, 2020].

In order to overcome the Si conductivity problem, a monolithic perovskite/Si heterojunction tandem cells with a recombination layer of nanocrystalline Si deposited by PECVD was constructed at low temperature resulting in a drop of parasitic absorption and reflection losses. So, the achieved parameters were 22.7% efficiency, 1,751 mV for V_{OC}, 16.8 mA/cm^2 for J_{SC} and 77.1% of FF while the area was 0.25 cm^2[Sahli et al, 2018].

Additionally, by comparing two types of recombination layer of both n-type µc-Si:H and n-type Si with nitrogen-doped cuprous oxide (Cu_2O: N) in resistance, it was proved that doping can augment the conductivity of Si. Where it was found that n-type µc-Si:H exhibited non-ohmic behavior while Cu_2O: N revealed ohmic contact with a low resistance of $3.9 \times 10^{-2}\Omega$/sq. This approach offered a whole new direction for achieving high efficiency [Kim et al, 2018]. Yet, the recombination layer of Si can be affected by SiO_x oxidation from Si bottom cell during the fabrication of top cell. it is why a Hoye et al. sputtered 30 nm ITO incorporated with nickel oxide as recombination layer to protect against oxidation which makes the TMOs becoming potential recombination layer materials [Hoye et al, 2018].

II-3-3-2 TMOs Based recombination layer

As recombination layers, the TMOs fabrication processing is more practical since they are a part of Si heterojunction cells. The ITOs as recombination layers in TPSCs treated at a low temperature reached 19.9% of efficiency with a J_{SC} of 14 mA cm^{-2}, a V_{OC} of 1.78 V, and an FF of 79.5% [Albrecht et al, 2016b].

Despite the fact the efficiency has been reduced due to the high absorption of ITO in the near-infrared spectrum this can be solved by shrinking the recombination thickness to improve photocurrent. This was examined by reducing the ITO recombination layer thickness from 80 to its half getting only a small improved absorption for bottom cells achieved due to the current mismatch elimination between the top and bottom solar cells. Furthermore, they optimized the thickness of n-type and p-type transport layers resulting in an efficiency of 28.4% and FF of 81% and also, the recombination layer thickness of ITO producing stabilized power output of 17% [Albrecht et al, 2016a].

Doping also can resolve the low carrier mobility when ITO is taken as TMOs which was causing an insufficient carrier recombination and voltage loss as shown on Figure II-11. IO:H was demonstrated to have an electron mobility over 100 cm^2/Vs [Barraud et al, 2013] and besides IO:H, the property of IZO-assisted high carrier mobility and low carrier concentration helped IZO to become a competitive recombination layer. This was realized in 2018 where recombination layer of IZO in 2T-TSCs-based perovskite was constructed and under an induced optical beam was used to identify defects in cells during the process of photocurrent collection and generation [Song et al, 2016]. An efficiency of 19.2% (area =1.22 cm^2) and 21.2% (area= 0.17 cm^2) were reached with the

recombination of sputtered IZO layer deposited at room temperature [Werner et al, 2016b]. As well, the influence of thickness influence was studied by changing the IZO thickness from 25 to 70 nm and the optimum situation was achieved by a 40 to 50 nm-thick IZO layer demonstrating the light management importance. Considering the high manufacturing process of 500°C, mesoscopic perovskite cells were limited to be implemented into monolithic TCs while IZO recombination layer can endure this temperature gaining the efficiency of 16%. Furthermore, by changing this time the thickness from 20 nm to 160 nm, it was noted that the larger contracts of refractive index between the transport layer and recombination layer can produce the internal reflection at this interface.

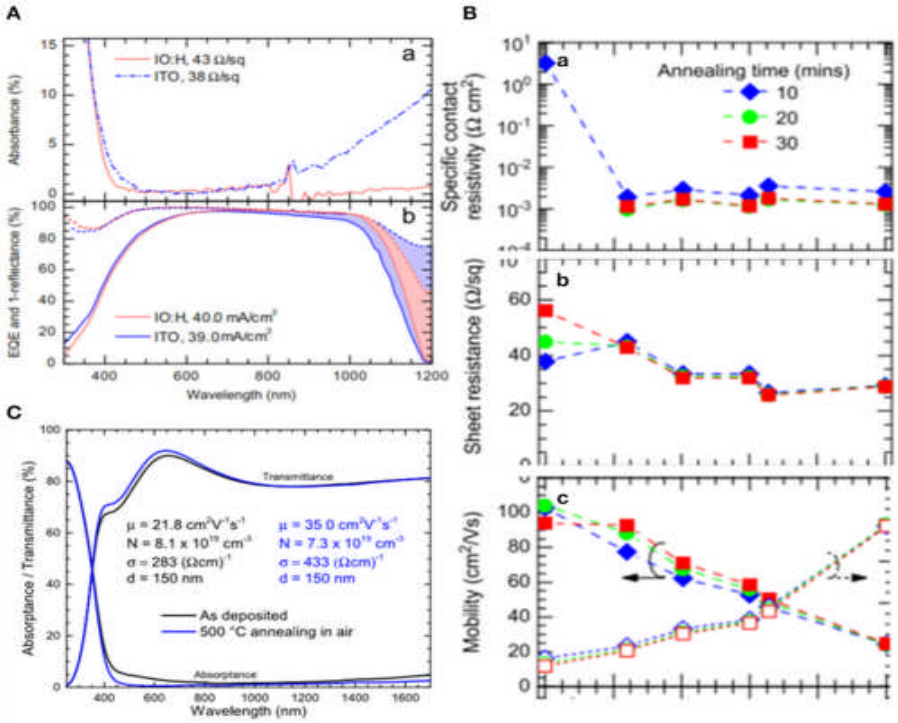

Figure II-11: A- Absorbance spectra, external quantum efficiency (solid), and 1-reflectance (dashed) spectra of IO:H and ITO films on glass. B- Specific contact resistivity, sheet resistance, and mobility and free electron density of IO:H/ITO bilayers on glass. C- UV-vis-NIR spectrophotometric of a 150 nm thick ZTO layer on glass before and after annealing at 50°C in air. Hall Effect characteristics are also given. μ¼ mobility; N¼ carrier density; r¼ conductivity; and d¼ thickness [Liu et al, 2020].

II-3-3-3 Organic molecule-based recombination layer

TMOs as the recombination layer can also be replaced by some special organic molecular with high transmittance because of the fact that the TMOs as a recombination layer work with

disadvantages, counting the optical loss in the near-infrared region of 800–1,000 nm and lateral current loss due to their reduced shunt resistance (Figure II-12).

2T TSCs with Spiro-OMeTAD/PEDOT:PSS/PEI/PCBM:PEI as recombination layer obtained a V_{OC} of 1.89 V, which was close to the sum of two subcells with no voltage loss [Jiang et al., 2016]. This encouraged the application of organic molecules as a recombination layer but some organic molecules were not suitable due to their unstable properties, PEDOT:PSS, for instance, it was not appropriate as a p-type recombination layer due to its acidic nature. So, to tackle this fact, a self-doped conducting polymer (SCP) was used in a stable and high efficiency tandem devices including ZnO nanoparticles as a recombination layer without PEDOT:PSS, which leads to 10.2% of PCE and prolonged long-term stability [Lee et al., 2016].

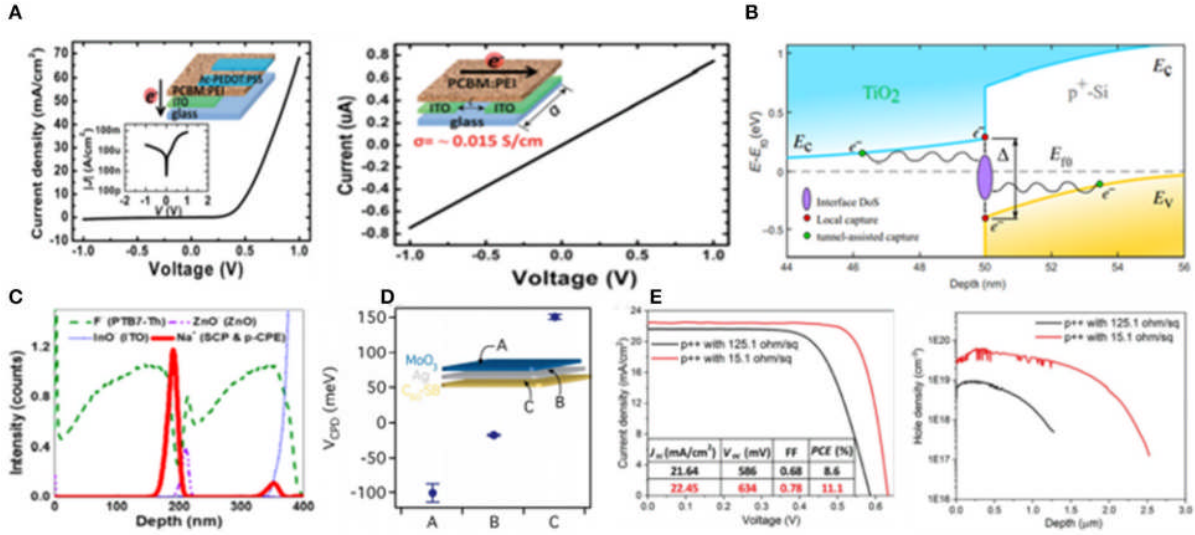

Figure II-12: A- J–V characteristics of the devices including the current flows vertically across the film and the current flows in parallel with the substrate. B- Contact behavior and simulated band diagram of TiO_2 /p^+ -Si interfaces. C- Time-of-Flight Secondary Ion Mass Spectrometry (TOF-SIMS) depth profile of the ITO/p-CPE:BHJ/ZnO/SCP/p^-CPE:BHJ structure. D- Surface potential (VCPD) of the recombination layers [C60-SB (30 nm)/Ultrathin Ag (10 nm)/MoO_3 (10 nm)] (reproduced from ref. 75, copyright 2016, ACS). E- The J–V curves and electrochemical capacitance–voltage measurements of Si bottom cells that have different p^{++} emitter profiles (black for 125.1 Ω/sq and red for 15.1 Ω/sq) [Liu et al, 2020]

Also, a developed multilayer stacking recombination layer approach using a graded recombination layer containing a zwitterionic fullerene, silver (Ag), and MoO_3 was fabricated and achieved 16 % of efficiency in perovskite/polymer TSCs [Liu et al, 2017].

By no adding extra recombination layer to bypass the optical and electrical loss in this recombination layer, the monolithic perovskite/homojunction Si TSCs was demonstrated for the

first time while dual-function SnO_2 served as an electron transport layer and an interface layer which has small lateral conductivity possibly restored by the p^{++}emitter of the Si cell. they reached a 21% of PCE (area= 4 cm^2) under reverse-sweep with a V_{OC} of 1.68 V, a J_{SC} of 16.1 mA/ cm^2 and a 78% of high FF [Zheng et al. [2018]. A steady-state PCE of 17.1% on a large area of 16 cm^2 was also achievable. Nevertheless, by employing n-type TiO_2 and Si fabricated by atomic layer deposition as recombination layer, has allowed to achieve an efficiency of 24.1% for passivating contact heterojunction perovskite/Si tandem cells [Shen et al, 2018]

II-3-Electron transport layer

Known as electron extraction layer too, the extraction (collection) and transportation of electrons, injected from the absorber is its mission. For this work, some requirements are needed from ETL such as the conduction band and valence bands must be lower than those of the absorber, for an effective charge extraction [Mahmood et al, 2017]. The bands misalignment of ETL with perovskite absorber affects seriously all the series, shunt and recombination resistance of the device making the interface between the perovskite absorber and ETL with significant importance for the device performance. So, to tackle these issues and as already mentioned about band matching, the chosen materials need to have high electron mobility and suitable band alignment leading to a better electron injection and hole blocking in the ETL/perovskite interface, achieving excellent current density and device performance [Kim et al,2020]. Figure II-13 summarizes various ETLs band energy diagram and possible approaches to attain efficient ETL layers.

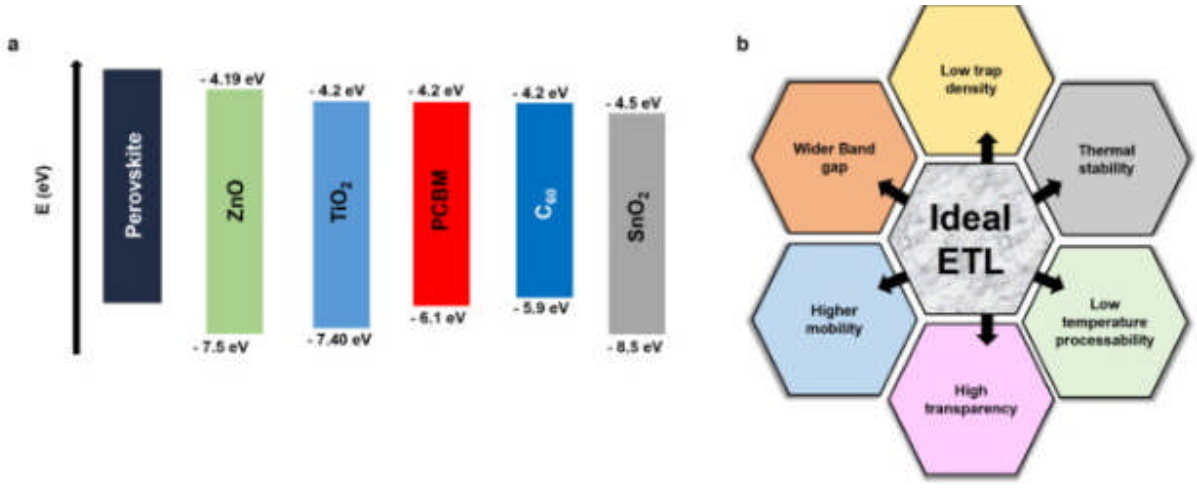

Figure II-12: Schematic representation a- Band structure and energy levels of various ETLs used in tandem devices, b- Approaches applied to reach efficient ETLs [Akhil et al, 2021]

Several approaches can be investigated in order to reach low-temperature processability, low trap density for better thermal stability and higher mobility in single-junction PSCs, some of them already discussed in recombination layer section.

The of charge collection imbalance between the ETL/Perovskite interface versus the HTL/perovskite interface controls the hysteresis of the device [Calado et al,2016] which can be reduced by using materials with efficient charge extraction from ETL/Perovskite interfaces. Compact and/or mesoporous n-type TiO_2 is the most broadly used material in TPSCs [Dong et al,2015]. They exhibited less hysteresis unlike planar devices without TiO_2 [Mahmood et al, 2017] because of the improved charge collection from the perovskite/ETL interface.

ETL thickness also take a significant part on influencing the device performance. The surface coverage of TiO_2 on fluorine doped tin oxide (FTOs) can be improvised by conventional treatment with $TiCl_4$ and UV ozone, enhancing a better deposition of TiO2 on FTOs, leading to excellent performances [Gao et al,2015]. Besides, the TiO_2 thickness layer also defines the recombination of charge carriers, the larger the thickness, more the recombination resistance is important.

So, if the thickness can add resistance to electron transport, it can also hinder the extraction of charge from TiO_2. An optimizing TiO_2 thickness layer of 40 nm was fixed after several studies, in order to have good recombination resistance and charge extraction and therefore reaching maximum device PCE [Choi et al,2016].

Incorporating graphene wafers in compact and mesoporous TiO_2 based ETL resulted in a reduction in the series resistance, which significantly ameliorate the EQE [Lamanna et al,2020]. Graphene wafers offer unbroken electron pathways [Kusuma et al,2018].

Despite the fact that TiO_2 is the candidate of choice for ETL, it its high sintering temperature of 500°C, hinders the thermal stability of a-Si:H in the lower cell and thus delays its commercialization. However, the deposition of TiO_2 in a perovskite device at 100°C [Paik et al,2020] is becoming true due to the latest advances in colloidal spray coating which allowed open doors to explore 2T tandem architectures with higher thermal stability. Table II-1 shows the various ETLs used for different tandem configurations.

Configuration	Top cell	Bottom cell	ETL	V_{oc}(V)	J_{sc}(mA/cm^2)	FF (%)	Area (cm^2)	PCE	Top cell P.C.E(%)	Bottom Cell P.C.E (%)	Year	Ref
2T	$CH_3NH_3PbI_3$	C-Si	SnO_2	1.78	14.00	79.5	1	18.1	–	–	2016	A
4T	$CH_3NH_3PbI_3$	C-Si	Al-ZnO	–	–	–	–	26.7	–	–	2018	B
4T	$CH_3NH_3PbI_3$	C-Si	C_{60}	–	–	–	–	24.6	16.23	8.37	2020	C
4T	CsFAMA	n-Si	SnO_2	–	39.50	–	–	28.2	19.00	24.00	2020	D
2T	$CH_3NH_3PbI_3$	C-Si	PCBM	1.69	15.80	79.90	0.17	21.2	–	–	2016	E
3T	$(MAPb(I_{0.95}Br_{0.05})_3$	C-Si	PCBM/ZnO	1.67	18.29	77.00	–	23.5	–	–	2019	F
3T	$(Cs_{0.05}(FA_{0.83}MA_{0.17})_{0.95}Pb(I_{0.83}Br_{0.17})_3)$	C-Si	SnO_2	–	–	–	0.78	17.1	11.7	5.4	2020	G
4T	$CH_3NH_3PbI_3$	C-Si	TiO2	–	–	–	3	21.2	14.80	6.40	2019	H
2T	$CH_3NH_3PbI_3$	p-Si	ZnO	1.77	20.19	82.22	–	28.5	–	–	2020	I
2T	CsFAMABrI	C-Si	TiO_2	1.80	18.81	75.6	1.20	26.3	–	–	2020	J
2T	CsMAPbBr	C-Si	C_{60}	1.82	19.2	74.4	–	26	–	–	2020	K
2T	$Cs_{0.05}MA_{0.15}FA_{0.8}Pb(I_{0.85}Br_{0.15})_3$	C-Si	C_{60} Anchored/a-NbO_x	1.8	19.5	75.9	–	27	–	–	2021	IL
2T	$FA_{0.83}Cs_{0.17}Pb(I_{0.80}Br_{0.20})_3$	C-Si	SnO_2-LiCl	1.9	16.9	77.9	0.50	25.4	–	–	2021	M

Table II-1: Various ET-Materials used for different tandem configurations [Akhil et al, 2021

	Reference		Reference
A	[Quiroz et al, 2018]	H	[Lee et al, 2019]
B	[Quiroz et al, 2018]	I	[Afrasiab et al, 2020]
C	[Ying et al, 2020]	J	[Lamanna et al, 2020]
D	[Chen et al,2020]	K	[Chen et al, 2020]
E	[Werner et al, 2016]	L	[Aydin et al, 2021]
F	[Park et al, 2019]	M	[Chen et al, 2021]
G	[Tockhorn et al, 2020]		

II-3 Hole Transport Layer

Hole transport layer must have high hole mobility, low electron affinity, compatible HOMO (highest occupied molecular orbital) and LUMO (lowest unoccupied molecular orbital) energy levels with perovskite, high thermal stability. Despite of many HTLs (small molecules, polymeric, carbon, and inorganic molecules) have been proposed and studied for single junction solar cells, not a lot is seen in the exploitation of these materials in tandem structures.

The main HTL function is to transport the holes generated in perovskite layer to the rear contact metal electrode. Acting as a barrier between the perovskite layer and counter electrode, it avoids the back transfer of electron. It influences V_{oc} by determining the division of quasi-Fermi – energy levels of the perovskite [Bakr et al,2017]. Generally, the wide band gap PSCs undergo the V_{OC} deficits larger than 0.65 V (defined as (Eg/q)-V_{OC}) that limit their performance [Unger et al,2017]. This is due to various factors, including light induced phase separation of perovskites and unmatched energy levels of HTLs. The HTL is deposited on top of perovskite absorber layer in n-i-p configuration and materials with good hydrophobicity (hydro=water, phobicity=lack of affinity) are preferred, for better humidity protection of perovskite layer. While less hydrophobicity materials can be employed get fine crystallization. Spiro-OMeTAD is an organic commonly used as HTL which has good thermal and optical stability but its lower conductivity and hole mobility together with higher cost limit the commercialization of these tandems. The addition of dopants such as Li-TFSI, FK209 and t-BP augments the conductivity, used in single junction perovskites in order to improve the HTLs conductivity. Whereas, these dopants effect negatively the stability of perovskite film due to its high hygroscopic nature. Thus, passivation of the interface at

perovskite – Spiro-OMeTAD by Al_2O_3 significantly recovers V_{OC}, dropping the V_{OC} deficit in wide bandgap mixed-halide in a 4T tandem configuration [Werner et al, 2015].

as well as other Spiro-OMeTAD disadvantages is its strong absorption and high reflection losses in UV and visible region that ascends because of the photo induced oxidation of the material, which tends to degrade the film rapidly. As solution, high bandgap and stable materials selection for HTLs could decrease the absorption in visible light region [Taghavi et al, 2016.; Jiang et al, 2016]. Figure II-13 a presents the spiro-OMETAD constrains to work as HTL for tandem configuration and Figure II-13 b gives some approaches to achieve an efficient HTL.

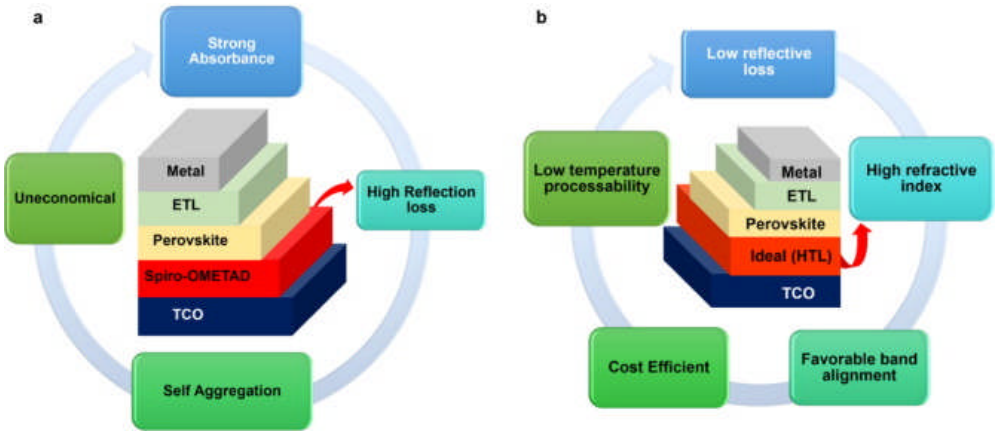

Figure II-13: a/ Limitations of using Spiro-OMETAD as HTL. b/ Required approaches to reach an efficient HTL [Akhil, 2021].

Even though the Spiro-OMeTAD is located at the bottom of the top PSC in the 4T-device, the highest parasitic absorption happens. As the oxidized Spiro-OMeTAD considerably absorbs light in the infrared and visible regions, only a small portion of light is transmitted into the lower Si cell leading to a considerable current loss (~1.8 mA cm^{-2}). Thus, the use of a thinner spiro-OMeTAD layer or the use of other HTMs with little parasitic absorption are vital.

The HTL width affects mainly the device performance and by reducing it (for instance spiro-OMeTAD in a monolithic device), it caused a reduction of parasitic absorption and higher light transmission [Albrecht et al., 17]. For the narrow HTL thickness, the high efficiency was reported and it is owing to the low recombination losses and also to reduced photoinduced oxidation of spiro-OMeTAD [Chen et al,2017].

With PCBM or ZnO electron-selective window layers that exhibit reduced parasitic absorption and improved stability, the inverted perovskite configurations are promising devices [You et al, 2016; Chen et al,2015]. In n-i-p and p-i-n (inverted) structures, the parasitic absorption is different as presented on the design of Figure II-14a

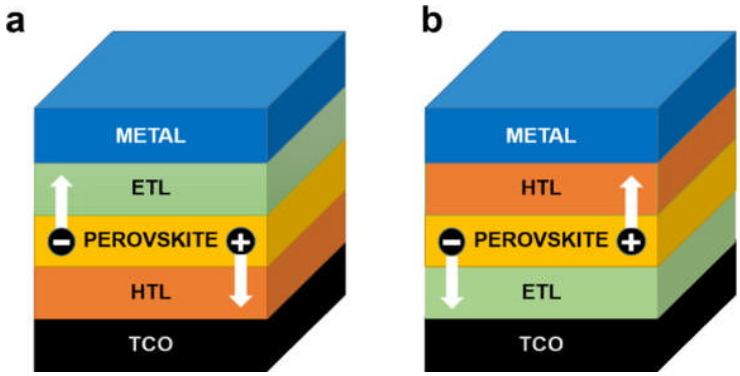

Figure II-14: a/ The p-i-n configuration (Inverted). b/ the n-i-p configuration [Akhil, 2021].

In the first structure (p-i-n), holes are collected at the transparent conductive oxides (TCOs) and electrons at the metallic back contact and contrarywise in the n-i-p configuration. The n-i-p architecture has been studied for 4T and monolithic devices. A monolithic device with an inverted p-i-n architecture and TiO2 as ETL allowed simulated efficiency up to 30% as well as minimized the parasitic loss of HTL [Filipič et al, 2015]. Furthermore, in p-i-n structure, the presence of spiro as HTL also exhibited lower parasitic absorption [Gilibert et al, 2020]. A comparative study of advanced p-i-n layer stacking (with C_{60} at the front) and n-i-p layer stacking (with spiro-OMeTAD) confirms that the earlier gave better performance [Bush et al, 2017], [Altazin et al,2018]. Similarly, the 3T configuration employs the Spiro-OMeTAD as the HTL to realize 17.1% of efficiency, where the device performance turned down when stacked with a united back-contact silicon sub-cell as a result of reflection loss [Tockhorn et al, 2020]. the Spiro-OMeTAD as HTL was also used in The three terminal heterojunction bipolar transistor device and effectively extract carriers to achieve an efficiency of 28.6% [Gilibert et al, 2020] PEDOT:PSS, composite PEDOT/graphene oxide (PEDOT:GO) (5.4 eV) [Zhang et al, 2018] , poly(triaryl amine) (PTAA) (5.4 eV) and nickel oxide (NiO_x) (5.4 eV) [Sun et al, 2018], as HTLs in perovskite solar cells are widely investigated but not that much studies are performed in tandem devices. Different HTMs in different tandem structures and their efficiency performance is presented in Table II-2. Figure II- 15 illustrates the relative HTLs energy levels.

Configuration	Top cell	Bottom cell	HTL	p-i-n/n-i-p configuration	V_{oc} (V)	J_{sc} (mA/ cm^2)	FF (%)	Area (cm^2)	P.C.E	Top Cell P.C.E (%)	Bottom Cell P.C.E (%)	Year	Ref
2T	$CH_3NH_3PbI_3$	C-Si	Spiro-OMeTAD	p-i-n	–	–	–		23.7	–	–	2020	N
4T	$Cs_{0.15}(CH_5N_2)_{0.85}Pb(I_{0.71}Br_{0.29})_3$	C-Si	Spiro-OMeTAD/ Al_2O_3	p-i-n	1.72	–	–	–	–	27.1	13.8	13.3	O
4T	$(FAPbI_3)_{0.95}(MAPbBr_3)_{0.05}$	P-Si	PTAA	p-i-n	0.65	13.5	80.10	–	26.0	18.9	7.1	2020	P
2T	$Cs_{0.17}FA_{0.8}Pb(Br_{0.17}I_{0.83})_3$	C-Si	NiO_x	p-i-n	1.65	18.1	79.00	–	23.6	–	–	2017	Q
3T	$MAPb(I_{0.95}Br_{0.05})_3$	C-Si	NiO_x	p-i-n	1.61	1.67	18.29	77	23.5	–	–	2019	R
3T	$(Cs_{0.05}(FA_{0.83}MA_{0.17})_{0.95}Pb(I_{0.83}Br_{0.17})_3)$	C-Si	Spiro-OMeTAD	n-i-p	–	–	–	–	17.1	11.7	5.4	2020	G
4T	$CH_3NH_3PbI_3$	P-Si	CuSCN	n-i-p	–	–	–	–	26.7	–	–	2018	B
2T	$Cs_mFA_nMA_{1-m-n}PbI_xBr_{3-x}$	C-Si	NiOx/poly-TPD	p-i-n	1.88	19.12	75.30	1	27.0	–	–	2020	U
2T	$(FAPbI_3)_{0.8}(MAPbBr_3)_{0.2}$	P-Si	PEDOT:GO	p-i-n	1.67	16.12	79.92	–	21.1	–	–	–	V
2T	$Cs_{0.05}(FA_{0.83}MA_{0.17})_{0.95}Pb(I_{0.8}Br_{0.2})_3$	C-Si	Poly TPD and NPD	p-i-n	1.74	17.93	74.31	–	25.2	–	–	–	W
2T	$CH_3NH_3PbI_3$	C-Si	PEDOT:PSS	n-i-p	1.78	14.70	80.40	–	21	–	–	2019	X

Table II-2: Different HTMs applied for different tandem cells configurations.

	Reference		Reference
N	[Abbasiyan etal, 2020]	U	[Xu et al, 2020]
O	[Abbasiyan et al, 2020]	V	[Wu et al,2017]
P	[Park et al,2020]	W	[Mazzarella et al,2019]
Q	[Bush et al,2017]	X	-[Ramírez et al,2019]
F	[Park et al,2019]	B	[Quiroz et al,2018]
G	[Quiroz et al,2018]		

A noticeable improvement could be achieved by replacing the low-loss, high-refractive-index inorganic HTL such as NiO_x in place of the spiro-OMeTAD layer [Quiroz et al, 2018]. By introducing NiO_x as HTL, the current density and V_{oc} output (more than 1.3V) of the upper perovskite cell can remarkably improve the thin component of NiO_x and its mesostructured scaffolding behavior makes it a good hole carrier for monolithic devices [Bush et al, 2017], Also, thermal damage to silicon is prevented due to its the lower annealing temperature. Consequently, a better Voc and stability which were obtained because of the interface (perovskite absorber/HTL) improvement (and reduced the formation of pinhole).

Moreover, a fabricated monolithic tandem cell with PTAA and NiOx showed less work function versus to PEDOT: PSS and therefore made better alignment of energy levels possible with the perovskite film, which results to an effective charge extraction, leading to enhance the J_{SC} and V_{OC}. Moreover, spin coating NiO_x deposition at relatively lower annealing temperature (220°C) on a 3T tandem configuration sidestepped the thermal damage of transparent contact and lower Si-cell [Santbergen et al, 2019]. Additionally, and fromnTableII-2 it is observable that high efficiencies can also result from a p-i-n configuration by employing proper ETLs.

Inorganic copper thiocyanate (CuSCN) has been largely proven in single junction cell, and also in tandem cells where it has been used as HTL. The CuSCN use as HTL and antireflection layer in 4T and p-i-n constructions decreases the optical loss because of the well-matched refractive index of the functional layers in the sub-cells. The reflected losses in a device are determined by material refractive index since the functional layers with approximately equal refractive index (RI) can diminish the optical reflection losses [Khan et al, 2019].

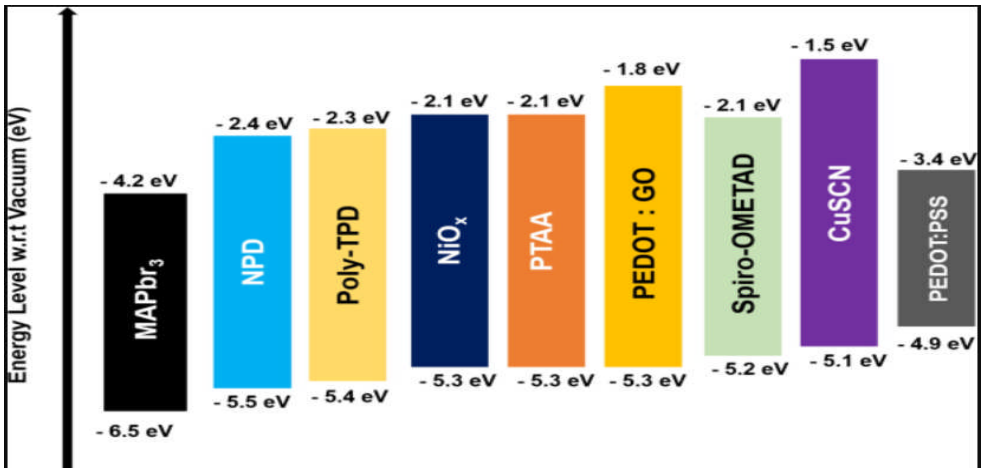

Figure II-15: Schematic representation of bandgap alignment of different HTMs used in tandem devices [Akhil, 2021].

In the following sections, the details on drift-diffusion modeling suitable for PSCs with an emphasis on the effect of mobile ions as well as how to treat the different recombination processes.

II- 4 Charge carriers transport modeling

II-4-1 Drift-diffusion (DD) model main equations

Typically, PSCs consist of two charge transport layers and in the middle a perovskite plus the electrodes. As presents Figure II-16 (a) a schematic representation of a characteristic energy diagram for a PSC with ETLs and HTLs plus the anode and cathode.

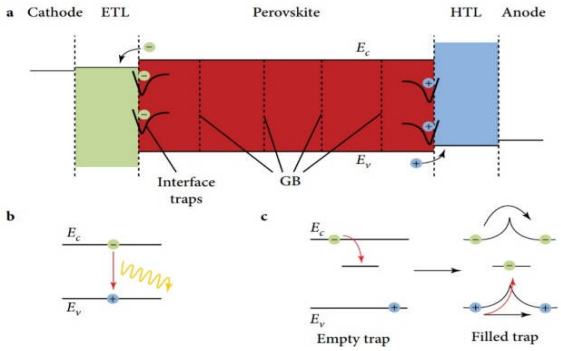

Figure II-16: a-Schematic energy diagram for a typical PSC prior to electrical contact. For the semiconductors, conduction and valence band are shown and for the electrodes work functions. In PSCs, mainly (b) band-to-band radiative recombination and (c) trap-assisted Shockley–Read–Hall recombination take place. As shown in (a) the trapping processes mostly happen at the perovskite/transport layer interfaces or at the grain boundaries [Vincent et al, 2020].

The drift diffusion modeling involves the three main sets of equations, here expressed in one dimension.

II-4-1-1-The current continuity equations

$$\begin{cases} \frac{\partial n(x,t)}{\partial t} = \frac{1}{q}\frac{\partial J_n(x,t)}{\partial x} + G(x,t) - R(x,t) \\ \frac{\partial p(x,t)}{\partial t} = -\frac{1}{q}\frac{\partial J_p(x,t)}{\partial x} + G(x,t) - R(x,t) \end{cases} \quad \text{II-1}$$

Where *x* and *t* are the coordinate position in the device and the time respectively. But, in a multilayer stack not only densities (the electron *n* and hole densities *p*) values are meant to change with *x* but also mobilities and dielectric constant values. Also, *Jn* and *Jp* the electron and hole currents, and G and R the electron/hole generation and recombination rate, respectively. These free charges movement is controlled either by diffusion because of the gradient in carrier density or by drift undergoing the electric field (recall that $\Delta\vec{V} = -gradE$, V is the electrostatic potential) and the electron and hole currents can be written as the charge transport equations [Selberherr, 1984]:

$$\begin{cases} J_n = -q.n.\mu_n \frac{\partial V}{\partial x} + qD_n \frac{dn}{dx} \\ J_p = -q.p.\mu_p \frac{\partial V}{\partial x} - qD_p \frac{dp}{dx} \end{cases} \quad \text{II-2}$$

with $\mu_{n,p}$ the charge electron and hole mobilities and $D_{n,p}$ the electron and hole diffusion coefficients as already detailed in chapter I. In solar cells, photon absorption dominates the generation rate G, in equation II-1, generally obtained by measuring the complex refractive index of all the layers and performing optical modeling based on the transfer matrix formalism [Burkhard et al., 2010]. And the recombination rate R, it is expressed by adding the contribution from the band-to-band/bimolecular recombination and trap-assisted SRH recombination.

Modelling PSCs is challenging compared to other semiconductors due to some reasons and among them is that ions as vacancies or interstitials can move through the structure. Henceforth, the continuity and *DD* equation also need to be written for anions X_a and cations X_c such as

$$\begin{cases} \frac{\partial X_a}{\partial t} = \frac{1}{q}\frac{\partial}{\partial x}\left(-qX_a\mu_a\frac{\partial V}{\partial x} + qD_a\frac{\partial X_a}{\partial x}\right) \\ \frac{\partial X_c}{\partial t} = \frac{1}{q}\frac{\partial}{\partial x}\left(-qX_c\mu_c\frac{\partial V}{\partial x} - qD_c\frac{\partial X_c}{\partial x}\right) \end{cases} \quad \text{II-3}$$

Generally, the movement of ions is limited to only the perovskite layer [Neukom et al., 2017;

Sherkar et al., 2017a; Tessler and Vaynzof, 2018; and Courtier et al., 2019a, 2019b]. But this limitation can be lifted in future explorations since it has been shown that the ions migrate inside the transport layers particularly during degradation [Matteocci et al., 2015; De Bastiani et al., 2016; Divitini et al., 2016; and Bi et al., 2017]. Moreover, the ions generation and recombination as well as the possibility that ions can act as trapping centers are generally ignored, which could also be taken into account. Poisson equation is main equation within transport equations

II-4-1-2-Poisson equation

$$\frac{\partial}{\partial x}\left(\varepsilon\frac{\partial V}{\partial x}\right) = -q(p - n + C_i) \qquad \text{II-4}$$

The ε is the permittivity, C_i can represent any other type of charge in the structure. In PSCs, the Poisson equation requires to be cautiously treated, as they contain plenty of potential charges for example: i- doping, especially in the transport layers; with N_A^- and N_D^+ being the ionized p-type and n-type doping respectively; ii- ions with X_c and X_a the cation and anion densities; and iii- the charged traps Σ_T^+ and Σ_T^- for hole and electron traps. So, the Poisson equation can be written as

$$\frac{\partial}{\partial x}\left(\varepsilon\frac{\partial V}{\partial x}\right) = -q(p - n + N_D^+ - N_A^- + X_c - X_a + \Sigma_T^+ - \Sigma_T^-) \qquad \text{II-5}$$

The interfaces with the anode and cathode can be chosen as boundaries conditions with the cathode at x=0 and the anode at x=L (L is the total thickness of the structure). In case of necessity, additional layers with different properties (mobilities, doping, dielectric constants, energy levels…) can be added when simulating to reproduce, for example, a typical solar cell stack with an energy diagram as shown in Figure II- 16 a. To numerically solve the aforementioned system of equations we need to specify the boundary conditions for the carrier densities

$$\begin{cases} n(0) = N_c e^{-\frac{\Phi_n}{V_T}} \\ n(L) = N_c e^{-\frac{E_{gap}-\Phi_p}{V_T}} \\ p(0) = N_v e^{-\frac{E_{gap}-\Phi_n}{V_T}} \\ p(L) = N_v e^{-\frac{\Phi_p}{V_T}} \end{cases} \qquad \text{II-6}$$

And the potential at the contacts

$$q\left(V(L) - V(0) + V_{app}\right) = W_c - W_a \qquad \text{II-7}$$

with N_c and N_v, the effective density of states for the conduction and valence band, φ_n and φ_p the electron and hole injection barrier at the cathode and anode, V_{app} being the externally applied voltage, and *Wa* and *Wc* the anode and cathode work functions, respectively. The built-in potential is given by $V_{bi} = (W_c - W_a)/q$. The E_{gap} in system equations II-6 can vary if there will be different layers in contact with the cathode and the anode.

II-4-2 Main recombination processes

The direct recombination of a free electron from the conduction band with a free hole from the valence band establish band-to-band recombination as shown in Figure II-16-b, typically associated by photon emission with same bandgap energy. Consequently, it is also so-called radiative recombination. The band-to-band recombination rate is given by:

$$R_B = \gamma(np - n_i^2) \qquad \text{II-8}$$

where γ is the band-to-band recombination rate constant and n_i is the intrinsic concentration of carriers. Values of γ generally vary between 10^{-11} and 10^{-9} cm^3/s in metal halide perovskites [Sherkar et al., 2017a, 2017b; Wolf et al., 2017; Ambrosio et al., 2018; Davies et al., al., 2018 Zhang et al., 2018; and Stolterfoht et al., 2019b]. Trap-assisted recombination process involves an electron and a hole recombination through a localized state in the bandgap as presented in Figure II-16 c. More details are already given in chapter I.

References of chapter II

[Lee et al., 2012] Lee, M. M., Teuscher, J., Miyasaka, T., Murakami, T. N., and Snaith, H. J. Efficient hybrid solar cells based on meso-superstructured organometal halideperovskites. *Science* 338, 643–647. doi: 10.1126/science.1228604, (2012).

[Zhou et al., 2014] Lee, M. M., Teuscher, J., Miyasaka, T., Murakami, T. N., and Snaith, H. JEfficient hybrid solar cells based on meso-superstructured organometal halideperovskites. *Science* 338, 643–647. doi: 10.1126/science.1228604, (2012).

[Dong et al., 2015] Dong, Q., Fang, Y., Shao, Y., Mulligan, P., Qiu, J., Cao, L., et al., Solar cellsElectron-hole diffusion lengths >175 mum in solution-grown CH3NH3PbI3single crystals. *Science* 347, 967–970. doi: 10.1126/science.aaa5760, (2015)

[Laboratory, 2019] Laboratory, N. R. E *Best Research-Cell Efficiency Chart.* https://www.nrel.gov/pv/assets/pdfs/best-research-cell-efficiencies. 20200925.pdf, . (2019).

[Malinkiewicz et al., 2013] Malinkiewicz, O., Yella, A., Lee, Y. H., Espallargas, G. M., Graetzel, M., Nazeeruddin, M. K., et al. Perovskite solar cells employing organic charge-transport layers. *Nat. Photonics* 8, 128–132doi: 10.1038/nphoton.2013.341, (2013).

[Rong et al., 2018] Rong, Y., Hu, Y., Mei, A., Tan, H., Saidaminov, M. I., Seok, S. I., et alChallenges for commercializing perovskite solar cells. *Science* 361ea at8235.,(2018).

[Enebe et al., 2019] G. C. Enebe, K. Ukoba, and T.-C. Jen, “Numerical modeling of effect of annealing on nanostructured CuO/TiO2 pn heter- ojunction solar cells using SCAPS,” AIMS Energy, vol. 7, pp. 527–538, 2019.

[Zulqarnain Haider et al., 2018] S. Zulqarnain Haider, H. Anwar, and M. Wang, “A com- prehensive device modelling of perovskite solar cell with inorganic copper iodide as hole transport material,” Semi-conductor Science Technology, vol. 33, p. 12, 2018.

[Lin et al., 2017] L. Lin, L. Jiang, Y. Qiu, and Y. Yu, “Modeling and analysis of HTM-free perovskite solar cells based on ZnO electron transport layer,” Superlattices and Microstructures, vol. 104, pp. 167–177, 2017.

[Kai Tan et al., 2016] K. Tan, P. Lin, G. Wang, Y. Liu, Z. Xu, and Y. Lin, “Con- trollable design of solid-state perovskite solar cells by SCAPS device simulation,” Solid-State Electronics, vol. 126, pp. 75–80, 2016.

[Hui Li and Wei Zhang,2020] Hui Li and Wei Zhang, Perovskite Tandem Solar Cells: From Fundamentals to Commercial Deployment, https://dx.doi.org/10.1021/acs.chemrev.9b00780,2020.

[Yin et al ,2015] Yin, W.-J.; Yang, J.-H.; Kang, J.; Yan, Y.; Wei, S.-H. Haliden Perovskite Materials for Solar Cells: a Theoretical Review. J. Mater. Chem., 3, 8926−8942 ,A 2015.

[Tong, et al ,2019] Tong, J.; Song, Z.; Kim, D. H.; Chen, X.; Chen, C.; Palmstrom, A. F.; Ndione, P. F.; Reese, M. O.; Dunfield, S. P.; Reid, O. G.; et al. Carrier Lifetimes of > 1 μs in Sn-Pb Perovskites Enable Efficient All- Perovskite Tandem Solar Cells. Science, 364, 475−479,2019.

[Yin et al ,2014] Yin, W.-J.; Shi, T.; Yan, Y. Unusual Defect Physics in CH3NH3PbI3 Perovskite Solar Cell Absorber. Appl. Phys. Lett., 104, 063903,2014.

[Snaith ,2013] Snaith, H. J. Perovskites: The Emergence of a New Era for Low-Cost, High-Efficiency Solar Cells. J. Phys. Chem. Lett., 4, 3623−3630,2013.

[Green et al ,2014] Green, M. A.; Ho-Baillie, A.; Snaith, H. J. The Emergence of Perovskite Solar Cells. Nat. Photonics, 8, 506−514,2014.

[eijtens et al,2018] L eijtens, T.; Bush, K. A.; Prasanna, R.; McGehee, M. D.Opportunities and Challenges for Tandem Solar Cells Using Metal Halide Perovskite Semiconductors. Nat. Energy, 3, 828−838,2018.

[Green et al,2014] Green, M. A.; Ho-Baillie, A.; Snaith, H. J. The Emergence of Perovskite Solar Cells. Nat. Photonics, 8 (7), 506−514,2014.

[Jena et al,2019] Jena, A. K.; Kulkarni, A.; Miyasaka, T. Halide PerovskitePhotovoltaics: Background, Status, and Future Prospects. Chem. Rev., 119, 3036−3103,2019.

[Stoumpos et al,2015] Stoumpos, C. C.; Frazer, L.; Clark, D. J.; Kim, Y. S.; Rhim, S.H.; Freeman, A. J.; Ketterson, J. B.; Jang, J. I.; Kanatzidis, M. G, Hybrid germanium iodide perovskite semiconductors: active lone pairs, structural distortions, direct and indirect energy gaps, and strong nonlinear optical propertiesHybrid Germanium Iodide Perovskite Semiconductors: Active Lone Pairs, Structural Distortions, Direct and Indirect Energy Gaps, and
Strong Nonlinear Optical Properties. J. Am. Chem. Soc., 137,6804−6819,2015.

[Noh et al,2013] Noh, J. H.; Im, S. H.; Heo, J. H.; Mandal, T. N.; Seok, S. I.Chemical Management for Colorful, Efficient, and Stable Inorganic−Organic Hybrid Nanostructured Solar Cells. Nano Lett., 13,1764−1769,2013.

[Kulbak et al,2015] Kulbak, M.; Cahen, D.; Hodes, G. How Important Is the Organic Part of Lead Halide Perovskite Photovoltaic Cells? Efficient CsPbBr3 Cells. J. Phys. Chem. Lett., 6, 2452−2456,2015.

[Anaya et al,2017] Anaya, M.; Lozano, G.; Calvo, M. E.; Míguez, H. ABX3 Perovskites for Tandem Solar Cells. Joule, 1, 769−793,2017.

[Luo et al,2020] Luo, D.; Su, R.; Zhang, W.; Gong, Q.; Zhu, R. Minimizing Non-Radiative Recombination Losses in Perovskite Solar Cells. Nat. Rev. Mater., 5, 44−60,2020.

[Kojima et al,2009] Kojima, A.; Teshima, K.; Shirai, Y.; Miyasaka, T. Organometal Halide Perovskites as Visible-Light Sensitizers for Photovoltaic Cells.J. Am. Chem. Soc., 131, 6050−6051,2009.

[Liang et al,2019] Liang, T. S.; Pravettoni, M.; Deline, C.; Stein, J. S.; Kopecek,R.; Singh, J. P.; Luo, W.; Wang, Y.; Aberle, A. G.; Khoo, Y. S. AReview of Crystalline Silicon Bifacial Photovoltaic Performance Characterisation and Simulation. Energy Environ. Sci., 12, 116−148,2019.

[Ramanujam and Singh,2017] Ramanujam, J.; Singh, U. P. Copper Indium Gallium Selenide Based Solar Cells−a Review. Energy Environ. Sci., 10, 1306−1319,2017.

[Chantana et al,2020] Chantana, J.; Kawano, Y.; Nishimura, T.; Kimoto, Y.; Kato, T.;Sugimoto, H.; Minemoto, T. 22%-Efficient Cd-Free Cu(In,Ga)-(S,Se)2 Solar Cell by All-Dry Process Using Zn0.8Mg0.2O andZn0.9Mg0.1O:B as Buffer and Transparent Conductive Oxide Layers.Prog. Photovoltaics, 28, 79−89,2020.

[Travis et al,2016] Travis, W.; Glover, E. N. K.; Bronstein, H.; Scanlon, D. O.;Palgrave, R. G. On theApplication of the Tolerance Factor to Inorganic and Hybrid Halide Perovskites: a Revised System. Chem. Sci., 7, 4548−4556,2016.

[Manser et al,2016] Manser, J. S.; Christians, J. A.; Kamat, P. V. Intriguing Optoelectronic Properties of Metal Halide Perovskites. Chem. Rev., 116, 12956−13008,2016.

[Park,2015] Park, N. G. Perovskite Solar Cells: an Emerging Photovoltaic Technology. Mater. Today, 18, 65−72,2015.

[Shen et al,2020] Shen, H. P.; Walter, D.; Wu, Y. L.; Fong, K. C.; Jacobs, D. A.; Duong, T.; Peng, J.; Weber, K.; White, T. P.; Catchpole, K. R. Monolithic Perovskite/Si Tandem Solar Cells: Pathways to Over 30% Efficiency. Adv. Energy Mater., 10, 1902840,2020.

[Eperon et al,2017] Eperon, G. E.; Horantner, M. T.; Snaith, H. J. Metal halide Perovskite Tandem and Multiple-Junction Photovoltaics. Nat. Rev.Chem., 1, 0095,2017.

[Sheng et al,2015] Sheng, R.; Ho-Baillie, A. W. Y.; Huang, S. J.; Keevers, M.; Hao, X. J.; Jiang, L. C.; Cheng, Y. B.; Green, M. A. Four-Terminal Tandem Solar Cells Using CH3NH3PbBr3 by Spectrum Splitting. J. Phys. Chem. Lett., 6, 3931−3934,2015.

[Weber et al,1978] Weber, D.. Z. Naturforsch., B: J. Chem CH3NH3PbX3, ein Pb(II)-System mit kubische Perowskitstruktur/CH3NH3PbX3, a Pb(II)-System with Cubic Per-ovskite Structure. Sci., 33b,1443−1445,1978.

[K. Tan et al,2016] K. Tan, P. Lin, G. Wang, Y. Liu, Z. Xu, and Y. Lin, “Con- trollable design of solid-state perovskite solar cells by SCAPS device simulation,” Solid-State Electronics, vol. 126, pp. 75–80,2016.

[. Lin et al,2017] L. Lin, L. Jiang, Y. Qiu, and Y. Yu, “Modeling and analysis of HTM-free perovskite solar cells based on ZnO electron transport layer,” Superlattices and Microstructures, vol. 104, pp. 167–177, 2017.

[Singh et al ,2017] N. Singh, A. Chaudhary, S. Saxena, M. Saxena, and N. Rastogi, “Electrical simulation of organic solar cell at different charge carrier mobility,” IOSR Journal of Applied Physics, vol. 9, no. 2, pp. 01–04, 2017.

[Mandadapu et al ,2017] U. Mandadapu, S. Victor Vedanayakam, and K.)yagarajan, “Simulation and analysis of lead based perovskite solar cell using SCAPS-1D,” Indian Journal of Science and Technology, vol. 10, no. 1, pp. 1–8, 2017.

[Zulqarnain et al ,2018] S. Zulqarnain Haider, H. Anwar, and M. Wang, “A com- prehensive device modelling of perovskite solar cell with inorganic copper iodide as hole transport material,” Semi-conductor Science Technology, vol. 33, p. 12, 2018.

[Slami et al ,2019] A. Slami, M. Bouchaour, and L. Merad, “Numerical study of ased perovskite solar cells by SCAPS-1D,” International Journal of Energy and Environment (IJEE), vol. 13, pp. 17–21, 2019.

[Enebe, et al ,2019] G. C. Enebe, K. Ukoba, and T.-C. Jen, “Numerical modeling of effect of annealing on nanostructured CuO/TiO2 pn heter- ojunction solar cells using SCAPS,” AIMS Energy, vol. 7,pp. 527–538, 2019.

[Liu et al, 2020] Na Liu, Lina Wang1, Fan Xu , Jiafeng Wu , Tinglu Song1and Qi Chen, ‘Recent Progress in Developing Monolithic Perovskite/Si Tandem Solar Cells ‘, Revue, Frontiers in chemistry, https://doi.org/10.3389/fchem.2020.603375 , 2020

Abrivation and words

[Beiley et al,2013]Beiley,Z.M.,Christoforo ,M.G., Gratia, P., Bowring, A. R., Eberspacher, P.,Margulis, G. Y. et al, Semi-transparent polymer solar cells with excellent sub-bandgap transmission for third generation photovoltaics. *Adv. Mater.* 25, 7020–7026. doi: 10.1002/adma.201301985,(2013)

[De et al,2009]De, S., Higgins, T. M., Lyons, P. E., Doherty, E. M., Nirmalraj, P. N., Blau, W. J., et al, Silver nanowire networks as flexible, transparent, conductingfilms: extremely high DC to optical conductivity ratios. *ACS Nano* 3, 1767–1774. doi: 10.1021/nn900348c,(2009)

[Margulis et al,2013]Margulis, G. Y., Christoforo, M. G., Lam, D., Beiley, Z. M., Bowring, A. R., Bailie, C. D., et al, Spray deposition of silver nanowire electrodes forsemitransparent solid-state dye-sensitized solar cells. *Adv. Energy Mater.* 31657–1663. doi: 10.1002/aenm.201300660,(2013)

[Chen et al,2019]Chen, H., Li, M., Wen, X., Yang, Y., He, D., Choy, W. C. H., et al, Enhanced silver nanowire composite window electrode protected by largesize graphene oxide sheets for perovskite solar cells. *Nanomaterials* 9:193. doi: 10.3390/nano9020193,(2019)

[Leijtens et al,2018]Leijtens, T., Bush, K. A., Prasanna, R., and McGehee, M. D.. Opportunitiesand challenges for tandem solar cells using metal halide perovskitesemiconductors. *Nat. Energy* 3, 828–838. doi: 10.1038/s41560-018-0190-4,(2018a)

[Zou et al,2014]Zou, J., Li, C. Z., Chang, C. Y., Yip, H. L., and Jen, A. K. Interfacialengineering of ultrathin metal film transparent electrode for flexible organicphotovoltaic cells. *Adv. Mater.* 26, 3618–3623. doi: 10.1002/adma.201306212,(2014).

[Yang et al,2015]Yang, Y. M., Chen, Q., Hsieh, Y.-T., Song, T.-B., Marco, N. D., Zhou, H., et al.. Multilayer transparent top electrode for solution processedperovskite/cu(in,ga)(se,s)2 four terminal tandem solar cells. *ACS Nano* 9, 7714–7721. doi: 10.1021/acsnano.5b03189,(2015)

[Chen et al,2016]Chen, B., Bai, Y., Yu, Z., Li, T., Zheng, X., Dong, Q., et al. Efficient semitransparent perovskite solar cells for 23.0%-efficiencyperovskite/silicon four-terminal tandem cells. *Adv. Energy Mater.* 6:1601128. doi: 10.1002/aenm.201601128,(2016).

[Loper et al,2015]Loper, P., Moon, S. J., de Nicolas, S. M., Niesen, B., Ledinsky, M., Nicolay, S., et al.. Organic-inorganic halide perovskite/crystalline silicon fourterminal tandem solar cells. *Phys. Chem. Chem. Phys.* 17, 1619–1629. doi: 10.1039/C4CP03788J,(2015)

[Liang et al,2018] Liang, F., Lin, Y., He, Z., Chen, W., Zhu, Y., Chen, T., et al. Promising ITOfree perovskite solar cells with WO3-Ag–SnO2 as transparent conductive oxide. *J. Mater. Chem. A* 6, 19330–19337. doi: 10.1039/C8TA08287A,(2018)

[Gluba et al,2013] Gluba, M. A., Amkreutz, D., Troppenz, G. V., Rappich, J., and Nickel, N. H. Embedded graphene for large-area silicon-based devices. *Appl. PhysLett.* 103:073102. doi: 10.1063/1.4818461,(2013)

[Lang et al,2015] Lang, F., Gluba, M. A., Albrecht, S., Rappich, J., Korte, L., Rech, B., et al. Perovskite solar cells with large-area CVD-graphene for tandem solar cells. *JPhys. Chem. Lett.* 6, 2745–2750. doi: 10.1021/acs.jpclett.5b01177,(2015).

[Yang et al,2019] Yang, Z., Yu, Z., Wei, H., Xiao, X., Ni, Z., Chen, B., et al. Enhancing electron diffusion length in narrow-bandgap perovskites forefficient monolithic perovskite tandem solar cells. *Nat. Commun.* 10:4498. doi: 10.1038/s41467-019-12513-x,(2019).

[Yoon et al,2017] Yoon, J., Sung, H., Lee, G., Cho, W., Ahn, N., Jung, H. S., et al. Super flexible, high-efficiency perovskite solar cells utilizing graphene electrodes: towards future foldable power sources. *Energy Environ. Sci.* 10,337–345. doi: 10.1039/C6EE02650H,(2017)

[Li et al,2014] Li, Z., Kulkarni, S. A., Boix, P. P., Shi, E., Cao, A., Fu, K., et al. Laminated carbon nanotube networks for metal electrode-free efficient perovskite solar cells. *ACS Nano* 8, 6797–6804. doi: 10.1021/nn501096h, 2014

[De and Coleman,2010] De, S., and Coleman, J. N. Are there fundamental limitations on the sheet resistance and transmittance of thin graphene films? *ACS Nano* 4, 2713–2720. doi: 10.1021/nn100343f,(2010)

[Raïssi et al, 2015] Raïssi, M., Vignau, L., Clout et, E., and Ratier, B.. Soluble carbonnanotubes/phthalocyanines transparent electrode and interconnection layers for flexible inverted polymer tandem solar cells. *Org. Electron.* 21, 86–91doi: 10.1016/j.orgel.2015.03.003,(2015)

[Chawla et al,2017] Chawla, R., Singhal, P., and Garg, A. K. Design and modelling of G–ZnO nanocomposite electrode for a-Si:H/µc-Si:H micromorph solar cell. *IntJ. Inform. Technol.* 10, 265–277. doi: 10.1007/s41870-017-0043-6, (2017)

[Bryant et al,2014] Bryant, D., Greenwood, P., Troughton, J., Wijdekop, M., Carnie, M., Davies, M.,

et al,. A transparent conductive adhesive laminate electrode for highefficiency organic-inorganic lead halide perovskite solar cells. *Adv. Mater.* 26, 7499–7504. doi: 10.1002/adma.201403939,(2014)

[Jiang et al,2015] Jiang, F., Liu, T., Zeng, S., Zhao, Q., Min, X., Li, Z., et al. Metal electrode–free perovskite solar cells with transfer-laminated conductingpolymer electrodes. *Opt. Express* 23, 7499–7504. doi: 10.1364/OE.23.000A83, (2015).

[Jesper Jacobsson et al,2016] Jesper Jacobsson, T., Correa-Baena, J.-P., Pazoki, M., Saliba, M., Schenk, K., Grätzel, M., et al. Exploration of the compositional space for mixedlead halogen perovskites for high efficiency solar cells. *Energy Environ. Sci.* 9, 1706–1724. doi: 10.1039/C6EE00030D, (2016)

[Lal et al,2014] Lal, N. N., White, T. P., and Catchpole, K. R. Optics and light trapping for tandem solar cells on silicon. *IEEE J. Photovol.* 4, 1380–1386. doi: 10.1109/JPHOTOV.2014.2342491, (2014)

[Yu et al,2016] Yu, Z., Leilaeioun, M., and Holman, Z. Selecting tandem partners forsilicon solar cells. *Nat. Energy* 1:16137. doi: 10.1038/nenergy.2016.137, (2016)

[Tanaka et al., 2003]Tanaka, K., Takahashi, T., Ban, T., Kondo, T., Uchida, K., and Miura, N. Comparative study on the excitons in lead-halide-based perovskite-typecrystals CH3NH3PbBr3 CH3NH3PbI3. *Solid State Commun.*127, 619–623. doi: 10.1016/S0038-1098(03)00566-0, (2003)

[Noh et al., 2013]Noh, J. H., Im, S. H., Heo, J. H., Mandal, T. N., and Seok, S. I. Chemicalmanagement for colorful, efficient, and stable inorganic-organic hybridnanostructured solar cells. *Nano Lett.* 13, 1764–1769. doi: 10.1021/nl400349b, (2013)

[Jesper Jacobson et al., 2016] Jesper Jacobsson, T., Correa-Baena, J.-P., Pazoki, M., Saliba, M., Schenk, K., Grätzel, M., et al. Exploration of the compositional space for mixedlead halogen perovskites for high efficiency solar cells. *Energy Environ. Sci.* 9, 1706–1724. doi: 10.1039/C6EE00030D, (2016).

[Chen et al., 2019]Chen, B., Yu, Z., Liu, K., Zheng, X., Liu, Y., Shi, J., et al. Grain engineeringfor perovskite/silicon monolithic tandem solar cells with efficiency of 25.4%.*Joule* 3, 177–190. doi: 10.1016/j.joule.2018.10.003, (2019)

[Xu et al., 2020] Xu, J., Boyd, C. C., Yu, Z. J., Palmstrom, A. F., Witter, D. J., Larson, B. W., et al. Triple-halide wide–band gap perovskites withsuppressed phase segregation for efficient tandems. *Science* 361, 1097–1104. doi: 10.1126/science aaz5074,(2020).

[Ju et al., 2017]Ju, M.-G., Dai, J., Ma, L., and Zeng, X. C. Lead-free mixed tin andgermanium perovskites for photovoltaic application. *J. Am. Chem. Soc.* 139, 8038–8043. doi: 10.1021/jacs.7b04219, (2017)

[Liu et al., 2017]Liu, J., Wang, G., Song, Z., He, X., Luo, K., Ye, Q., et al. FAPb1-xSnxI3mixed metal halide perovskites with improved light harvesting and stabilityfor efficient planar heterojunction solar cells. *J. Mater. Chem. A.* 5, 9097–9106. doi: 10.1039/C6TA11181E, (2017).

[Williams et al., 2017]Williams, S. T., Rajagopal, A., Jo, S. B., Chueh, C.-C., Tang, T. F. L., Kraeger, A., et al. Realizing a new class of hybrid organic-inorganic multifunctional perovskite. *J. Mater. Chem. A* 5, 10640–10650. doi: 10.1039/C7TA01327B, (2017).

[Lee J. W. et al, 2015] Lee, Y., Park, C., Balaji, N., Lee, Y.-J., and Dao, V. A. High-efficiency silicon solar cells: a review. *Isr. J. Chem.* 55, 1050–1063. doi: 10.1002/ijch.201400210, (2015).

[Smith et al, 2014]Smith, I. C., Hoke, E. T., Solis-Ibarra, D., McGehee, M. D., and Karunadasa, H. I. A layered hybrid perovskite solar-cell absorber withenhanced moisture stability. *Angew. Chem. Int. Ed. Engl.* 53, 11232–11235. doi: 10.1002/anie.201406466,(2014)

[Stoumpos et al, 2016] Stoumpos, C. C., Cao, D. H., Clark, D. J., Young, J., Rondinelli, J. M., Jang, J. I., et al. Ruddlesden–popper hybrid lead iodideperovskite 2D homologous semiconductors. *Chem. Mater.* 28, 2852–2867. doi: 10.1021/acs.chemmater.6b00847, (2016)

[Tsai et al., 2016]Tsai, H., Nie, W., Blancon, J.-C., Stoumpos, C. C., Asadpour, R., Harutyunyan, B., et al. High-efficiency two-dimensional ruddlesden–popper perovskitesolar cells. *Nature* 536, 312–316. doi: 10.1038/nature18306, (2016).

[Liu et al., 2020a,b]Liu, N., Liu, P., Ren, H., Xie, H., Zhou, N., Gao, Y., et al. (2020a). Probing phase distribution in 2D perovskites for efficient device design. *ACS Appl. MaterInterfaces* 12, 3127–3133. doi: 10.1021/acsami.9b17047

[Liang et al., 2016] Liang, J., Wang, C., Wang, Y., Xu, Z., Lu, Z., Ma, Y., et al.. All inorganic perovskite solar cells. *J. Am. Chem. Soc.* 138, 15829–15832. doi: 10.1021/jacs.6b10227, (2016)

[Bush et al., 2018] Bush, K. A., Frohna, K., Prasanna, R., Beal, R. E., Leijtens, T., Swifter, S. A., et al. Compositional engineering for efficient wide band gap perovskites withimproved stability to photoinduced phase segregation. *ACS Energy Lett.* 3, 428–435. doi: 10.1021/acsenergylett.7b01255, (2018).

[Mailoa et al, 2015 ;] Mailoa, J. P., Bailie, C. D., Johlin, E. C., Hoke, E. T., Akey, A. J., Nguyen, W. H., et al. A 2-terminal perovskite/silicon multijunction solar cell enabled by a silicon tunnel junction. *Appl. Phys. Lett.* 106:121105. doi: 10.1063/1. 4914179;(2015).

[Hoye et al, 2018]Hoye, R. L. Z., Bush, K. A., Oviedo, F., Sofia, S. E., Thway, M., Li, X., et al.. Developing a robust recombination contact to realize monolithic perovskitetandems with

industrially common p-Type silicon solar cells. *IEEE J. Photovol*8, 1023–1028. doi: 10.1109/JPHOTOV.2018.2820509, (2018)

[Albrecht et al, 2016b] Albrecht, S., Saliba, M., Correa-Baena, J.-P., Jäger, K., Korte, L., Hagfeldt, A., et al. Towards optical optimization of planar monolithicperovskite/silicon-heterojunction tandem solar cells. *J. Optics* 18:064012doi: 10.1088/2040-8978/18/6/064012, (2016a)

[Barraud et al,2013] Barraud, L., Holman, Z. C., Badel, N., Reiss, P., Descoeudres, A., Battaglia, C., et al. Hydrogen-doped indium oxide/indium tin oxide bilayers for highefficiency silicon heterojunction solar cells. *Solar Energy Mater. Solar Cells* 115, 151–156. Doi 10.1016/ j. solmat.2013.03. 02 4, (2013).

[Song et al,2016] Song, Z., Werner, J., Shrestha, N., Sahli, F., De Wolf, S., Niesen, B., et al. Probing Photocurrent nonuniformities in the subcells of monolithicperovskite/silicon tandem solar cells. *J. Phys. Chem. Lett.* 7, 5114–5120. doi: 10.1021/acs.jpclett.6b02415, (2016).

[Werner et al, 2016b] Werner, J., Walter, A., Rucavado, E., Moon, S.-J., Sacchetto, D., Rienaecker, M., et al. Zinc tin oxide as high-temperature stable recombination layer formesoscopic perovskite/silicon monolithic tandem solar cells. *Appl. Phys. Lett.* 109:233902. doi: 10.1063/1.4971361, (2016b).

[Lee et al., 2016] Lee, J., Kang, H., Kee, S., Lee, S. H., Jeong, S. Y., Kim, G., et al. Long-term stable recombination layer for tandem polymer solar cells usingself-doped conducting polymers. *ACS Appl. Mater. Interfaces* 8, 6144–6151. doi: 10.1021/acsami.5b11742, (2016).

[Jiang et al., 2016] Jiang, F., Liu, T., Luo, B., Tong, J., Qin, F., Xiong, S., et alA two-terminal perovskite/perovskite tandem solar cell. *J. Mater. Chem. A* 4, 1208–1213 doi: 10.1039/C5TA08744A, (2016).

[Zheng et al. [2018] Zhang, D., Najafi, M., Zardetto, V., Dörenkämper, M., Zhou, X., Veenstra, S., et al. High efficiency 4-terminal perovskite/c-Si tandem cells. *Solar EnergyMater. Solar Cells* 188, 1–5. Doi : 10.1016/j.solmat.2018.07.032, (2018).

[Shen et al, 2018] Shen, H., Omelchenko, S. T., Jacobs, D. A., Yalamanchili, S., Wan, Y., Yan, D., et al *In situ* recombination junction between p-Si and TiO2 enables high-efficiency monolithic perovskite/Si tandem cells. *Sci. Adv.* 4: eaau 9711.doi: 10.1126/ sciadv.aau9711, (2018)

[Bi et al., 2015] Bi, C., Wang, Q., Shao, Y., Yuan, Y., Xiao, Z., and Huang, J. Non-wetting surface-driven high-aspect-ratio crystalline grain growth for efficient hybrid perovskite solar cells. *Nat. Commun.* 6 :7747. doi : 10.1038/ncomms8747, (2015).

[Sahli et al, 2018] Sahli, F., Kamino, B. A., Werner, J., Bräuninger, M., Paviet-Salomon, B., Barraud, L., et al. Improved optics in monolithic perovskite/silicon tandem solar cells with a nanocrystalline silicon recombination junction. *Adv. Energy Mater* 8:1701609. doi: 10.1002/aenm.201701609, (2018).

[Kim et al, 2018] Kim, J., Takiguchi, Y., and Miyajima, S. Characterization of p-type nitrogen-doped cuprous oxide/n-type hydrogenated microcrystalline silicontunnel recombination junction for perovskite/crystalline silicon tandem solarcells. *Japan. J. Appl. Phys.* 57:08RB05. doi: 10.7567/JJAP.57.08RB05, (2018).

[Mahmood et al, 2017] K. Mahmood, S. Sarwar, M.T. Mehran, **Current status of electron transport layers in perovskite solar cells: materials and properties** RSC Adv, pp. 17044-17062, (2017)

[Kim et al,2020] T. Kim, J. Lim, S. Song **Recent Progress and Challenges of Electron Transport Layers in Organic-Inorganic Perovskite Solar Cells** Energies, 13 (2020)

[Calado et al, 2016] P. Calado, A.M. Telford, D. Bryant, X. Li, J. Nelson, B.C. O'Regan, P.R.F. Barns**Evidence for ion migration in hybrid perovskite solar cells with minimal hysteresis** Nat. Commun, p. 13831., 7 (2016)

[Dong et al,2015] Q. Dong, Y. Fang, Y. Shao, P. Mulligan, J. Qiu, L. Cao,J.Huang **Electron-hole diffusion lengths >175 μm in solution-grown $CH_3NH_3PbI_3$ single crystals** Science,347, p. 967, (2015)

[Gao et al,2015]Q. Gao, S. Yang, L. Lei, S. Zhang, Q. Cao, J. Xie, J. Li, Y. Liu **An Effective TiO2 Blocking Layer for Perovskite Solar Cells with Enhanced Performance** Chem. Lett., 44 , pp. 624-626,(2015).

[Choi et al, 2016] J. Choi, S. Song, M.T. Hörantner, H.J. Snaith, T. Park **Well-Defined Nanostructured, Single-Crystalline TiO2 Electron Transport Layer for Efficient Planar Perovskite Solar Cells** ACS Nano, 10 , pp. 6029-6036, (2016)

[Lamanna et al,2020]E. Lamanna, F. Matteocci, E. Calabrò, L. Serenelli, E. Salza, L. Martini, F. Menchini, M. Izzi, A. Agresti, S. Pescetelli, S. Bellani, A.E. Del Río Castillo, F. Bonaccorso, M. Tucci, A. Di Carlo, Mechanically Stacked, Two-Terminal Graphene-Based Perovskite/Silicon Tandem Solar Cell with Efficiency over 26%, Joule 4 865-881, (2020).

[Kusuma et al,2018] J. Kusuma, R.G. Balakrishna, S. Patil, M.S. Jyothi, H.R. Chandan, R. Shwetharani **Exploration of graphene oxide nanoribbons as excellent electron conducting network for third generation solar cells** Sol. Energy Mater. Sol. Cells, 183 , pp. 211-219,(2018).

[Williams and Seger,2008] G. Williams, B. Seger, P.V. Kamat, **TiO2-Graphene Nanocomposites, UV-Assisted Photocatalytic Reduction of Graphene Oxide** ACS Nano, 2 , pp. 1487-1491, (2008)

[Paik et al,2020]M.J. Paik, Y. Lee, H.-S. Yun, S.-U. Lee, S.-T. Hong, S.I. Seok,**TiO2 Colloid-Spray Coated Electron-Transporting Layers for Efficient Perovskite Solar Cells** Adv. Energy Mater., 10 , p. 2001799, (2020)

[Albrecht et al,2016]S. Albrecht, M. Saliba, J.P.C. Baena, F. Lang, L. Kegelmann, M. Mews, L. Steier, A. Abate, J. Rappich, L.J.E. Korte, E. Science, Monolithic perovskite/silicon-heterojunction tandem solar cells processed at low temperature, 9 81–88, (2016).

[Quiroz et al,2018] C.O.R. Quiroz, Y. Shen, M. Salvador, K. Forberich, N. Schrenker, G.D. Spyropoulos, T. Heumüller, B. Wilkinson, T. Kirchartz, E. Spiecker, **Balancing electrical and optical losses for efficient 4-terminal Si–perovskite solar cells with solution processed percolation electrodes** J. Mater. Chem. A, 6 , pp. 3583-3592, (2018)

[Ying et al, 2020] Z. Ying, Y. Zhu, X. Feng, J. Xiu, R. Zhang, X. Ma, Y. Deng, H. Pan, Z. He **Sputtered Indium-Zinc Oxide for Buffer Layer Free Semitransparent Perovskite Photovoltaic Devices in Perovskite/Silicon 4T-Tandem Solar Cells**
, p. 2001604, (2020).

[Chen et al,2020]B. Chen, S.-W. Baek, Y. Hou, E. Aydin, M. De Bastiani, B. Scheffel, A. Proppe, Z. Huang, M. Wei, Y.-K.J.N.c. Wang, Enhanced optical path and electron diffusion length enable high-efficiency perovskite tandems, 11 1–9,(2020).

[Werner et al,2016]J. Werner, C.-H. Weng, A. Walter, L. Fesquet, J.P. Seif, S. De Wolf, B. Niesen, C.J.T.j.o.p.c.l. Ballif, Efficient monolithic perovskite/silicon tandem solar cell with cell area >1 cm2, 7 161–166,(2016).

[Park et al,2019] I.J. Park, J.H. Park, S.G. Ji, M.-A. Park, J.H. Jang, J.Y. Kim, **A Three-Terminal Monolithic Perovskite/Si Tandem Solar Cell Characterization Platform**, Joule, 3, pp. 807-818,(2019)

[Tockhorn et al, 2020] P. Tockhorn, P. Wagner, L. Kegelmann, J.-C. Stang, M.Mews, S. Albrecht,L. Korte, **Three-Terminal Perovskite/Silicon Tandem Solar Cells with Top and Interdigitated Rear Contacts**, ACS Appl. Energy Mater.,3 , pp. 1381-1392 ,2020

[Lee et al,2019] S.-W. Lee, S. Bae, K. Cho, S. Kim, J.-K. Hwang, W. Lee, S. Lee, J.Y. Hyun, S. Lee, S.B Choi, H. Chun, W.M. Kim, Y. Kang, H.-S. Lee, D. Kim,**Sputtering of TiO2 for High-Efficiency Perovskite and 23.1% Perovskite/Silicon 4-Terminal Tandem Solar Cells**,ACS Applied Energy Materials, 2 , pp. 6263-6268, (2019).

[Afrasiab et al, 2020] A.D. Afrasiab, F.E. Khan, A.D. Subhan, S.D. Khan, M.S. Khan, M.S. Ahmad, M. Rehan, **Noman, Optimization of efficient monolithic perovskite/silicon tandem solar cell** , Optik, 208 , Article 164573,(2020).

[Lamanna et al,2020] E. Lamanna, F. Matteocci, E. Calabrò, L. Serenelli, E. Salza, L. Martini, F.Menchini, M. Izzi, A. Agresti, S. Pescetelli,Mechanically Stacked, Two-Terminal Graphene-Based Perovskite/Silicon Tandem Solar Cell with Efficiency over 26% Joule (2020)

[Chen et al, 2020] B. Chen, J.Y. Zhengshan, S. Manzoor, S. Wang,W. Weigand, Z. Yu, G. Yang, Z. Ni, X. Dai, Z.C. Holman, Blade-coated perovskites on textured silicon for 26%-efficient monolithic perovskite/silicon tandem solar cells,Joule, 2020

[Aydin et al, 2021] E. Aydin, J. Liu, E. Ugur, R. Azmi, G.T. Harrison, Y. Hou, B. Chen, S. Zhumagali, M. De Bastiani, M. Wang, W. Raja, T.G. Allen, A.u. Rehman, A.S. Subbiah, M. Babics, A. Babayigit, F.H. Isikgor, K. Wang, E. Van Kerschaver, L. Tsetseris, E.H. Sargent, F. Laquai, S. De Wolf, Ligand-bridged charge extraction and enhanced quantum efficiency enable efficient n–i–p perovskite/silicon tandem solar cells, Energy Environ. Sci. 14 4377–4390, 2021

[Chen et al, 2021] B. Chen, P. Wang, R. Li, N. Ren, Y. Chen, W. Han L. Yan,Q. Huang, D. Zhang, Y. Zhao, X. Zhang,Composite electron transport layer for efficient N-I-P type monolithic perovskite/silicon tandem solar cells with high open-circuit voltage, Journal of Energy, Chemistry ,2021

[Bakr et al, 2017] Z.H. Bakr, Q. Wali, A. Fakharuddin, L. Schmidt-Mende, T.M. Brown, R. Jose, **Advances in hole transport materials engineering for stable and efficient perovskite solar cells**, Nano Energy, 34 , pp. 271-305,(2017)

[Ledwani and Sangwai,2020] L. Ledwani, J.S. Sangwai (Eds.), Nanotechnology for Energy and Environmental Engineering, Springer International Publishing, pp. 145-168, Cham (2020)

[Unger et al,2017] E.L. Unger, L. Kegelmann, K. Suchan, D. Sörell, L. Korte, S. Albrecht **Roadmap and roadblocks for the band gap tunability of metal halide perovski,**J. Mater. Chem. A, pp. 11401-11409, 5 (2017)

[Werner et al,2015]J. Werner, G. Dubuis, A. Walter, P. Löper, S.-J. Moon, S. Nicolay, M. Morales-Masis, S. De Wolf, B. Niesen, C. Ballif,**Sputtered rear electrode with broadband transparency for perovskite solar cells**,Sol. Energy Mater. Sol. Cells, pp. 407-413, 141 (2015)

[Taghavi et al,2016]M.J. Taghavi, M. Houshmand, M.H. Zandi, N.E. Gorji,**Modeling of optical losses in perovskite solar cells**,Superlattices Microstruct, pp. 424-428., 97 (2016)

[Jiang et al,2016]Y. Jiang, I. Almansouri, S. Huang, T. Young, Y. Li, Y. Peng, Q. Hou, L. Spiccia, U. Bac h, Y.-B. Cheng, M.A. Green, A. Ho-Baillie ,**Optical analysis of perovskite/silicon tandem solar cells**,J. Mater. Chem. C, pp. 5679-5689, 4 (2016)

[Chen et al,2017]B. Chen, X. Zheng, Y. Bai, N.P. Padture, J. Huang **Progress in Tandem Solar Cells Based on Hybrid Organic-Inorganic Perovskites** Adv. Energy Mater, p. 1602400., 7 (2017)

[You et al,2016]J. You, L. Meng, T.-B. Song, T.-F. Guo, Y. Yang, W.-H. Chang, Z. Hong, H. Chen, H. Zhou, Q. Chen, Y. Liu, N. De Marco, Y. Yang **Improved air stability of perovskite solar cells via solution-processed metal oxide transport layers**,Nat. Nanotechnol, pp. 75-81., 11 (2016)

[Chen et al,2015] W. Chen, Y. Wu, Y. Yue, J. Liu, W. Zhang, X. Yang, H. Chen, E. Bi, I. Ashraful, M. Grätzel, L. Han,**Efficient and stable large-area perovskite solar cells with inorganic charge extraction layers** Science, p. 944, 350 (2015)

[Zhang et al,2018]S. Zhang, M. Stolterfoht, A. Armin, Q. Lin, F. Zu, J. Sobus, H. Jin, N. Koch, P. Meredith , P.L. Burn, D. Neher,**Interface Engineering of Solution-Processed Hybrid Organohalide Perovskite Solar Cells** ACS Appl. Mater. Interfaces, pp. 21681-21687, 10 (2018)

[Sun et al,2018] J. Sun, J. Lu, B. Li, L. Jiang, A.S.R. Chesman, A.D. Scully, T.R. Gengenbach, Y.-

B. Cheng, J.J. Jasieniak, **Inverted perovskite solar cells with high fill-factors featuringchemical bath deposited mesoporous NiO hole transporting layers** Nano Energy, pp. 163-171, 49 (2018)

[Altazin et al,2018] L.S.S. Altazin, J. Werner, B. Niesen, C. Ballif, B. Ruhstaller, **Design of perovskite/crystalline-silicon monolithic tandem solar cells** Opt. Express, pp. A579-A590, 26 (2018)

[Bush et al,2017] K.A. Bush, A.F. Palmstrom, Z.J. Yu, M. Boccard, R. Cheacharoen, J.P. Mailoa, D.P. McMeekin, R.L.Z. Hoye, C.D. Bailie, T. Leijtens, I.M. Peters, M.C. Minichetti, N. Rolston, R. Prasanna, S. S ofia, D. Harwood, W. Ma, F. Moghadam, H.J. Snaith, T. Buonassisi, Z.C. Holman, S.F. Bent, M. D. McGehee ,**23.6%-efficient monolithic perovskite/silicon tandem solar cells with improved stability, Nature**, Energy, p. 17009, 2 (2017)

[Tockhorn et al,2020] P. Tockhorn, P. Wagner, L. Kegelmann, J.-C. Stang, M. Mews, S. Albrecht, L. Korte,**Three-Terminal Perovskite/Silicon Tandem Solar Cells with Top and Interdigitated Rear Contacts** ACS Appl. Energy Mater, pp. 1381-1392, 3 (2020)

[Gilibert et al,2020] G. Giliberti, A. Martí, F. Cappelluti, Perovskite-Si solar cell: a three-terminal heterojunction bipolar transistor architecture, in: 2020 47th IEEE Photovoltaic Specialists Conference (PVSC), pp. 2696–2699, 2020

[Albrecht et al,2016]S. Albrecht, M. Saliba, J.P. Correa Baena, F. Lang, L. Kegelmann, M. Mews, L. Steier, A. Abate, J. Rappich, L. Korte, R. Schlatma nn, M.K. Nazeeruddin, A. Hagfeldt, M. Grätzel, B. Rech,**Monolithicperovskite/silicon-heterojunction tandem solar cells processed at low temperature** Energy Environ. Sci, pp. 81-88., 9 (2016)

[Filipič et al,2015] M. Filipič, P. Löper, B. Niesen, S. De Wolf, J. Krč, C. Ballif, M. Topič **CH3NH3PbI3 perovskite/silicon tandem solar cells: characterization based optical simulations** Opt. Express, pp. A263-A278, 23 (2015)

[Park et al,2019] I.J. Park, J.H. Park, S.G. Ji, M.-A. Park, J.H. Jang, J.Y. Kim,**A Three-Terminal Monolithic Perovskite/Si Tandem Solar Cell Characterization Platform**,Joule, pp. 807-818, 3 (2019)

[Quiroz et al,2018] C.O.R. Quiroz, Y. Shen, M. Salvador, K. Forberich, N. Schrenker, G.D. Spyropoulos, T. Heumüller, B. Wilkinson, T. Kirchartz, E. Spiecker, **Balancing electrical and optical losses for efficient 4-terminal Si–perovskite solar cells with solution processed percolation electrodes**. Mater. Chem. A, pp. 3583-3592, 6 (2018)

[Wu et al,2017] Y. Wu, D. Yan, J. Peng, Y. Wan, S.P. Phang, H. Shen, N. Wu, C. Barugkin, X. Fu, S. Surve, **Monolithic perovskite/silicon-homojunction tandem solar cell with over 22% efficiency** Energy Environ. Sci, pp. 2472-2479., 10 (2017)

[Mazzarella et al,2019] L. Mazzarella, Y.H. Lin, S. Kirner, A.B. Morales-Vilches, L. Korte, S. Albrecht, E. Crossland, B. Stannowski, C. Case, H.J. Snaith **Infrared light management using a nanocrystalline silicon oxide interlayer in monolithic perovskite/silicon heterojunction tandem solar cells with efficiency above 25%** Adv. Energy Mater, p. 1803241., 9 (2019)

[Jaysankar et al,2018] M. Jaysankar, B.A. Raul, J. Bastos, C. Burgess, C. Weijtens, M. Creatore, T. Aernouts, Y. Kuang, R. Gehlhaar, A. Hadipour, **Minimizing voltage loss in wide-bandgap perovskites for tandem solar cells** ACS Energy Lett, pp. 259-264., 4 (2018)

[Abbasiyan et al,2020] A. Abbasiyan, M. Noori, H. Baghban **Quasi-periodic selective intermediate structure for perovskite/Si tandem solar cells** Sol. Energy, pp. 461-468, 198 (2020)

[Park et al,2020] H.H. Park, J. Kim, G. Kim, H. Jung, S. Kim, C.S. Moon, S.J. Lee, S.S. Shin, X. Hao, J.S. Yun **Transparent Electrodes Consisting of a Surface-Treated Buffer Layer Based on Tungsten Oxide for Semitransparent Perovskite Solar Cells and Four-Terminal Tandem Applications** Small Methods, p. 2000074, 4 (2020)

[Xu et al,2020] J. Xu, C.C. Boyd, J.Y. Zhengshan, A.F. Palmstrom, D.J. Witter, B.W. Larson, R.M. France, J. Werner, S.P. Harvey, E.J. Wolf, **Triple-halide wide–band gap perovskites with suppressed phase segregation for efficient tandems** Science, pp. 1097-1104, 367 (2020)

[Ramírez et al,2019] C.O. Ramírez Quiroz, G.D. Spyropoulos, M. Salvador, L.M. Roch, M. Berlinghof, J. Darío Perea, K. Forberich, L.I. DionBertrand, N.J. Schrenker, A. Classen, N. Gasparini, G. Chistiakova, M. Mews, L. Korte, B. Rech, N. Li, F. Hauke, E. Spiecker, T. Ameri, S. Albrecht, G. Abellán, S. León, T. Unruh, A. Hirsch, A. Aspuru-Guzik, C.J. Brabec,**Interface Molecular Engineering for Laminated Monolithic Perovskite/Silicon Tandem Solar Cells with 80.4% Fill Factor**,Adv. Funct. Mater, p. 1901476., 29 (2019)

[Khan et al,2019] S.B. Khan, S. Irfan, Z. Zhuanghao, S.L. Lee,**Influence of Refractive Index on Antireflectance Efficiency of Thin Films** Materials, 12 (2019

[Santbergen et al,2019] R. Santbergen, H. Uzu, K. Yamamoto, M.J.I.J.o.P. Zeman, Optimization of Three-Terminal Perovskite/Silicon Tandem Solar Cells, 446–451,9 (2019)

[Selberherr, 1984] Selberherr, S., *Analysis and Simulation of Semiconductor Devices* (Springer, Vienna, 1984).

[Burkhard et al., 2010]. Burkhard, G. F., Hoke, E. T., and McGehee, M. D., "Accounting for interference, scattering, and electrode absorption to make accurate internal quantum efficiency measurements in organic and other thin solar cells," Adv. Mater **22**(30), 3293–3297 (2010).

[Neukom et al., 2017]. Neukom, M. T., Züfle, S., Knapp, E., Makha, M., Hany, R., and Ruhstaller, B., "Why perovskite solar cells with high efficiency show small IV-curve hysteresis," Sol. Energy Mater. Sol. Cells **169**, 159–166 (2017).

[Sherkar et al., 2017a]. Sherkar, T. S., Momblona, C., Gil-Escrig, L., Ávila, J., Sessolo, M., Bolink, H. J., and Koster, L. J. A., "Recombination in perovskite solar cells: Significance of grain boundaries, interface traps, and defect ions," ACS Energy Lett. **2**(5), 1214–1222 (2017a).

[Tessler and Vaynzof, 2018]. Tessler, N. and Vaynzof, Y., "Preventing hysteresis in perovskite solar cells by undoped charge blocking layers," ACS Appl. Energy Mater. **1**(2), 676–683 (2018).

[Courtier et al., 2019a]. Courtier, N. E., Cave, J. M., Foster, J. M., Walker, A. B., and Richardson, G., "How transport layer properties affect perovskite solar cell performance: Insights from a coupled charge transport/ ion migration model," Energy Environ. Sci. **12**(1), 396–409 (2019a).

[Courtier et al. 2019b] Courtier, N. E., Cave, J. M., Walker, A. B., Richardson, G., and Foster, J. M., "IonMonger: A free and fast planar perovskite solar cell simulator with coupled ion vacancy and charge carrier dynamics," J. Comput. Electron. **18**(4), 1435–1449 (2019b).

[Matteocci et al 2015]. Matteocci, F., Busby, Y., Pireaux, J. J., Divitini, G., Cacovich, S., Ducati, C., and Di Carlo, A., "Interface and composition analysis on perovskite solar cells," ACS Appl. Mater. Interfaces **7**(47), 26176–26183 (2015).;

[Divitini et al. 2016] Divitini, G., Cacovich, S., Matteocci, F., Cinà, L., Di Carlo, A., and Ducati, C., "*In situ* observation ofheat-induced degradation of perovskite solar cells," Nat. Energy **1**(1), 15012 (2016).

[De Bastiani et al., 2016]. De Bastiani, M., Dell'Erba, G., Gandini, M., D'Innocenzo, V., Neutzner, S., Kandada, A. R. S., Grancini, G., Binda, M., Prato, M., Ball, J. M., Caironi, M., and Petrozza, A., " Ion migration and the role of preconditioning cycles in the stabilization of theJ-Vcharacteristics of inverted hybrid perovskite solar cells," Adv. Energy Mater. **6**(2), 1501453 (2016).

[Bi et al., 2017]. Bi, E., Chen, H., Xie, F., Wu, Y., Chen, W., Su, Y., Islam, A., Grätzel, M., Yang, X., and Han, L., "Diffusion engineering of ions and charge carriers for stable efficient perovskitesolar cells,"Nat.Commun. **8**(1), 15330 (2017).

[Sherkar et al., 2017a]., Sherkar, T. S., Momblona, C., Gil-Escrig, L., Ávila, J., Sessolo, M., Bolink, H. J., and Koster, L. J. A., "Recombination in perovskite solar cells: Significance of grain boundaries, interface traps, and defect ions," ACS Energy Lett. **2**(5), 1214–1222 (2017a)

[Sherkar et al., 2017b] Sherkar, T. S., Momblona, C., Gil-Escrig, L., Bolink, H. J., and Koster, L. J. A., "Improving perovskite solar cells: Insights from a validated device model," Adv. Energy Mater **7** (13), 1602432 (2017b).

[Wolf et al., 2017]. Wolf, C., Cho, H., Kim, Y.-H., and Lee, T.-W., "Polaronic charge carrier-lattice interactions in lead halide perovskites," ChemSusChem **10**(19), 3705–3711 (2017).

[Ambrosio et al., 2018]. Ambrosio, F., Wiktor, J., De Angelis, F., and Pasquarello, A., "Origin of low electron–hole recombination rate in metal halide perovskites," Energy Environ. Sci. **11**(1), 101–105 (2018).

[Davieset al., al., 2018]. Davies, C. L., Filip, M. R., Patel, J. B., Crothers, T. W., Verdi, C., Wright, A. D., Milot, R. L., Giustino, F., Johnston, M. B., and Herz, L. M., "Bimolecular recombination in methylammonium lead triiodide perovskite is an inverse absorption process," Nat. Commun. **9**(1), 293 (2018).

[Zhan et al., 2018]. . Zhang, X., Shen, J.-X., Wang, W., and Van de Walle, C. G., “First-principles analysis of radiative recombination in lead-halide perovskites,” ACS Energy Lett. **3** (10), 2329–2334 (2018).

[Stolterfoht et al., 2019b]. Stolterfoht, M., Le Corre, V. M., Feuerstein, M., Caprioglio, P., Koster, L. J. A., and Neher, D., “Voltage-dependent photoluminescence and how it correlates with the fill factor and opencircuit voltage in perovskite solar cells,” ACS Energy Lett. **4**(12), 2887–2892 (2019b).

CHAPTER III

RESULTS AND DISCUSSION

Chapter III Results and discussion

III-1 Introduction

Despite so many efforts to obtain high efficiency from tandem solar cells. It is still lower than that of monolayer perovskite solar cells. Thus, the researchers mainly focus on the simulation of perovskite tandem solar cells. By realizing this via optimization of individual top and bottom perovskite cells. This shortcoming drew the researcher's attention towards the development of these devices and lead-free perovskite solar cells [Sani et al., 2018].

Silvaco Atlas [Silavo, 2019] is one of various software incorporating this objective by using the drift diffusion model to model the transport of charge carriers within the device under light, wave-spectrum and bias conditions. It is two-dimensional physical based simulator where it can be included all possible physical phenomena such us size grain impact, defect type and density, different wave spectrum as lighting sources, configurations and material constituents and also fraction rate contents in all the composite materials.

In this part of work, first a perovskite solar cell will be explored via choosing perovskite material as absorber than two solar cells will be built as a tandem

Thus, this part of the work therefore includes the simulation of a lead-free -perovskite tandem solar cell based on methyl ammonium germanium halide and mixed halide layers which has not yet been so explored in the literature. Furthermore, it appears that, individual $CH_3NH_3GeI_3$ and $MASnGeI_3$-based layers are compatible with low temperature and solution processing methodology [Stoumpos et al., 2015; Ito et al., 2018]. Thus, in terms of temperature constraints and deposition method, both layers are compatible for the application of all-perovskite tandem solar cells. Additionally, this document also describes the ETL combination with the proposed lead-free all-perovskite tandem solar cells, because the ETL layer plays a crucial role in the proper facilitation of electrons from the perovskite layer to the electrodes. Facing issues such as limitation of deposition methods and the high cost, the simulation ways are adopted to comprehend the influence of electron transport materials on the perovskite tandem solar cell performances.

In addition, the effect of perovskite absorber layer material is also explored and in this case a Lead based material was used. The simulation was performed using Atlas-Silvaco software.

III-2 Results and discussion

III-2-1 Device configuration

III-2-1-1 Absorber material ($CH_3NH_3GeI_3$)

For the purpose of choosing absorber material, and because they exhibit outstanding photovoltaic performances, the metal halide perovskites such as methyl-ammonium germanium halide ($CH_3NH_3GeI_3$) are considered as potential candidates for lead-free perovskite absorber layer [Liao et al., 2017; Ran et al., 2018; Zhang et al., 2019; Chang et al., 2019; Song et al., 2017; Leijtens et al., 2017; Stoumpos et al., 2015; Sun et al., 2016; Y; Kanoun et al., 2019]. Besides the germanium-based perovskite layer quite a lot of tin-based perovskite layer were also used for the application of lead-free perovskite solar cell [Liao et al., 2017; Ran et al., 2018]. Nonetheless, the efficiency of Sn based perovskite layer exceeds that of the Pb based perovskite layer, again because of the fast oxidation of Sn^{2+} to Sn^{4+} and due to the presence of pair isolated causes severe device degradation which leads eventually to reduce the device stability.

In this work the SrSnO3 is used as electronic transport layer (ETL), it is why a brief definition is allocated in the next section

III-2-1-2 ETL material ($SrSnO_3$)

Alkaline-earth stannates $ASnO_3$ (A= Ca, Sr, and Ba) are of great interest due to their intriguing dielectric properties and applications such as in thermally stable capacitors [Mahapatra et al, 2006; Yoon et al, 1988; Parkash et al, 1996]. Recently, these perovskites have also received considerable attentions as new TCO films based on the unique features of high optical transparency and high carrier mobility [Sun et al, 2018; Li et al, 2017; Fa et al, 2018; Wang et al, 2018; Thoutam et al, 2019].

Among $ASnO_3$, $SrSnO_3$ (SSO) shows the semiconductor behavior with the band gap of 4.1 eV and has an orthorhombic structure with the lattice constants of a=5.708 Å, b=5.703 Å, and c=8.065 Å [Zang et al, 2006].

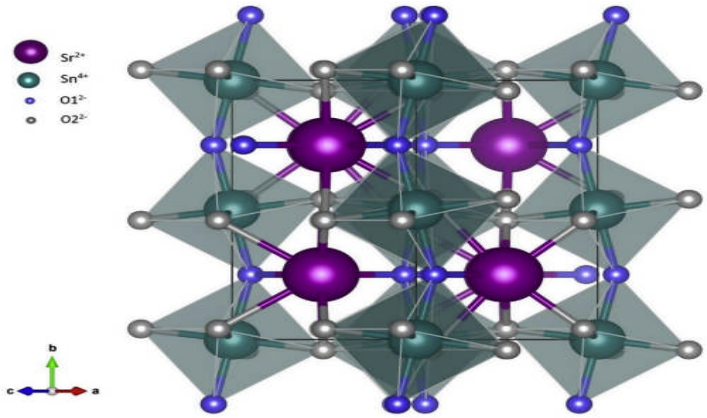

FigureI-1: Crystal structure of SrSnO3 compound [M.de Freitas et al, 2019]

The pure SSO films are not conductive. To further improve the conductivity of SSO films, many elements have been chosen to dope SSO films to generate carriers by replacing the A site or B site, such as La for Sr sites [Baba et al, 2015], and Ta for Sn sites [Liu et al, 2017]. Selecting proper doping element and appropriate dopant concentration is crucial to obtain high-performance TCO films, as well as optimized growth condition. Nb element is often adopted to substitute partially for TCO films, as more carriers tend to generate in the material system benefiting from the high valence-state Nb^{5+} cations. Indeed, the high density of carriers created by introducing Nb ions has been demonstrated according to the experimental and first principal calculation results. For examples, Nb-doped TiO2 films exhibited the room-temperature resistivity as low as 2×10^{-4} Ωcm [Furubavashi et al, 2005], and Nb-doped ZnO films showed the lowest resistivity of 8.95×10^{-4} Ωcm [Shao et al, 2010]. Physically, the Nb donors will contribute by one electron to the conduction band of SSO as the Sn ions are substituted by Nb due to the similar ionic radii of Nb^{5+}(0.64 Å) and Sn^{4+}(0.69 Å), resulting in an enhanced conductivity in electron-doped SSO films. On the other hand, the physical properties of TCO films can also be tuned under different deposition oxygen pressures and temperatures during the film growth.

In order to understand the photovoltaic performance of perovskite tandem solar cell, firstly a single layer perovskite solar cell based on $CH_3NH_3GeI_3$ and $CH_3NH_3SnI_3$ will be compared than the choice of tandem structure will be based.

The device configurations for single layer and tandem perovskite solar cell are presented in Figure III-2. Table III-1 summarizes the initial device parameters which are taken for the simulation of single layer perovskite solar cell and tandem solar cell. Table III-2 presents the considered

parameters for the front and back metal contacts. Device parameters for the interface defects between HTM/perovskite interface and perovskite/ETM interface are given in Table III.3.

To understand the effect of different electron transport layers on the device performance of perovskite tandem solar cell, all the parameters of electron transport layers are given in Table III-4 as well as the involved other materials

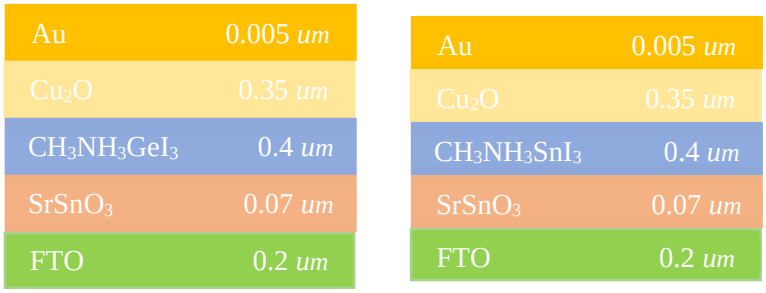

Figure III-2: Simulated structure(p-i-n) of $CH_3NH_3GeI_3$ and $CH_3NH_3SnI_3$ based perovskite solar cell -(left and middle) (b) FAMASnGeI3 based perovskite solar cell.

Material and properties	Cu_2O	$MAGeI_3$	$MASnI_3$	$MAPbI_3$	$SnSrO_3$	FTO
Thickness (nm)	0.350	0.4	750	0.4	0.07	0.20
Band gap E_g (eV)	2.17	1.9	1.3	1.55	3.20	3.50
Electron affinity χ (eV)	3.2	3.98	4.17	3.9	4.00	4.00
Dielectric permittivity ε_r	7.11	10.0	8.2	6.5	8.70	9.00
Conduction band density of states(N_c (cm^{-3}))	$2.02x10^{17}$	10^{16}	108	$2.2x10^{18}$	$1.7x10^{19}$	$2.2x10^{18}$
Valance band density of states (N_v (cm^{-3}))	$1.1x10^{19}$	10^{16}	10^7	$1.8x10^{19}$	$2x10^{20}$	$1.8x10^{19}$
Electron thermal velocity (cm/s)	10^7	10^7		10^7	10^7	10^7
Hole thermal velocity-cm/s	10^7	10^7		10^7	10^7	10^7
Electron mobility (cm2/Vs)	200	$1.62x10^5$	1.6	2	$5.3x10^3$	20
Hole mobility (cm2/Vs)	80	$1.01x10^5$	1.6	2	$6.6x10^2$	10
N_D (cm^{-3})	0	10^9	0	$5.21x10^9$	$2x10^{16}$	10^{18}
N_A (cm^{-3})	10^{18}	10^9	10^{16}	$5.21x10^9$	0	0
References	[Hossain et al.,2015]	[Kanoun et al.,2019]		[Burgelman et al, 2018]	[Bishnol&Pandy, 2018]	[Manadadapu et al.,2017]

Tables III-1: The device layer properties for hole transport layer, absorber layers based methylammonium (MA=CH_3NH_3), electron transport layer and transparent conductive oxide.

Contact properties	Front contact	Back contact
Thermionic emission /Surface Recombination velocity of electrons (cm/s)	10^7	10^7
Thermionic emission /Surface Recombination velocity of holes (cm/s)	10^7	10^7
Metal Work Function (eV)	4.3	5.1

Table III-2: Parameters for front and back contact [Anwar et al., 2017].

parameters	HTM/perovskite	Perovskite/ETM
Defect Type	Neutral	Neutral
$A_e(cm^2)$: Cross Section area of electrons	10^{18}	10^{15}
$A_h(cm^2)$: Cross Section area of holes	10-^{16}	10^{-15}
Energetic Distribution	Single	Single
Reference for defect energy level Et	Above the highest E_V	Above the highest E_V
Energy with respect to reference (eV)	0.050	0.600
Total density (cm^{-3})	10^{12}	10^{11}

Table III-3: Interface defects Parameters [Shasti and Mortezaali, 2019].

III-2-1-2 Model and Material statements included in the simulation:

- **Perovskite Material**

As perovskite is organic material, it could contain both type of recombination, (Radiative and non-radiative). Each recombination mechanism depends differently on the hole and electron concentrations and its rate constants.

The Langevin mechanism exists in the organic materials, happening as a direct consequence of the fact that electron and hole possibly meet in the same field which is due to their low mobility. The recombination model in this case is referred to Langevin Model (Bimolecular Langevin Recombination), to enable the exchange between charged carriers and singlet and triplet. This model must be declared in Material statement by A.Langevin and in Model statement by NI.Langevin. the expression of this recombination rate is given by:

$$R_{Ln,p} = r_L(x,y,t)(np - NI_L^2) \qquad \text{III-1}$$

With r_L is Langevin recombination rate coefficient given by:

$$r_L = A.Langevin\frac{q(\mu_n(E)+\mu_p(E))}{\varepsilon_r\varepsilon_0} \qquad \text{III-2}$$

Where μ_n, μ_p are the electron and hole mobilities, *p*,*n* are the hole and electron concentrations, ε_r is the relative permittivity and *q* is the electron charge. When NILangevin is included so its value is NI= n_i otherwise it is zero

However, on the ns-s timescale, it was showed a regeneration of the charge carrier population. Which attributed this to the annihilation of triplet states resulting in the generation of higher-excited singlet and triplet excitons that now have sufficient energy to undergo charge separation at the polymer–fullerene (fullerene type of PCBM) interface and thus recreate a small pool of charges. This study demonstrates that triplet-state formation is not exclusive to the low-bandgap systems but may be a more general phenomenon in polymer–fullerene blends in which the polymer's triplet level is sufficiently low to be populated from interfacial triplet charge transport states that are created during nongeminate charge recombination [Laquai et al, 2017].

First, two solar cell's structures using the $CH_3NH_3GeI_3$ and $CH_3NH_3SnI_3$ to investigate the role of B atom-methylammonium halide on J-V characteristics are simulated on Atlas-Silvaco as shown in Figure III-2.

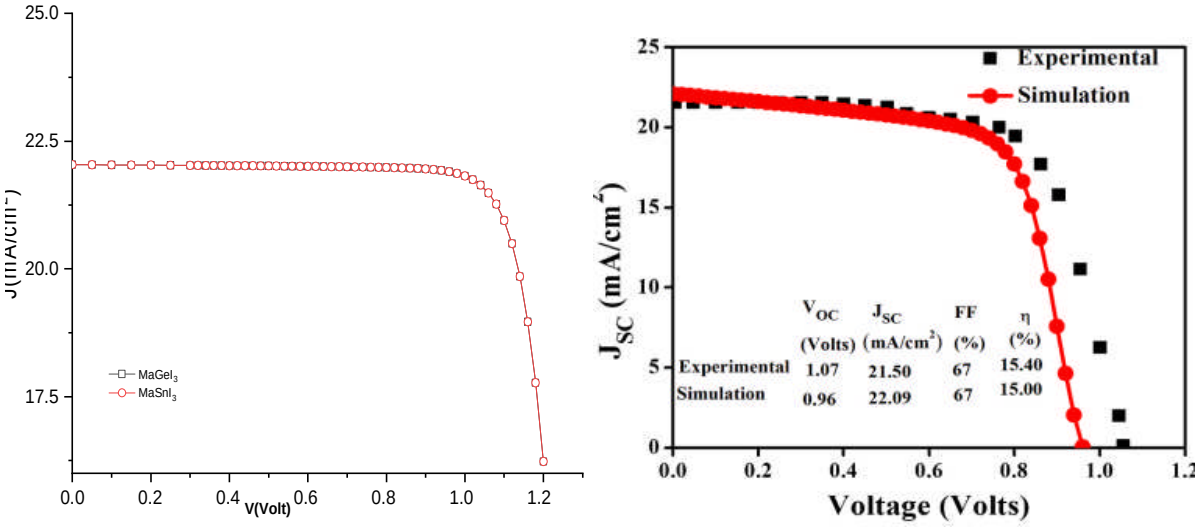

Figure III-3: (left) J-V characteristics of MaGeI3 and MaSnI3 for a single Perovskite-solar cell. (right) the Compared experimental and simulated JV characteristic for MaGeI3 [Singh et al, 2020]

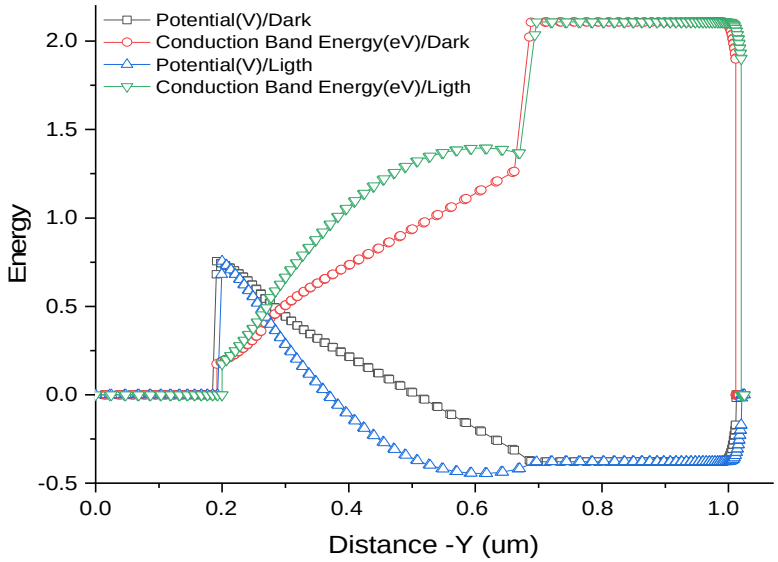

Figure III-4: Potential and conduction band energy along the thickness of structure at the middle (x=0.5 *u*m) showing how the presence of the light upgrades the energy of electron inside the absorber material.

As it is noticeable, there is no influence observed between the two structure responses (MAGeI3, MASnI3) which can be due to the lack of our essential data to be included especially the reflection index (via *. nk file) that through which the gap energy can be surely introduced in the calculation. We believe strongly that the refractive index has a great influence which makes difference [Nuggehalli and Ravindra, 2020].

Thus, the next section will add a $MaPbI_3$ as absorber layer regarding to the availability of its data parameters aiming to explore its effect on this type of configuration (p-i-n structure). The table III-4 shows the possible ETL and HTL used for this $MAPbI_3$ absorber.

Parameters for ETL	PCBM	IGZO	SnO_2	**TiO_2**	ZnO
E_g(ev)	2	3.05	3.5	**3.2**	3.3
χ (ev)	3.9	4.16	4	**3.9**	4.1
ε_r	3.9	10	9	**9**	9
$N_{c\ (cm^{-3})}$	2.5×10^{21}	5×10^{18}	2.2×10^{17}	**10^{21}**	4×10^{18}
$N_{v(cm^{-3})}$	2.5×10^{21}	5×10^{18}	2.2×10^{16}	**2×10^{20}**	10^{19}
$\mu_{n(cm^2/Vs)}$	0.2	15	20	**20**	100
$\mu_{p(cm^2/Vs)}$	0.2	0.1	10	**10**	25
$N_{d(cm^{-3})}$	2.93×10^{17}	10^{18}	10^{17}	**10^{19}**	10^{18}
$N_{a(cm^{-3})}$	0.0	0.0	0.0	**1.0**	10^{5}
$N_{t(cm^{-3})}$	10^{15}	10^{15}	10^{15}	**10^{15}**	10^{17}
Parameters for HTL	Spiro-OMeTAD	P3HT	CuI	**NiO**	CuSCN
E_g(ev)	3.00	1.85	2.98	**3.6**	3.4
χ (ev)	2.45	3.1	2.1	**1.46**	1.9
εr	3.00	3.4	6.5	**11**	10
N_c(cm-3)	10^{19}	10^{22}	2.8×10^{22}	**1.6×10^{19}**	1.7×10^{19}
N_v(cm-3)	10^{19}	10^{22}	10^{22}	**1.10^{19}**	2.5×10^{21}
$\mu_n(cm^2/Vs)$	2×10^{-4}	10^{-4}	1.7×10^{-4}	**50**	10^{-4}
$\mu_p(cm^2/Vs)$	2×10^{-4}	10^{-3}	2×10^{-4}	**50**	10^{-1}
$N_d(cm^{-3})$	0.0	0.0	0.0	**0.0**	0.0
$N_a(cm^{-3})$	2×10^{18}	3.17×10^{13}	10^{18}	**1.8×10^{18}**	10^{18}
$N_t(cm^{-3})$	10^{15}	10^{14}	10^{15}	**10^{14}**	10^{14}

Table III-4: Physical properties of some ETmaterials and HTmaterials [Azri, 2019].

Figure III-5 and III-6 present the difference effect on changing the electron transport material on the conduction band energy and consequently the potential within the solar cell. TiO2 and SrSnO3 are used in this case, and despite that TiO_2 is commonly used for this technology (MAPbI3), the SrSnO3 shows better band adjustment.

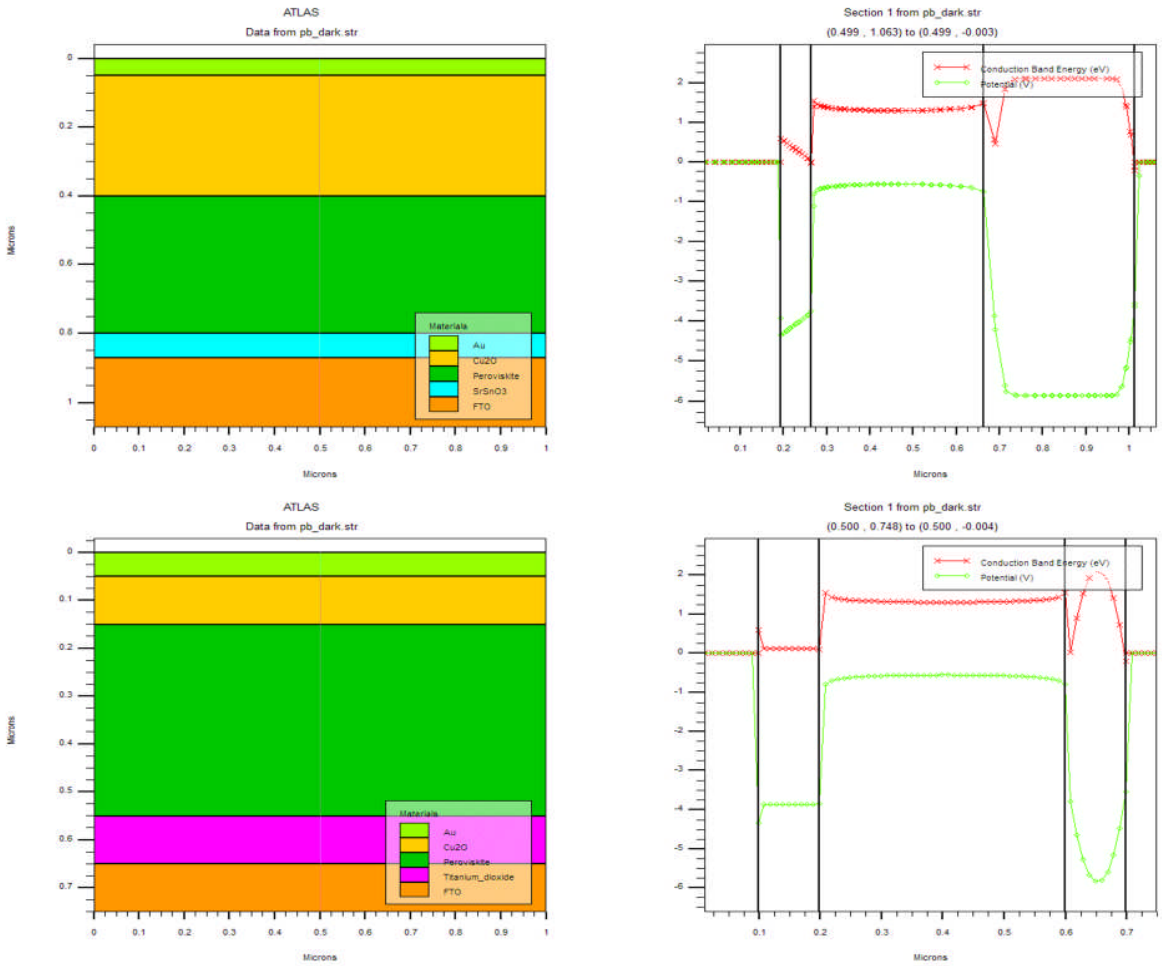

Figure III- 5: The structure and equivalent conduction band energy and potential across the structure at the middle length x=0.5um, for both solar cells ($MAPBI_3$-TiO_2 and $MAPBI_3$-$SrSnO_3$).

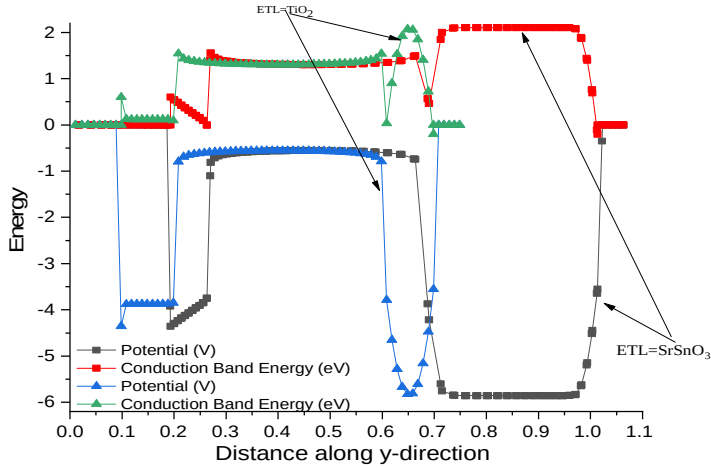

Figure III- 6: $MAPBI_3$-TiO_2 and $MAPBI_3$-$SrSnO_3$ Conduction band energy and Potential.

Keeping the same dimensions of each layer in solar cell configuration and changing only the perovskite material gives the results presented on figure III-7 and III-8.

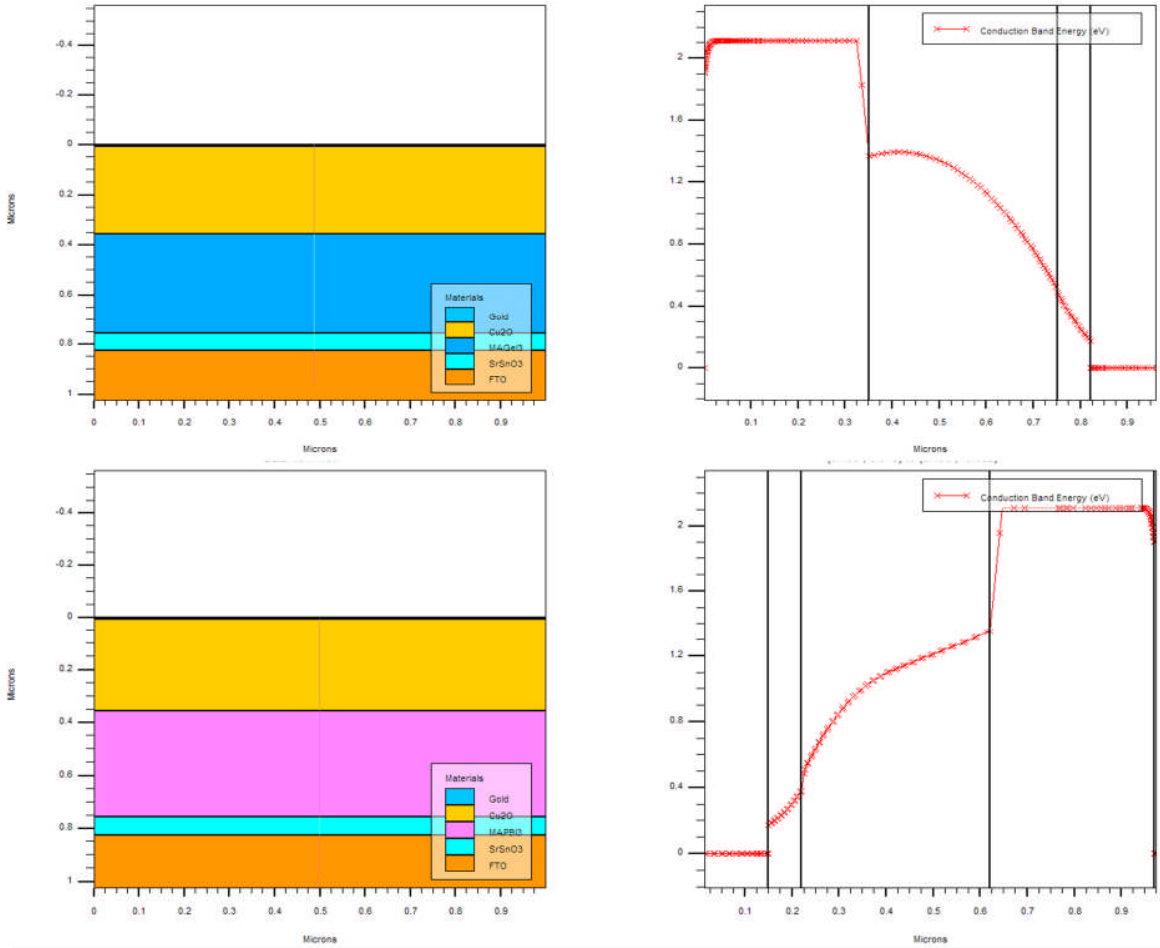

Figure III-7: The structure and conduction band energy along the structure in Y-direction for (on top) the $MAGeO_3$ and (bottom) the $MAPbI_3$ Perovskite solar cell.

Figure III-8: The conduction band energy in $MAGeO_3$ and $MAPbI_3$ Perovskite solar cell.

Furthermore, organic-inorganic mechanically stacked tandem solar cell is built. Using the lead-free absorber (MAGeI3) as top cell connected to inorganic bottom solar cell as shown in figure III-9. The inorganic solar cell consists of CdS (n-type, N_d =1e18 cm^{-3})-CIGS (p-type, Na= 2e16 cm^{-3})-Silicon (substrate). the connection was done via a tunneling layer based on highly doped Silicon material. An auxiliary quantum tunneling mesh was specified as it is required to model quantum tunneling between the two cells of the tandem device.

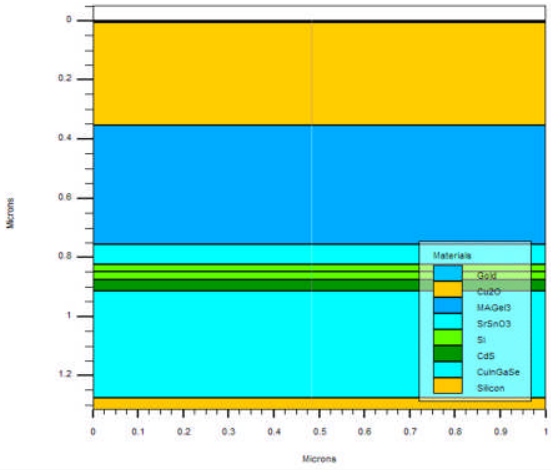

Figure III-9: Tandem configuration based on $MAGeI_3$ organic top cell and CdS/CIGS bottom cell.

The tandem based on MAPbI3 also was realized under the same conditions as MAGeI3 illustrated by in figure III-10.

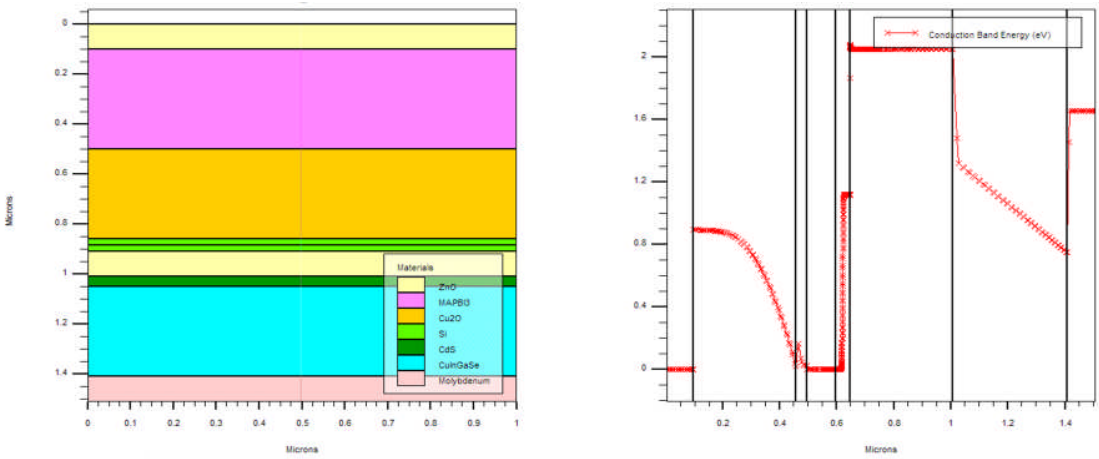

Figure III-10: Tandem configuration based on $MAPbI_3$ organic top cell and CdS/CIGS bottom cell.

The defects in each material were along the simulation taken into account as well as the interface traps.

Reference of Chapter III

[Liao et al., 2017] Liao, Y., Liu, H., Zhou, W., Yang, D., Shang, Y., Shi, Z., Li, B., Jiang, X., Zhang, L., Quan, L.N., Quintero-Bermudez, R., Sutherland, B.R., Mi, Q., Sargent, E.H., Ning, Z.' Highly oriented low-dimensional tin halide perovskites with enhanced stability and photovoltaic performance'. J. Am. Chem. Soc. 139, 6693–6699. https:// doi.org/10.1021/jacs.7b01815, 2017

[Leijtens et al, 2017] Leijtens, T., Prasanna, R., Gold-Parker, A., Toney, M.F., McGehee, M.D.,. Mechanism of tin oxidation and stabilization by lead substitution in tin halide perovskites. ACS Energy Lett. 2, 2159–2165. https://doi.org/10.1021/ acsenergylett.7b00636, 2017

[Ran et al, 2018] Ran, C., Xi, J., Gao, W., Yuan, F., Lei, T., Jiao, B., Hou, X., Wu, Z., 'Bilateral interface engineering toward efficient 2D–3D bulk heterojunction tin halide lead-free perovskite solar cells. ACS Energy Lett. 3, 713–721. https://doi.org/10.1021/ acsenergylett.8b00085, 2018

[Chang et al, 2019] Chang, X., Marongiu, D., Sarritzu, V., Sestu, N., Wang, Q., Lai, S., Mattoni, A., Filippetti, A., Congiu, F., Lehmann, A.G., Quochi, F., Saba, M., Mura, A., Bongiovanni, G., 2019. Layered Germanium hybrid perovskite bromides: insights from experiments and first-principles calculations. Adv. Funct. Mater. 29, 1–9. https://doi.org/10.1002/adfm.201903528

[Song et al, 2017] Song T.B, Yokoyama T, Aramaki S, Kanatzidis M.G, Performance enhancement of lead-free tin- based perovskite solar cells with reducing atmosphere assisted dispersible additive. ACS Energy Lett. 2, 897–903. https://doi.org/10.1021/ acsenergylett.7b00171, 2017.

[Stoumpos et al, 2015] Stoumpos C.C, Frazer, L, Clark, D.J, Kim, Y.S, Rhim, S.H, Freeman A.J, Ketterson, J. B, Jang J.I., Kanatzidis M.G., 'Hybrid germanium iodide perovskite semiconductors: Active lone pairs, structural distortions, direct and indirect energy gaps, and strong nonlinear optical properties', J-Am-Chem, 6804–6819. https://doi.org/10.1021/jacs.5b01025 ,2015.

[Zhang et al, 2019] Zhang, C, Li Z., Deng X., Yan B, Wang Z, Chen X., Sun Z, Huang S,' Enhancing photovoltaic performance of perovskite solar cells utilizing germanium nanoparticles', Sol. Energy 188, 839–848. https://doi.org/10.1016/j. solener.2019.06.069, 2019

[Zang et al, 2006] Zhang WF, Tang J, Ye J,' Photoluminescence and photocatalytic properties of $SrSnO_3$ perovskite,' Chem. Phys. Lett. 418:174–178, 2006

[Baba et al, 2015] Baba E, Kan D, Yamada Y, Haruta M, Kurata H, Kanemitsu Y, Shimakawa Y 'Optical and transport properties of transparent conducting La-doped $SrSnO_3$ thin films', J. Phys. D: Appl. Phys. 48:455106, 2015

[Liu et al, 2017] Liu Q, Jin F, Gao G, Wang W, 'Ta doped $SrSnO_3$ epitaxial films as transparent conductive oxide', J. Alloys Compd. 717:62–68, 2017

[Furubayashi et al, 2005] Furubayashi Y, Hitosugi T, Yamamoto Y, Inaba K, Kinoda G, Hirose Y, Shimada T, Hasegawa T A transparent metal: Nb-doped anatase TiO_2. Appl. Phys. Lett. 86:252101', 2005

[Shao et al, 2010] Shao J, Dong W, Li D, Tao R, Deng Z, Wang T, Meng G, Zhou S, Fang X,' Metal-semiconductor transition in Nb-doped ZnO thin films prepared by pulsed laser deposition', Thin Solid Films 518:5288–5291, 2010

[Mahapatra et al, 2006] Mahapatra MK, Singh P, Kumar D, Parkash O, 'Synthesis, crystal structure, microstructure and electrical behavior of systems $Sr_{1-x}La_xSnO_3$ and $SrSn_{1-x}Ni_xO_3$ ($x \leq 0.10$)', Br. Ceram. Trans. 105:280–284, 2006

[Yoon et al, 1988] Yoon. KH, Kim JH, Jo KH, Song HI, Yoon SO, Kim CS Structural and dielectric studies in the $(Ba_{0.9}Ca_{0.1})(Ti_{1-x}Sn_x)O_3$ system. J. Mater. Sci. 23:61–64, 1988

[Parkash et al, 1996] Parkash O, Mandal KD, Christopher CC, Sastry MS, Kumar D Dielectric properties of the $Sr_{1-x}La_xSn1\text{-}xCo_xO_3$ system. J. Mater. Sci. 31:4705–4708, 1996

[Sun et al, 2018] Sun W, Fan J, Xu R, Zhang X, Kan C, Liu W, Zhang L, Ma C, Hu D, Ji Y, Zhu Y, Yang H' 'High optical transmittance and anomalous electronic transport in flexible transparent conducting oxides Ba0.96La0.04SnO3 thin films,' Ceram. Int. 44:18001–18006, 2018

[Li et al, 2017] Li B, Zhang Y, Liu Z, Geng L,' Structural, electrical, and optical properties of $Ba_{1-x}Sm_xSnO_3$ epitaxial thin films on MgO substrates by pulsed laser deposition'. J. Alloys Compd. 708:1117–1123, 2017

[Fa et al, 2018] Fan F-Y, Zhao W-Y, Chen T-W, Yan J-M, Ma J-P, Guo L, Gao G-Y, Wang F-F, Zheng R-K, 'Excellent structural, optical, and electrical properties of Nd-doped BaSnO3 transparent thin films,' Appl. Phys. Lett. 113:202102, 2018

[Wang et al, 2018] Wang T, Prakash A, Dong Y, Truttmann T, Bucsek A, James R, Fong DD, Kim J-W, Ryan PJ, Zhou H, Birol T, Jalan B,' Engineering $SrSnO_3$ phases and electron mobility at room temperature using epitaxial strain,' ACS Appl. Mater. Interfaces 10:43802–43808, 2018

[Thoutam et al, 2019] Thoutam LR, Yue J, Prakash A, Wang T, Elangovan KE, Jalan B,'Electrostatic control of insulator-metal transition in La-doped SrSnO3 films', ACS Appl. Mater. Interfaces 11:7666–7670, 2019

[M. de Freitas et al, 2019] Sabrina M. de Freitas, Gilberto J.B. Júnior, Ricardo D.S. Santos, Marcos V. dos S. Rezende,' Defects and dopant properties of SrSnO3 compound: A computational study ', Elsevier B.V., Computational Condensed Matter 21, 2019

[Sani et al, 2018] Sani, F, Shafie, S., Lim, H.N., Musa, A.O.,' Advancement on lead-free organic-inorganic halide perovskite solar cells' A review. Materials (Basel). 11, 1–17. doi.org/10.3390/ma11061008,2018.

[Nuggehalli and Ravindra, 2020] Aneer Lamichhane, Nuggehalli and M. Ravindra, 'Energy Gap-Refractive Index Relations in Perovskites', Materials 13, 1917; doi:10.3390/ma13081917, 2020,

[Singh et al, 2020] Neelima Singh, Alpana Agarwal and Mohit Agarwal,'Numerical simulation of highly efficient lead-free all-perovskite tandem solar cell', Elsevier, Solar Energy, 208, 399-410, 2020

[Anwar et al, 2017] Anwar. F, Mahbub. R., Satter. S.S, Ullah. S.M., 'Effect of different HTM layers and electrical parameters on ZnO nanorod-based lead-free perovskite solar cell for high efficiency performance', Int. J. https://doi.org/10.1155/2017/ 9846310, Photoenergy 2017

[Bishnoi and Pandey] Bishnoi.S, Pandey.S.K,' Device performance analysis for lead-free perovskite solar cell optimisation'. IET Optoelectron. 12, 185-190 https://doi.org/10. 1049/ietopt. 2017.0135 ,2018.

[Hossain et al, 2015] Hossain, M.I., Alharbi, F.H., Tabet, N., Copper oxide as inorganic hole transport material for lead halide perovskite based solar cells. Sol. Energy 120, 370–380. https://doi.org/10.1016/j.solener.2015.07.040. 2015

[Shasti and Mortezaali, 2019] Shasti, M., Mortezaali, A., Numerical study of Cu2O, SrCu2O2, and CuAlO2 as hole-transport materials for application in perovskite solar cells. Phys. Status Solidi Appl. Mater. Sci. 216, 1–10. https://doi.org/10.1002/pssa.201900337. 2019.

[Minemoto et al, 2020] Minemoto. T, Kawano. Y, Nishimura.T, Shen. Q, Yoshino. K, Iikubo. S, Hayase.S, Chantana, J, 'Theoretical analysis of band alignment at back junction in Sn–Ge perovskite solar cells with inverted p-i-n structure', Sol.EnergyMater. Sol. Cells 206, 110268.https://doi.org/10.1016/j.solmat.2019.110268, 2020.

[Laquai et al, 2017] Frédéric Laquai, Denis Andrienko, Carsten Deibel, and Dieter Neher Charge Carrier Generation, Recombination, and Extraction in Polymer–Fullerene Bulk Heterojunction Organic Solar Cells' Springer International Publishing Switzerland 2017 K. Leo (ed.), Elementary Processes in Organic Photovoltaics, Advances in Polymer Science 272, DOI 10.1007/978-3-319-28338-8_11.2017

[You, 2019] Z. Q. Zhao, S. You J. Huang, L. Yuan, a Z. Y. Xiao,a Y. Cao, N. Cheng, L. Hu,b J. F. Liua and B. H. Yu Molecular modulator for stable inverted planar perovskite solar cells with efficiency enhanced by interface engineering', Journal of Materials Chemistry C, 2019.

[Sariciftci et al, 1992] N. S. Sariciftci et al,' Photoinduced electron transfer from a conducting polymer to a buckminsterfullerene', Science, 258, 1474–1476; DOI: 0.1126/science. 258.5087. 1474. 1992

[Hauff et al, 2005] E. Hauff et al Study of field effect mobility in PCBM films and P3HT:PCBM blends,., Sol. Energy Mater. Sol. Cells, 87 149–156; DOI: 1016/j.solmat.2004.06.014. 2005,

Some definitions

PCBM is a solubilized version of the buckminsterfullerene, C_{60}, and is one of the most commonly used electrons accepting materials in organic photovoltaic devices. The solubility enables PCBM to be dissolved in common solvents used for donor polymers, allowing the simultaneous casting of polymer and fullerene and the formation of an efficient bulk heterojunction. When used in a device with a donor polymer, PCBM enables rapid and efficient charge transfer and exciton dissociation [Sariciftci et al, 1992], and has a high electron mobility [Hauff et al, 2005].

IGZO : Indium Gallium Zinc Oxide, also known as IGZO, or a-IGZO in its amorphous form ($In_2Ga_2ZnO_7$) is a transparent amorphous oxide semiconductor (TAPS) used in thin-film transistors (TFTs) and LED devices.

Conclusion

The current solar cell based on a single p–n junction was originally proposed in the 1950s [Chapin et al, 1954] and has come a long way in those photovoltaic technologies that are starting to be economically viable these days [Chapin et al, 1954]. Despite the improvement realized over decades, using silicon and other material technologies, usually leading to long progress plateaus with an ambiguous path for further growth, and funding cycles being influenced by the price of fossil fuels.

Actually, no single-junction technology can exceed the SQ limit (~ 33%) [Shockley and Queisser, 1961] and this is true regardless of the state of development, Therefor, the use of multi-junction solar cells, with two or more absorber photovoltaic cells are stacked monolithically on top of each other achieves higher efficiencies. But tandem solar cells (multi-junction) have realized just small field of product applications because of many problems as material and process compatibility, inadequate efficiency and the price.

Among all the available solar cell combinations, just two technologies have been able to realize two-terminal tandem devices integrated monolithically which can reach the market. The amorphous silicon based is the first, as it provides many features such as a relative low-cost and low efficiency solar cell that remains a viable solution for consumer electronic products [Yang et al, 1997].

At the other extremity of the performance scale are the III–V multi-junction solar cells which accomplish the present efficiency record of 46% using GaInP/GaAs; GaInAsP/GaInAs systems [Todorov et al, 2016], as the first to exceed the Shockley–Queisser limit and are, at present, the typical solution for the most efficient concentrator and space PV applications. Still other muti-junction based solar cells using crystalline silicon, CdTe and CIGS materials facing significant fabrication challenges for monolithic integration.

Perovskite materials appeared as a conceivable solution, provided that design optimization and thoughtful matters with stability and environmental friendliness could be solved. Among the advantages of multi-junction solar cells, is the efficient absorption of wider range of the solar spectrum. So, for best absorption, the higher band-gap p–n junctions are set on the top of those with a lower bandgap. In this way, higher energy photons from incident solar radiation are

efficiently absorbed by the upper band gap layers, thus reducing the difference between the photon energy and the absorber band gap energy.

First Au-Cu2O- $CH_3NH_3GeI_3$- $SrSnO_3$ perovskite solar cell was realized under Atlas – Silvaco simulator and compared results were done with sufficient agreement.

The solar cells used perovskite ($CH_3NH_3GeI_3$) lead free and with lead (Pb) such as ($CH_3NH_3PbI_3$) are used separably to build top solar cells. $SrSnO_3$ and TiO_2 were involved as electronic transport materials while Cu_2O was included as hole transport material.

The effect on the light is explored through the variation in shape of conduction band energy. The influence of $SrSnO_3$ and TiO_2 is also investigated when using the $MAPbI_3$ perovskite solar cell.

Despite the multiple p–n junctions are electrically connected by means of tunnel junctions or shared electrode leading to a series electrical connection. The two-junction tandem device was chosen that operate under planar and spectral light available in Silvaco (solar 03-example) package library

The employed tunneling layer consists on (P^+ and N^+)-Silicon

the organic-inorganic mechanically stacked tandem solar cell is built used the lead-free absorber (MAGeI3) as top cell connected to inorganic bottom solar cell. The inorganic solar cell is made up of CdS (n-type, N_d =1e18 cm^{-3})-CIGS (p-type, Na= 2e16 cm^{-3})-Silicon (substrate).

References of conclusion

[Chapin et al, 1954] D. M. Chapin, C. S. Fuller and G. L. Pearson, 'A new silicon p-n junction photocell for converting solar radiation into electrical power' J. Appl. Phys25, 676–677. https://doi.org/10.1063/1.1721711, 1954

[Breyer and Gerlach, 2013] C. Breyer and A. Gerlach, 'Global overview on grid parity',Progr. Photovolt.: Res. Appl., 2013, 21, 121–136, https://doi.org/10.1002/pip.1254

[Shockley and Queisser, 1961] W. Shockley and H. J. Queisser,' Detailed balance limit of efficiency of p-n junction solar cells', J. Appl. Phys, 1961, 32, 510–519.

[Yang et al,1997] J. Yang, A. Banerjee and S. Guha,' Triple-junction amorphous silicon alloy solar cell with 14.6% initial and 13% stable conversion efficiency', Appl. Phys. Lett, 70, 2975–2977, https://doi.org/10.1063/1.118761 , 1997

[Todorov et al, 2016] T. Todorov, O. Gunawana and S. Guhab, 'A road towards 25% efficiency and beyond: perovskite tandem solar cells', The Royal Society of Chemistry, Mol. Syst. Des. Eng., 1, 370–376, DOI: 10.1039/c6me00041j, 2016